SOVIET ATOMIC ENERGY

АТОМНАЯ ЭНЕРГИЯ
(ATOMNAYA ÉNERGIYA)

TRANSLATED FROM RUSSIAN

$\frac{c}{b}$ CONSULTANTS BUREAU

SOVIET ATOMIC ENERGY

Soviet Atomic Energy is a cover-to-cover translation of *Atomnaya Energiya*, a publication of the Academy of Sciences of the USSR.

An arrangement with Mezhdunarodnaya Kniga, the Soviet book export agency, makes available both advance copies of the Russian journal and original glossy photographs and artwork. This serves to decrease the necessary time lag between publication of the original and publication of the translation and helps to improve the quality of the latter. The translation began with the first issue of the Russian journal.

Subscription
(12 Issues): $95

Single Issue: $30
Single Article: $15

Order from:

CONSULTANTS BUREAU

227 West 17th Street, New York, New York 10011

SOVIET ATOMIC ENERGY

A translation of *Atomnaya Énergiya*

Volume 22, Number 1 January, 1967

CONTENTS

CONTENTS

(continued)

Engl./Russ.

NOTE

This index lists all material that appears in the original Russian journal. Items originally published in English or generally available in the West are not included in the translation and are shown in brackets. Whenever possible, the English-language source containing the omitted items is given.

The Russian press date (podpisano k pechati) of this issue was 1/4/1967. Publication therefore did not occur prior to this date, but must be assumed to have taken place reasonably soon thereafter.

STUDY OF AN AUTORESONANCE METHOD OF ACCELERATING PARTICLES BY ELECTROMAGNETIC WAVES

A. A. Vorob'ev, A. N. Didenko,
A. P. Ishkov, A. A. Kolomenskii,
A. N. Lebedev, and Yu. G. Yushkov

UDC 621.384.62

Aspects of the autoresonance acceleration of particles by fast waves in smooth wave-guides are considered. The results are confirmed by experiments carried out in the 10-cm waveband. The maximum energy of electrons so accelerated was about 700 keV.

Existing methods of accelerating charged particles by electromagnetic waves in linear accelerators assume the use of slow waves in diaphragmed waveguides with a longitudinal component of the electric field. The technological difficulties associated with the manufacture of such accelerating systems are generally known. In view of this, other methods of acceleration free from this failing and using a uhf field of high intensity present special interest.

It was shown in [1-4] that it was possible to effect resonance acceleration of particles by a transverse electromagnetic wave by applying a longitudinal magnetic field and selecting appropriate initial conditions (autoresonance method of acceleration). In this paper we present the results of an experimental investigation into this method of acceleration. We shall only consider acceleration by 10-cm electromagnetic waves set up inside smooth rectilinear waveguides. This is because as yet there are no ways of obtaining the strong fields required to produce appreciable acceleration over large volumes in other frequency ranges (including the visible).

If the magnetic field is directed along the z axis, then for a particle of energy $\mathscr{E}$ moving in the field of a plane levorotatory electromagnetic TEM wave propagating along the z axis with a phase velocity v_φ the integral of motion is [1-4]

$$\mathscr{E}\,(1 - \beta_\varphi \beta_z) = \text{const.} \tag{1}$$

Here $\beta_\varphi = v_\varphi/c$ and $\beta_z = v_z/c$, where v_z is the component of particle velocity along the z axis.

Condition (1), once satisfied, remains valid on increasing the energy. The condition is satisfied for both homogeneous and inhomogeneous waves in the transverse plane. Hence the fields of quadrupole lenses may be used for acceleration. If $\beta_\varphi = 1$, then the conditions of autoresonance acceleration will be satisfied in a magnetic field constant along the z axis. If, however, $\beta_\varphi \neq 1$, then, as shown in [3], the magnetic field must increase along the z axis in order to maintain synchronism.

In practice it is very difficult to create a rf field satisfying the requirements indicated. Firstly, rf fields of high intensity can only be set up in waveguides in which the waves are not transverse. Secondly, it is very difficult to excite waves simultaneously traveling in the z direction and rotating to left or right in waveguides.

In view of this we tried to establish an autoresonance mechanism of acceleration by using simpler electromagnetic waves such as the H_{11} wave of a circular waveguide and the structurally-similar H_{10} wave of a rectangular waveguide. For this purpose we first made some calculations in order to ascertain what waves existing in waveguides satisfied relation (1). This may be shown most simply for the H_{11} wave of the circular waveguide. Let the external magnetic field and the axis of the circular waveguide in which the H_{11} wave, (either standing or traveling with respect to z) is excited be directed along the z axis. In this case, if we write down the equation of motion along the z axis and the energy-balance equation

$$\frac{d\mathscr{E}}{dt} = e\,(\mathbf{v}\mathbf{E}),$$

1

for an H wave traveling with respect to θ and z, we obtain the relation

$$\mathscr{E}\left(1-\frac{z}{c}\cdot\frac{k}{k_z}\right) = \mathscr{E}\left(1-\beta_z\beta_\varphi\right) = \text{const}, \tag{2}$$

where k_z is the z component of the wave vector.

Relation (2) is an integral of motion analogous to that studied in [1-3] for levorotatory electromagnetic TEM waves. If we take an H wave traveling with respect to z and standing with respect to θ, we may obtain exactly such an integral of motion. This means that the autoresonance mechanism of acceleration is possible not only on using waves of right- or left-handed polarization but also on using a superposition of these waves.

If we take an H wave standing with respect to z and traveling with respect to θ, we obtain the relation

$$\frac{d}{dt}\left(\mathscr{E}\dot{z}\right) = \frac{ck_z\,\text{tg}\,k_z z}{k_z}\cdot\frac{d\mathscr{E}}{dt}. \tag{3}$$

We see from Eq. (3) that the integral of motion (1) does not exist for H waves standing with respect to z. This means in particular that the autoresonance mechanism of acceleration is not established if TEM or H waves standing with respect to z are excited in the waveguide.

Let us estimate the maximum energy to which particles can be accelerated in an autoresonance accelerator with definite parameters. Multiplying the equation of motion in r by $r\mathscr{E}/c^2$ and the equation in θ by $r\dot{\theta}\mathscr{E}/c^2$ and combining them, we obtain

$$\frac{1}{c}\cdot\frac{d}{dt}\left[(\mathscr{E}\dot{r})^2+(\mathscr{E}r\dot{\theta})^2\right] = \mathscr{E}\left(1-\frac{\beta_z}{\beta_\varphi}\right)(E_r\dot{r}+E_\theta r\dot{\theta}). \tag{4}$$

Hence after making some transformations we obtain the following integral of motion

$$\frac{\gamma^2(\dot{r}^2+r^2\dot{\theta}^2)}{2c^2} = \frac{\varkappa^2}{k^2}\cdot\frac{\gamma^2}{2}+\frac{\gamma\gamma_c}{\beta_\varphi}(1-\beta_\varphi\beta_{z,\,0})+\text{const} \tag{5}$$

or

$$\frac{\gamma^2\beta_\perp}{2}-\frac{\gamma_0\beta_{\perp 0}}{2} = \frac{\varkappa^2}{2k^2}(\gamma-\gamma_0)+\frac{\gamma_0(1-\beta_\varphi\beta_{z,\,0})}{\beta_\varphi^2}(\gamma-\gamma_0), \tag{6}$$

where $\beta_\perp^2 = \frac{\dot{r}^2+r^2\dot{\theta}^2}{c^2}$.

Assuming $\dot{r}\ll r\dot{\theta}$ and expressing $\beta_\perp$ in terms of H, γ, and $r(\beta_\perp = eHr/mc^2\gamma)$, we write the integral of motion in the following form:

$$\left(\frac{eHr_{\kappa}}{mc^2}\right)^2\left(1-\frac{r_H^2}{r_{\kappa}^2}\right) = \frac{\varkappa^2}{2k}(\gamma-\gamma_0)+\frac{\gamma_0(1-\beta_\varphi\beta_{z,\,0})}{\beta_\varphi^2}(\gamma-\gamma_0), \tag{7}$$

where $\varkappa = \sqrt{k^2-k_z^2}$.

Assuming that r_K in this expression is equal to the radius of the waveguide, we can determine the maximum energy attainable in the autoresonance accelerator with a waveguide of fixed radius For our case $r_K = 3.8$ cm; hence for this waveguide $\mathscr{E}_{\max} = 1.8$ MeV ($\mathscr{E}_{kin} = 1.3$ MeV) if $r_H = 0$ (initial velocity directed along the z axis), and at the initial instant $\beta_{z,\,0} = 0$.

Since the waves in the waveguide propagate with a phase velocity exceeding the velocity of light, we find that, strictly speaking, for a magnetic field constant with respect to z, a continuous energy rise in the wave is impossible, as indicated in [1-3]. Let us therefore determine the length of the segment along the z axis over which acceleration will take place. If, on motion in the γf field of the waveguide, the phase of the particle relative to the wave remains constant during acceleration, then, by differentiating the phase expression $\varphi_1 = \omega t - n\theta - k_z z$ (n = number of variations with respect to θ) with respect to time, we find that the angular velocity of the particle should vary in accordance with

$$\dot{\theta} = \frac{\omega-k_z z}{n} = \frac{kc}{n}\left(1-\frac{\beta_z}{\beta_\varphi}\right). \tag{8}$$

2

On the other hand, for autoresonance acceleration, the angular velocity of the particle equals

$$\dot{\theta}_{res} = \frac{kc}{n}(1 - \beta_\varphi \beta_z).$$ (9)

For this law of variation of the velocity of the autoresonance particle, the phase will vary in accordance with

$$\varphi_2 = \omega t - n\theta - \frac{z}{k_z}.$$

Assuming that the energy will rise until the particle phase lags behind the wave by not more that π, we may use (8) and (9) to find an expression for the waveguide length over which the energy rises:

$$z = -\frac{n\beta_\varphi \lambda}{2(1-\beta_\varphi)}.$$ (10)

In order to check the autoresonance method of acceleration, we set up an experimental apparatus to study the mechanism of autoresonance acceleration for an H_{11} wave in a circular waveguide and an H_{10} wave in a rectangular waveguide. The apparatus is shown as a block diagram in Fig.1.

The rf power was fed into the accelerating system along a waveguide channel from a nonadjustable magnetron pulse generator operating at a frequency of $f \approx 3000$ MHz. The duration of the rf pulse was 3 μsec at a repetition rate of 50 cps. The pulse power fed to the accelerating system was no greater than 600 kW.

The accelerating system was a 72×44-mm rectangular waveguide, in which an H_{10} wave is excited, or a circular waveguide with a 76-mm diameter, in which an H_{11} wave is excited. In order to set up conditions for traveling-wave propagation along the z axis, the waveguide in question was loaded with a matched load. The lengths of the accelerating systems varied in the experiments between 150 and 1000 mm.

The waveguides were evacuated to a pressure of 10^{-5} mm Hg with diffusion pumps. Standard quartz windows were used to separate the evacuated part from the atmosphere. Electrons were injected into the waveguide through an aperture 5 mm in diameter at an angle of 90° to the z axis and then rotated by a special magnet and directed along the axis of the waveguide. The incident angles at which the electrons passed into the accelerating system could be varied by varying the angle of rotation of the electron beam.

The constant magnetic field along the z axis was set up by means of a solenoid, the length of which could also be changed from 150 to 1000 mm. The x-ray radiation was recorded with a "Kaktus" x-ray meter and also by means of the signal obtained from a detector consisting of a stilbene crystal and a photomultiplier. When rf power passed along the accelerating waveguide, radiation was observed for a magnetic field of $H_z = 1000$ Oe.

As shown earlier, for $\beta_\varphi > 1$ the length of the section in which the energy increased was quite short. In our case, for an H_{11} wave in a circular waveguide, $\beta_\varphi = 2$; hence from expression (10) we find that this length $z = 3.6$ cm. Hence if the length of the homogeneous magnetic solenoid is greater than 3.6 cm, the energy should vary periodically along the waveguide. In order to observe the "beats" of energy, the inner wall of the waveguide was coated with a thin layer of phosphor. For an optimum magnetic field, luminous rings appeared on the waveguide walls. The distance between the rings was $l = 6$ to 7 cm; i.e., approximately twice the length of the section in which the energy rise took place. On varying the magnetic field in the neighborhood of resonance, slight displacements of the rings along the waveguide took place. Sharp distortion of the magnetic field at any point along the solenoid led to the vanishing of the luminous rings in this region and to a fall in the intensity of x-ray radiation.

Fig.1. Block diagram of the apparatus. 1) Magnetron generator; 2) vacuum pump; 3) wave transformer; 4) accelerating system; 5) electron gun; 6) rotating magnet; 7) solenoid; 8) rf load; 9) matching plunger; 10) observation window.

The kinetic energy of the accelerated electrons was determined by passing the electrons through aluminum

3

foils; it was $\mathscr{E}_{kin} = 600$ keV for an electric field of 3 to 5 kV/cm. This energy is considerably higher than that attainable with ordinary cyclotron acceleration under analogous conditions.

Detuning the match between the accelerating waveguide and the rf load led to the appearance of substantial reflections in the channel and to a disruption of acceleration (in this case a ferrite decoupler was included in the rf channel between the accelerating waveguide and the magnetron generator).

For a more detailed check on acceleration in the systems in question (using a standing wave along the z axis) we prepared a resonator in which H_{108} oscillations were excited. In this system no acceleration was recorded. This fact indicates once more that in this case there is no cyclotron acceleration whereby the replacement of the traveling wave by a standing wave need not change the final energy.

Thus the experimental results indicate the existence of an autoresonance mechanism of acceleration and agree closely with both the theoretical considerations developed in [1-4] and those of the present investigation. Electrons accelerated in accelerators of this type may find technological applications such as the efficient injection of particles into magnetic traps [5, 6].

LITERATURE CITED

1. A. A. Kolomenskii and A. N. Lebedev, Dokl. AN SSSR, 145, 1259 (1962).
2. A. A. Kolomenskii and A. N. Lebedev, ZhÉTF, 44, 261 (1963).
3. A. A. Kolomenskii and A. N. Lebedev, In: Transactions of the International Conference on Accelerators, Dubna, 1963 [in Russian]. Moscow, Atomizdat, p.1030 (1964).
4. V. Ya. Davydovskii, ZhÉTF, 43, 886 (1962).
5. B. S. Akshanov, Yu. Ya. Volkolupov, and K. D. Sinel'nikov, ZhÉTF, 36, 595 (1966).
6. B. S. Akshanov, Yu. Ya. Volkolupov, and K. D. Sinel'nikov, ZhÉTF, 36, 603 (1966).

4

USING L. S. PONTRYAGIN'S MAXIMUM PRINCIPLE IN MINIMUM-CRITICAL-SIZE AND MAXIMUM-POWER REACTOR PROBLEMS

T. S. Zaritskaya and A. P. Rudik

UDC 621.039.50

L. S. Pontryagin's maximum principle is used for solving problems in which it is necessary to find the minimum critical size of a reactor for a given power or to find the maximum power for a given critical size. Recently Pontryagin's maximum principle [1] has been successfully used both for determining the optimum transient conditions for reactors [2, 4] and for finding the optimum spatial arrangement for reactors with prescribed physical characteristics [1]. In the present study this principle is used in two other problems encountered in the theory of reactor design.

STATEMENT OF THE PROBLEM OF FINDING THE MINIMUM CRITICAL SIZE FOR A PRESCRIBED REACTOR POWER

It is assumed that the reactor power W is given and that the structural materials are distributed uniformly through the reactor. Resonance absorption and neutron absorption and multiplication during moderation are ignored. The uranium concentration U(z) is considered variable over the volume of the reactor within the limits:

$$0 \leqslant U(z) \leqslant U_{max} . \tag{1}$$

The power per unit of reactor volume, $\rho (z) \ N(z)U(z)$, is limited:

$$p = N(z) \, U(z) - D \leqslant 0, \tag{2}$$

where N(z) is the thermal-neutron density at point z and D is a constant. It is required to find the distribution U(z) which will yield the minimum critical reactor size for a prescribed power W and under conditions (1) and (2). The problem is solved in a two-group approximation for a symmetric slab reactor. The initial equations describing the thermal-neutron density, [N(z)], and the moderated-neutron density [n(z)], have the usual form [6]

$$
\left.
\begin{aligned}
\frac{d^2N}{dz^2} - \frac{1 + U(z)}{L_0^2} N &= -n; \\
\frac{d^2n}{dz^2} - \frac{n}{\tau} &= -\frac{\eta U}{\tau L_0^2} N,
\end{aligned}
\right\}
\tag{3}
$$

where L_0^2 is the square of the diffusion length of the medium, where the structural materials are taken into account but the uranium is not; τ is the square of the moderation length (the variation in τ for different uranium concentrations is neglected); η is the effective number of neutrons produced in fission.

PONTRYAGIN'S METHOD

In order to use the mathematical theory of optimal processes [1], we write (3) in the form of four first-order equations, introducing the notation $x^{(1)} \equiv N$; $x^{(2)} \equiv dN/dz$; $x^{(3)} \equiv n$; $x^{(4)} \equiv dn/dz$ and adding an

equation for $x^{(5)}$, making use of the fact that the reactor power is specified and is equal to $W = \int_0^H N(x)U(z)dz$ (where H is the desired half-width of the reactor). As a result, we obtain the following system of equations:

5

$$\left.\begin{array}{l} \dfrac{dx^{(1)}}{dz} = x^{(2)} \equiv f^{(1)}; \\[2mm] \dfrac{dx^{(2)}}{dz} = \dfrac{1+U}{L_0^2}\, x^{(1)} - x^{(3)} \equiv f^{(2)}; \\[2mm] \dfrac{dx^{(3)}}{dz} = x^{(4)} \equiv f^{(3)}; \\[2mm] \dfrac{dx^{(4)}}{dz} = \dfrac{x^{(3)}}{\tau} - \dfrac{\eta U}{\tau L_0^2}\, x^{(1)} \equiv f^{(4)}; \\[2mm] \dfrac{dx^{(5)}}{dz} = U x^{(1)} \equiv f^{(5)}. \end{array}\right\} \tag{4}$$

The functions $x^{(i)}$ satisfy the following boundary conditions:

$$x^{(1)}(H) = x^{(3)}(H) = 0; \quad x^{(2)}(0) = x^{(4)}(0) = 0; \quad x^{(5)}(0) = 0; \quad x^{(5)}(H) = W. \tag{5}$$

The Hamiltonian of the system (4) is formed according to the rule [1]:

$$\left.\begin{array}{l} \mathcal{H} = \displaystyle\sum_{\alpha=1}^{5} \psi_i f^{(i)} \equiv \chi + U\varphi; \\[2mm] \chi = \psi_1 x^{(2)} + \dfrac{1}{L_0^2}\, \psi_2 x^{(1)} - \psi_2 x^{(3)} + \\[2mm] \quad + \psi_3 x^{(4)} + \dfrac{1}{\tau}\, \psi_4 x^{(3)}; \\[2mm] \varphi = x^{(1)}\left[\dfrac{1}{L_0^2}\left(\psi_2 - \dfrac{\eta}{\tau}\,\psi_4\right) + \psi_5\right], \end{array}\right\} \tag{6}$$

where the auxiliary functions ψ_i satisfy the equations

$$\frac{d\psi_i}{dz} = -\frac{\partial\mathcal{H}}{\partial x^{(i)}} + \lambda\,\frac{\partial p}{\partial x^{(i)}}, \tag{7}$$

and the function p is given by formula (2). The function λ is defined as follows: if $p < 0$, then $\lambda \equiv 0$; if $p = 0$, then λ is defined by the condition

$$\frac{\partial\mathcal{H}}{\partial U} = \lambda\,\frac{\partial p}{\partial U}. \tag{8}$$

Taking into account the boundary conditions (5) for the functions $x^{(i)}$ and the transversality conditions for the functions ψ_i, we obtain the following boundary conditions:

$$\psi_1(0) = \psi_3(0) = 0; \qquad \psi_2(H) = \psi_4(H) = 0. \tag{8'}$$

Pontryagin's maximum principle* requires that in order to find the optimum distribution U(z), we must find a continuous and not identically equal to zero vector function ψ (with components ψ_i, $i = 1, \ldots, 5$) such that, first of all, the Hamiltonian $\mathcal{H}$ as a function of the independent variable U reaches a supremum $\mathcal{H} = \sup_U \mathcal{H} \equiv M$ everywhere in the region $0 \le z \le H$; secondly, the supremum of the Hamiltonian $\mathcal{H}$ is a constant positive number; and thirdly, the condition $\lambda \ge 0$ is satisfied in the zone where $p = 0$, if such a zone exists.

ADMISSIBLE TYPES OF CONTROL

Pontryagin's maximum principle enables us at once to determine the admissible types of control; i.e., to determine the types of zones, with known control functions of which the reactor can consist. It is evident that in the present problem the Hamiltonian as a function of the independent variable U will attain a supremum in the following cases:

1. $U(z) = U_{max}$, if $\varphi > 0$.

2. $U(z) = 0$, if $\varphi(z) < 0$.

3. $U(z) = U_0(z)$,

---

* According to the terminology of [1], this problem of the minimum critical size belongs to the class of fast-response problems.

6

Arrangement.	I	II	III	IV	V	VI
First zone $(0 \leqslant z \leqslant h)$	$p=0$	$p=0$	$U(z)=U_{max}$	$U(z)=0$	$U(z)=U_{max}$	$U(z)=0$
Second zone $(h \leqslant z \leqslant H)$	$U(z)=U_{max}$	$U(z)=0$	$p=0$	$p=0$	$U(z)=0$	$U(z)=U_{max}$

where $U_0(z)$ is determined from the condition $\partial \mathcal{H}/\partial U = 0$ (the case of the classical calculus of variations). It is easily verified that in this case $\psi_i \equiv 0$, and consequently there cannot be any zones with $U(z) = U_0(z)$*.

4. $U(z) = D/x^{(1)}(z)$. This zone corresponds to the case in which strict equality occurs in condition (2): $p = 0$.

POSSIBLE ARRANGEMENTS OF A TWO-ZONE REACTOR

Now we must construct an optimum reactor from three types of admissible zones: $U(z) = U_{max}$, $U(z) = 0$, and $p = 0$. Unfortunately, there is no mathematical algorithm for finding the optimum arrangement. We must test all possible arrangements and select the one which satisfies Pontryagin's maximum principle. We shall consider only a two-zone reactor (h is the boundary between the zones).

The six possible arrangements for a two-zone reactor are shown above.

Obviously, arrangements III and IV cannot be constructed because of boundary conditions (5). Arrangement VI must lead to a larger critical size than arrangement V, in which the uranium is concentrated at the center. Thus, we must analyze arrangements I, II, and V. We shall analyze arrangement I and show that it is the optimum arrangement. In addition, we shall compare the critical sizes for arrangements II and IV with the critical size for arrangement I.

OPTIMUM TWO-ZONE ARRANGEMENT

Solution of System of Equations for $x^{(i)}$.

The system of equations (3) or (4) can easily be solved analytically for $x^{(i)}$. Since the solution is rather cumbersome, we shall not give it here and shall confine ourselves to making one remark. In the first zone, if we use the condition $p = 0$, the system of equations (3) will no longer be homogenous in $N(z)$ and $n(z)$. Consequently, when we match the solutions at the zone boundary in the case $z = h$, we will not obtain a criticality condition, i.e., we will not find a value h. The zone boundary h is found from the following considerations. Since the Hamiltonian is constant and the functions $x^{(i)}$ and ψ_i are continuous functions of the independent variable z, the control function $U(z)$ must be a continuous function. Hence, if $\varepsilon > 0$, we have

$$\lim_{\varepsilon \to 0} U(h - \varepsilon) = U_{max} . \qquad (9)$$

Obviously these considerations are valid only when $\varphi(h) \neq 0$. As will be shown in the following section, $\varphi(h) \neq 0$ when we have the optimum arrangement I.

Solution of System of Equations for ψ_i.

We shall write the system of equations (7) for the functions ψ_i in explicit form:

$$\begin{cases} \dfrac{d\psi_1}{dz} = -\dfrac{1+U}{L_0^2}\,\psi_2 + \dfrac{\eta U}{\tau L_0^2}\,\psi_4 - U\psi_5 + \lambda U; \\[2mm] \dfrac{d\psi_2}{dz} = -\psi_1; \\[2mm] \dfrac{d\psi_3}{dz} = \psi_2 - \dfrac{\psi_4}{\tau}; \\[2mm] \dfrac{d\psi_4}{dz} = -\psi_3; \\[2mm] \dfrac{d\varphi_5}{dz} = 0. \end{cases} \qquad (10)$$
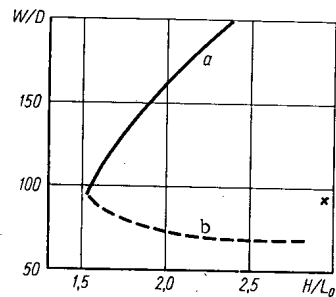
Fig.1. W/D as a function of H/L_0 for arrangements I (a) and V (b) when $\eta = 1.07$, $\tau/L_0^2 = 0.01$, and $U_{max} = 35.19$ (the × corresponds to arrangement II.)

* It should be noted that since the function $\varphi(z)$, according to (6), is the product of a function which depends only on $x^{(i)}$ and a function which depends only on ψ_i, it follows that $U_0(z) \equiv 0$. The statement that no such zone can exist means that there cannot be zones $U(z) = 0$ in which $\varphi(z) = 0$.

7
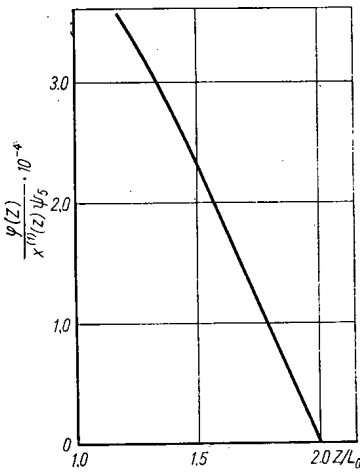
Fig.2. Graph of $\varphi(z)/x^{(1)}(z)$ in the second zone of the reactor for arrangement I.

In the first zone, according to formula (8), the function λ has the form

$$\lambda = \left[\frac{1}{L_0^2} \left(\psi_2 - \frac{\eta}{\tau} \psi_4 \right) + \psi_5 \right], \qquad (11)$$

i.e., the functions ψ_i are independent of U. In the second zone $\lambda = 0$, and the system of equations (10) includes $U(z) = U_{max}$.

Figure 1 shows the function $W/D = f(H/L_0)$ for arrangements I and V. As the calculations show, the critical size is even larger for arrangement II than for arrangement V (Fig.1 shows one of the points for arrangement II). Figure 2 shows the function $\varphi(z)/x^{(1)}(z)$ in the second zone of the reactor for arrangement I. We can see that the Hamiltonian attains a supremum in this zone. Furthermore, the analysis shows that the condition $\lambda > 0$ is satisfied in the first zone. Thus, arrangement I is in fact optimal.

RELATIONSHIP OF THE MINIMUM-CRITICAL-SIZE PROBLEM TO THE MAXIMUM-POWER PROBLEM

In the above paragraphs we consider the problem of finding the minimum critical size for a given reactor power. Now we shall examine the inverse problem: for a prescribed reactor size and the assumptions given above, find the arrangement which will yield the maximum reactor power. We shall show that arrangement I will be optimal in this case as well.

What is the difference in form between the statements of these two problems?

In the minimum-critical-size problem we were looking for the minimum of a functional $J = + \int_0^H dz$ for a prescribed value of the functional $W = \int_0^H x^{(1)} U dz$. In the maximum-power problem the functional J is given and we must find the maximum of the functional W. The other equations for $x^{(i)}$ in the inverse problem are exactly the same as in the direct problem.

Let us find how the Hamiltonians and the equations for ψ_i differ in these two problems. Let us denote $J(z)$ by $x^{(0)}$ and $W(z)$ by $x^{(5)}$. In the direct problem the increment added to the Hamiltonian is

$$\Delta \mathscr{H}_{dir} = -\psi_0 + x^{(1)} U \psi_5, \qquad (12)$$

while in the inverse problem it is

$$\Delta \mathscr{H}_{inv} = -\psi_0 + x^{(1)} U \psi_5, \qquad (13)$$

i.e., the form of the Hamiltonian is the same in the direct and inverse problems. Hence, according to Eq.(7), it follows that the systems of equations for ψ_i are also identical. Let us now compare the boundary conditions. In the direct problem $x^{(0)}(0) = 0$; ψ_0 is an undetermined constant [$\psi_0 \leq 0$, since we are trying to find the minimum of $x^{(0)}(H)$]; $x^{(5)}(0) = 0$ and $x^{(5)}(H) = W$; ψ_5 is a constant found by solving the equations simultaneously for $x^{(i)}$ and ψ_i. It is important to note that, according to one of the requirements of the maximum principle, the supremum of the Hamiltonian must be a constant positive number, and so we find that $\psi_5 > 0$.

In the inverse problem $x^{(0)}(0) = 0$ and $x^{(0)}(H) = H$; i.e., the constant ψ_0 is not determined by the boundary conditions; $x^{(5)}(0) = 0$; ψ_5 is an undetermined constant [$\psi_5 \geq 0$, since we are trying to find the maximum of $x^{(5)}(H)$]. Thus, the constants ψ_0 and ψ_5 in the direct and inverse problems are not determined by the boundary conditions but are found as solutions of the systems of equations for $x^{(i)}$ and ψ_i. Since the solutions are unique and the systems are identical, all $x^{(i)}$ and ψ_i (including ψ_0 and ψ_5) are identical for the two problems. Consequently, if we have solved the problem of minimum critical size for a given power, we automatically obtain the solution of the problem of maximum power for a given critical size.

The above considerations hold true whenever we are looking for the optimum of any functional for a prescribed value of a second functional: the solutions of the direct and inverse problems are identical. However, depending on the signs of the constants ψ_0 and ψ_5, we may have different cases: if $\psi_0 < 0$, and $\psi_5 > 0$, then in the direct case we are looking for the minimum of the functional $x^{(0)}$ and in the inverse case for the maximum of $x^{(5)}$; if $\psi_0 > 0$ and $\psi_5 > 0$, then we are looking for maxima in both cases;

8

if $\psi_0 < 0$ and $\psi_5 < 0$, we are looking for minima in both cases; if $\psi_0 > 0$ and $\psi_5 < 0$, then we are looking for a maximum in the direct case and the minimum in the inverse case.

In conclusion, it should be pointed out that the use of Pontryagin's maximum principle has made it possible to find an exact solution of the problem of minimum critical reactor size. The solution process is divided into two stages: rigorously defining the type of zones from which the reactor may be made up, and then making up a reactor from these zones. There is no algorithm for the second stage; it consists simply in analyzing different variant arrangements for optimality.

The results obtained here can easily be extended to problems with cylindrical and spherical geometry, as well as to multigroup problems. However, if the resonance absorption in the uranium is taken into consideration, we will obviously have to use numerical calculation methods and cannot obtain solutions in analytic form.

LITERATURE CITED

1. L. S. Pontryagin et al., Mathematical Theory of Optimal Processes [in Russian], Moscow, Fizmatgiz (1961).
2. Joshikumi Shinohara and Jean Valat, C. r. Acad. Sci., 259, Groupe 6 (1964).
3. Z. Rosztoczy and L. Weaver, Nucl. Sci. Eng. 20, 318 (1964).
4. J. Roberts and H. Smith, Nucl. Sci. Eng., 22, 470 (1965).
5. B. P. Kochurov, Atomnaya Énergiya, 20, 243 (1966).
6. A. D. Galanin, Theory of Thermal-Neutron Nuclear Reactors [in Russian], Moscow, Atomizdat (1959).

FAST BOILING REACTORS WITH THE FUEL
IN THE FORM OF A FUSED SALT

Miecislaw Taube

UDC 621.039.526

An attempt is made to classify fast reactors. Versions of a fast reactor with liquid
fuel in a boiling coolant - solvent are considered separately. The advantages of this type
of reactor and the feasibility of its construction are evaluated; the basic characteristics
of the reactor are derived.

A characteristic feature of the current state of development of nuclear power generation is that
in the sphere of fast reactors, solid-fueled (oxide) reactors cooled by liquid metal (sodium) are being
given primary consideration. The main efforts are concentrated on the future improvement and intro-
duction of reactors of this type in energy generation. Nevertheless, the investigations and developments
of other types of reactors are worthy of note, for example with a gaseous and vapor coolant. In part-
icular, it is proposed to use helium (p $\approx$ 70 atm, T $\approx$ 660°C) [1, 2], and also steam (p $\approx$ 170 atm,
T $\approx$ 540°C) [3]. It is assumed that uranium and plutonium oxides will be used as the fuel in all the pro-
jects mentioned.

There is a significant difference in a reactor with liquid fuel in the form of a three-component alloy
of plutonium (e.g., the LAMPRE-II reactor) [1]. Reactors with liquid fuel in the form of fused
chlorides (UCl_3, $PuCl_3$, NaCl, $MgCl_2$, etc.) are at the stage of discussion and evaluation. Two different
versions of a reactor of this type are known: a) with indirect cooling (via a heat-exchanger system)
[4-7] and b) with direct cooling, in which the removal of heat by the coolant (liquid lead) is accomplished
by means of contact heat exchange with the liquid chlorides (fuel) [2,4,8].

In considering the possible routes of development of fast reactors, it is possible to see feasibilities
of developing other types of reactors (Table 1). In this paper, we consider the fast reactor with a liquid
fuel and a boiling solvent. In this type of boiling reactor, part of the coolant exists in the liquid state
and part in the vapor state. The existence of several versions of such reactors is possible, in principle
(Table 2); at the end of 1965, two types of fast reactors with boiling coolant were proposed, designated
respectively WARS [15] and SAWA [16].

The basic characteristics of the reactors are given in Table 3. We note the special features which
are common to both versions. The fuel is in the form of fused chlorides $U^{238}Cl_3$ and $Pu^{239}Cl_3$; NaCl as
diluent; melting point of the fuel ~ 450°C; molar ratio U:Pu=4:1; specific heat ~ 0.30 kcal/kg; specific
weight ~ 5.0 kg/liter. The coolant enters the reactor in liquid form. Boiling of the coolant takes place
in the reactor core at a temperature of 750-800°C under a pressure of 20-40 atm. The vapor is fed
directly into the turbine or into the heat exchanger; the partial pressure of the uranium and plutonium
chlorides is about six to eight orders less than that of the coolant. The coolant is chemically inert
relative to the fuel components, but reacts with certain fission products.

Part of the fission products are removed by the coolant vapors. The stability of operation of a
fast reactor depends, to a considerable degree, upon the coefficient of thermal expansion of the boiling
coolant, which introduces negative reactivity. This ensures a relatively high reactor stability [17],
although the possibility of transition to the oscillatory conditions cannot be excluded. Reloading of the
fuel can be carried out continuously and part of the fission products can be separated from the liquid
or vapor coolant. The problem of fuel regeneration is solved relatively simply. The problem of
corrosion of the structural materials (for example, an alloy of the INOR-8 type) in a chloride medium
(in particular, aluminum trichloride in the SAWA reactor or to a certain extent by contact with liquid
mercury in the WARS reactor) requires special investigations; however, this obviously can be solved
positively.

TABLE 1. Principle Versions of Fast Reactors

Fuel	Coolant	Type of cooling	Remarks
Gaseous	Liquid	Indirect	Gaseous-fueled reactor, cooled by sodium
		Direct	Gaseous-fueled and liquid-cooled reactor (technologically inexpedient)
	Liquid-gas(boiling)	Indirect	No technological advantages
		Direct	Impossible, because of irreversible mixing of fuel and coolant
	Gaseous	Indirect	No technological advantages
		Direct	Impossible, because of irreversible mixing of fuel and coolant.
Liquid	Liquid	Indirect	LAMPRE [1] liquid-metal reactor, sodium-cooled. Liquid-salt reactor, sodium-cooled [4, 7]
		Direct	Liquid-salt reactor, cooled by liquid lead [2, 5, 8]
	Boiling	Indirect	No technological advantages
		Direct	Liquid-fueled with boiling coolant (see Table 2)
	Gaseous	Indirect	No technological advantages
		Direct	Liquid-fueled, with straight-through gas cooling
Solid	Liquid	Indirect	No technological advantages
		Direct	Oxide-fueled reactor, cooled by liquid sodium [1, 9-13]
	Boiling	Indirect	No technological advantages
		Direct	Solid-fueled reactor with boiling potassium [14]
	Gaseous	Indirect	No technological advantages
		Direct	Oxide-fueled reactor with gaseous coolant [1, 3]

The fundamental differences between the two versions consists in the following. In the WARS reactor, mercury is used as the coolant and it is almost insoluble in the liquid uranium, plutonium, and sodium chlorides, as a result of which a heterogeneous dispersion is obtained. The development of bubbles of mercury vapors can be controlled quite adequately. The possibility of formation of mercury chloride must be taken into account (the monochloride transforms to the dichloride at a temperature of 560°C). In the SAWA reactor, the coolant is aluminum trichloride, which easily dissolves the uranium, plutonium, and sodium chlorides with the formation of a homogeneous solution. The development of

11

TABLE 2. Fast Reactors with Liquid Fuel and Directly Boiling Coolant

Liquid fuel (mp $\sim 450°C$)	Boiling coolant(boiling point $\sim 800°C$, under a pressure of several tens of atm.)	Fuel-coolant system	Remarks
Metallic* (alloys of Pu, Fe, Co, Ce, etc.)	Metallic	Homogeneous	Liquid-metal fueled reactor, boiling coolant - mercury
		Heterogeneous	Liquid-metal fueled reactor, boiling coolant - sodium
	Salt	Homogeneous	Impracticable, because of poor solubility of salt in metals
		Heterogeneous	Impracticable, because of poor solubility of metals in salts
Salt (fused chlorides UCl_3, $PuCl_3$, diluted with chlorides KCl, $MgCl_2$, NaCl, $CaCl_2$, etc.)	Metallic	Homogeneous	Impracticable, because of poor solubility of metals in salts
		Heterogeneous	Liquid-salt fueled reactor, boiling coolant - mercury (WARS type)
	Salt	Homogeneous	Liquid-salt fueled reactor, boiling coolant - aluminum trichloride (SAWA type)
		Heterogeneous	Impracticable, because of mutual solubility of salts or because of mutual reaction

* The use of uranium is excluded in consequence of the temperature conditions.

TABLE 3. Comparative Characteristics of Fast Reactors

Characteristic	Reactor			
	BN-350	–	SAWA	WARS
Cooling	Indirect	Indirect	Direct	
Coolant	Liquid		Boiling	
Fuel	Solid (oxides)	Liquid (chlorides)	Liquid (chlorides)	
Thermal power, MW	1000	2500	1000	1000
Core volume, liter	2000	10,000	6,000	10,000
Specific power, kW/liter	500	250	165	100
Fuel concentration, kg Pu/liter	0.4	–	0.33	0.33
Specific power, kW/kg Pu	1200	580	1000	1000
Coolant	Sodium	Sodium	Aluminum trichloride	Mercury
Mean specific heat of liquid coolant, kcal/ kg·deg C	0.30	0.30	0.27	0.033
Heat of boiling of coolant, kcal/kg	Does not boil	Does not boil	37.8	68.13
Coolant supply, kg/sec	–	–	1340	3300
Thermal expansion/°C	$1.3 \cdot 10^{-6}$	$1.5 \cdot 10^{-4}$ (salt)	$2 \cdot 10^{-2}$	$2 \cdot 10^{-3}$
State of work	To be constructed [9]	Preliminary planning [6]	Preliminary development [15,16]	

12

bubbles of aluminum trichloride vapor takes place spontaneously and it is very difficult to control. This problem has been insufficiently discussed in the literature and requires special investigation.

LITERATURE CITED

1. M. Whitman et al. Report No. 3/1 Presented at London Conference on Fast Breeder Reactors, 17-19 May 1966.
2. R. Moore and S. Fawcett, See [1], Report No. 1/7
3. R. Mueller et al. See [1], Report No. 1/6
4. L. Alexander, Molten Salt Fast Reactors. Conference Breeding and Safety in Large Fast Reactors, ANL-6792 (1963).
5. L. Alexander, Ann. Rev. Nucl. Scie., 14, 287 (1964).
6. M. Taube, Symposium Power Reactor Experim., Report No. SM-21/19. Vienna, IAEA (1961).
7. P. Nelson et al. Trans. Amer. Nucl. Soc., 8, 153 (1965).
8. H. Killingback, A Molten Salt Fast Reactor, Winfrith AEE. Preprint, April (1966).
9. A. Leipunskii et al. See [1], Report No. 3/1
10. A Frame et al. See [1], Report No. 3/1
11. C. Pursel and E. Link, See [1], Report No. 3/5
12. I. Tattersall et al. See [1], Report No. 3/6
13. G. Vendreys et al. See [1], Report No. 1/3
14. A. Fraas, Nucleonics, No. 1, 72 (1964).
15. M. Taube et al. Nukleonika, No. 9-10, 641 (1965).
16. M. Taube et al. Nukleonika, No. 9-10, 639 (1965).
17. M. Taube et al. Nukleonika, No. 9, 631 (1966).
18. E. Nesis, Usp. fiz. nauk, 87, 651 (1965).

SODIUM TECHNOLOGY AND EQUIPMENT OF THE BN-350 REACTOR

A. I. Leipunskii, M. S. Pinkhasik,
Yu. E. Bagdasarov, R. P. Baklushin,
V. M. Poplavskii, A. A. Rineiskii,
E. N. Chernomordik, V. I. Sharanov,
I. K. Petrovichev, V. V. Stekol'nikov,
S. M. Blagovolin, K. B. Grigor'ev,
and I. D. Dmitriev

UDC 621.039.526+621.039.534.6

Information relating to the installation of a dual-purpose atomic station with a BN-350 reactor on the Mangyshlak peninsula in the USSR was presented in contributions to the Third International Conference on the Peaceful Use of Atomic Energy (Geneva, 1964), and the Detroit Conference in 1965. The present paper is devoted to a description of the main technological equipment and experimental work carried out in the construction process; it also includes a discussion of certain questions on sodium technology.

CIRCULATION PUMP

A console pump with a free fixed level of sodium, biological shielding, and mechanical sealing was chosen for the BN-350 reactor. Adequate experience in the use of such pumps has been gained in the USSR. The parameters of the pumps of the first and second circuits are shown in the table.

There is no fundamental design difference between the pumps of the first (Fig.1) and second circuits. The pump in the second circuit has no biological shielding.

The shaft of the pump has one radial and one radial-thrust slide bearing. The distance between the axes of the working wheel and lower bearing is 2 m. The biological shielding is situated inside the pump tank and part of the shielding is in the sodium. Between the roof of the pump tank and the lower bearing is a cooling belt for reducing the axial flow of heat in the direction of the bearings, and also for preventing sodium vapor from passing into the bearing cavity of the pump. A sodium-potassium alloy is used to cool the belt. A system for cooling the shaft, operating from a common oil supply, is provided, and measures are taken to prevent the passage of oil vapor or the oil itself into the sodium. The pumping part proper is removed from the tank without cutting the sodium-containing conduits. The bearings and upper oil seal may be inspected and repaired without withdrawing the removable part of the pump. The gas cavity is sealed in this case by a special "standing" seal, which operates with the pump disconnected. Part of the coolant flow is closed "on itself"; the remainder is taken away through a special overflow line to the pump inlet. No speed regulation is provided, but the pump is able to operate under different conditions. Three, four, or five pumps may be connected in parallel, and in addition the pump may operate at one-quarter speed.

Design Parameters of the Circulating Pumps of the First and Second Circuits

Circuit	Rating, m^3/h	Head of sodium column, m	Shaft speed, rpm	Maximum power of electric motor, kW
First	3220	110	1000/250	1700
Second	3850	70	1000/250	1100

Experiments in developing the design of the pump are continuing at the present time.

A 1:4.5 scale model has been used to choose the geometry of the flow section and the control apparatus, to determine the number and direction of internal flows, to carry out cavitation tests, to determine the degree and direction of hydraulic forces, and to find the efficiency of the pump (which turns out to be 70%).

The pump uses sealing of the type used in hydrogen-cooled generators. The heat from the friction pairs is transferred to the oil and eliminated with a built-in cooling system. A special testing system was set up to develop the construction and select the materials of the friction pairs. Preference was given to a combination of graphite and a chromium-plated steel surface.

A full-scale test-bed, comprising the under-carriage of the pump with all its components except the rotor (the weight of which was imitated by a metal disc), was set up to finish the bearings and to check the thermal state of the shaft, both when the oil-cooling system and cooling belt were in operation and when they were switched off.

At the present time a sodium test-bed has been set up for testing standard pumps. This is equipped with all necessary measuring and control systems. The test circuit contains about 20 m^3 of sodium. The test-bed will be used to test pumps under conditions similar to those found in practice and also to test the electric motor and its auxiliary systems, the fittings, the reverse valve, the level gage, and the flow meter. The main purpose of the test-bed, however, is the all-round "capability testing" of earlier-developed principal components of the pumping system and the pumping system as a whole.

The test-beds for the pumps of the first and second circuit are placed together; by setting up a connection between them, it is proposed to carry out tests on the reverse valve under conditions simulating the shut-down of one of the pumps in the BN-350 reactor.

INTERMEDIATE HEAT EXCHANGER

The intermediate heat exchanger (Fig.2) of shell-and-tube construction consists of two parallel sections. Each section is made in the form of a horizontal rectangular tank with three heat-transfer pipe beds immersed in it. Each bed consists of 343 U-shaped pipes 28 mm in diameter and 2 mm thick with a spacing of 35 mm along the front and in depth. Kh18N9 steel is used. The beds in each section are connected in series. The sodium of the first circuit passes into the inter pipe space, where it transfers heat to the sodium of the second circuit moving inside the pipes. The vertical U-shaped pipe
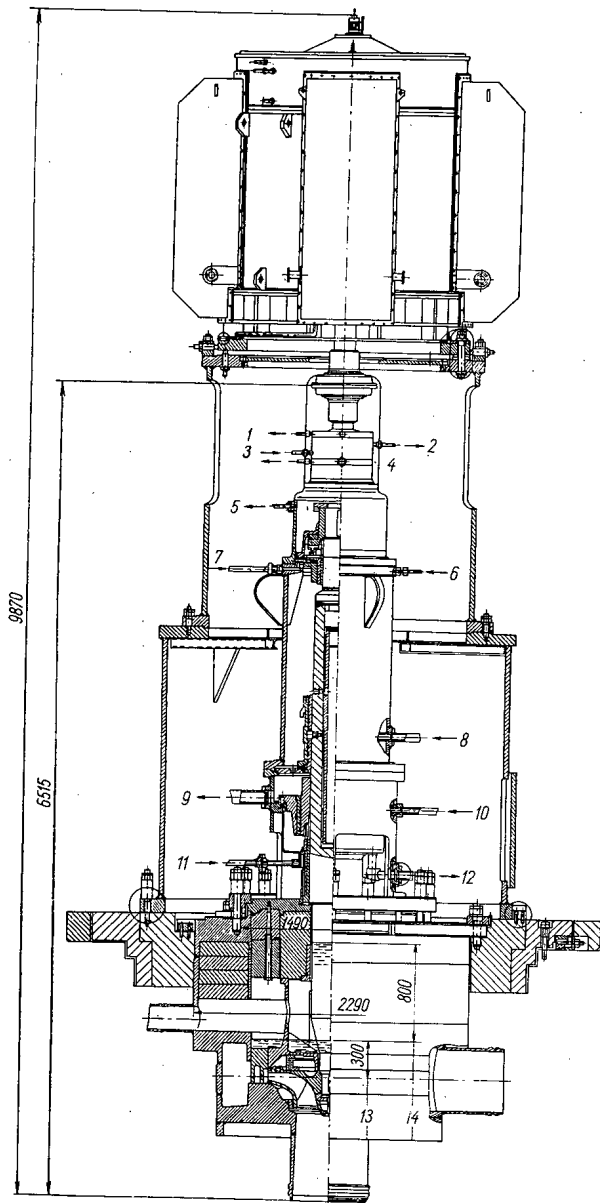

Fig. 1. Sodium circulation pump of the first circuit: 1) flow of oil from the shaft gas-sealing unit; 2) water from shaft gas-sealing unit; 3)water for cooling the shaft gas-sealing unit; 4) oil passing into the shaft gas-sealing unit; 5) gas for scavenging; 6) oil passing into the upper bearing; 7) oil passing into the pivot; 8) oil passing into the shaft; 9) oil from the pivot, upper bearing, and shaft; 10) oil passing into the lower bearing; 11) Na-K for cooling the shaft; 12) oil from the lower bearing; 13) initial lining level; 14) maximum level.
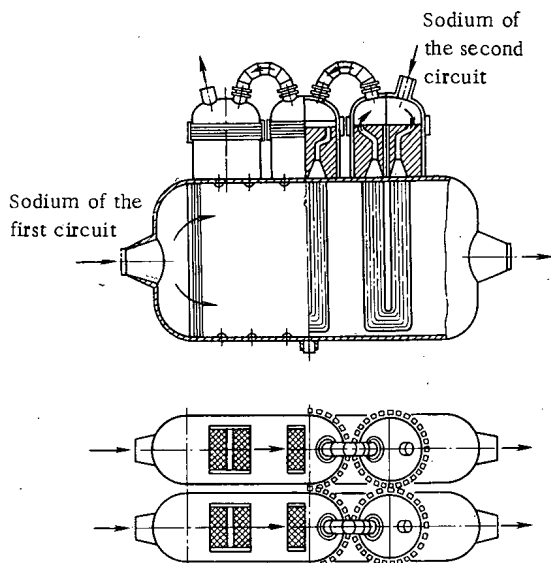
15

Fig.2. Intermediate heat exchanger.

bed has a cylindrical form; hence, in order to ensure a uniform distribution of the coolant over the width of the body, the pipe system of each bed is filled out to rectangular form with a set of stationary, nonoperating, straight pipes.

In order to create a uniform flow of the sodium of the first circuit, an equalizing grid is placed at the entrance to the first bed. Any bed of the heat exchanger may be taken out and replaced by a new one. In order to ensure access to the entrance and exit chambers, biological shielding, with special channels for passing the sodium of the second circuit, is provided.

At the present time the following experiments have been carried out:

1. The hydrodynamic characteristics of the interpipe space of the heat exchanger have been studied (on a 1:2.5 model).

Principal Characteristics of the Heat Exchanger

Thermal power.	$200 \cdot 10^3$ kW
Temperature of first-circuit sodium	
at the entrance.	500°C
at the exit	300°C
Temperature of second-circuit sodium	
at the entrance.	273°C
at the exit	453°C
Heat-transfer surface	1120 m²
Hydraulic resistance of first circuit.	0.146 kg/cm²
Hydraulic resistance of second circuit	2.24 kg/cm²

The results of the tests showed that the configuration of the input part of the model failed to ensure uniform flow of the sodium around the first pipe bed.

By suitable remodeling, this nonuniformity was eliminated. The experimentally determined over-all hydraulic-resistance coefficient of the heat exchanger, equal to 2.8, agreed closely with calculation.

2. Vibrational tests of the heat-exchanger tubes with transverse coolant flow were conducted on the model. The geometry of the bed, its lay-out, and its materials, were similar to those in the design. The tests were carried out with water. The experiments indicated that the dynamic stresses arising in the tubes under the influence of a transverse coolant flow were small for the design in question and could not have any marked effect on the efficiency of the heat exchanger.

In addition to the model tests, vibration tests were carried out on a full-scale heat exchanger, with the circulation of water through both the first and second circuits at the rated flow velocities.

3. A sodium test-bed of 3000 kW thermal power was also assembled and tested in order to secure an experimental verification of the thermotechnological characteristics of the heat exchanger.

STEAM GENERATOR

The steam generator (Fig.3) consists of two sections connected in parallel with respect to the sodium and water-steam circuits, a gas vessel, and connecting tubes. Each section contains one evaporator and one steam super-heater.

The evaporator is made in the form of a vertical vessel, with natural circulation of water inside Field tubes and separation of the steam in the steam space of the body. Sodium passes into the evaporator from the superheater and moves upward through the interpipe space, giving up heat to the water.
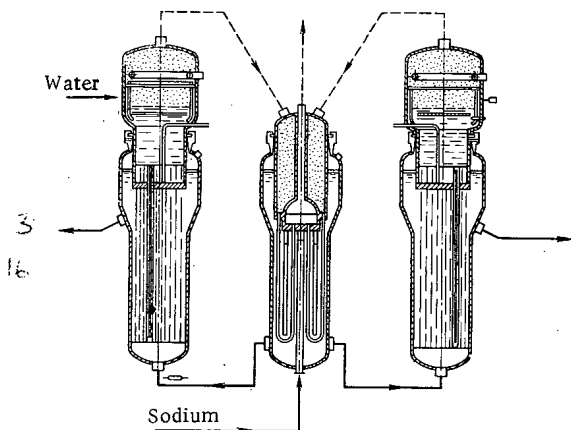
16

Fig. 3. Principle of the steam generator.

The boiler water from the water space of the evaporator passes into the inner, downcoming channel of the Field tube, moves downward, and passes into a ring-shaped gap, where it receives heat from the sodium, and, partly evaporating, again moves upward. The water-steam mixture thus formed is brought out through the steam exhaust pipes into the steam space of the evaporator.

The tube panel separates the body of the evaporator into two cavities: the upper, (steam-water) and the lower, (sodium). In the upper space or cavity are the collector of the feed-water supply, the scavenging collector, lines for the emergency removal of water from the evaporator, a jet-quenching sheet with downcoming tubes, and separation systems.

The lower (sodium) space may be arbitrarily divided into three parts: the entrance chamber, the working part, and the exit chamber with the gas space. In the entrance chamber is a double perforated sheet intended to produce a uniform distribution of the flow of sodium over the cross section of the evaporator. The working part consists of a body 1400 mm in diameter with a wall thickness of 24 mm. In the body are 816 Field tubes arranged in a triangular lattice with 44-mm spacing. Each Field tube consists of an outer tube of diameter 32 × 2 mm and an inner tube of diameter 16 × 1.4 mm. The lower end of the former is lapped and sealed, and the latter is fixed by its upper end in a steam waste vessel 600 mm high set in a socket of the tube panel. In the upper part of the exit chamber is a gas space for the withdrawal of gaseous products of the reaction between sodium and water in the case of accidental unsealing of the tube system.

The steam superheater is a vertical U-shaped heat-exchange system with the sodium and steam entrance and exit chambers in an upper position. The heat-transfer surface is made up of 805 U-shaped tubes 16 mm in diameter and 6 × 2 mm thick. The ends of the tubes are fixed into tube panels with apertures arranged in a triangle with a 23-mm spacing.

The components of the evaporator and steam superheater are made of 1 × 2M steel.

The gas vessel is a cylindrical vessel with hemispherical ends; it is intended for the partial trapping of sodium which may be thrown out together with hydrogen from the steam-generator space if there is any significant unsealing of the heating surface.

In the line of each evaporator is a feed regulator and a fast-acting irreversible cut-off valve, which operates if any leak appears in the steam generator. In order to secure rapid elimination of the dangerous state if substantial leaks of water into the sodium occur, an emergency line is provided for ejecting the water from the evaporators.

For removing reaction products there are tubes linking the gas cavities of the evaporator with the gas vessel. The latter is connected to a reaction-product separator installed outside the steam-generator room by means of a system of pipes incorporating a safety device.

Principal Characteristics of the Steam Generator

Steam-production rating.	276 tons/h
Superheated-steam pressure.	50 kg/cm²
Pressure in evaporator	52 kg/cm²
Temperature of superheated steam	435°C
Temperature of feed water.	158°C
Temperature of sodium at entrance to steam superheater	453°C
Temperature of sodium at exit from steam superheater.	416°C
Temperature of sodium at exit from evaporator.	273°C
Resistance of steam generator with respect to steam	1.5 kg/cm²
Resistance of steam generator with respect to sodium	0.93 kg/cm²

Evaporator heating surface . . . . 820 m^2
Steam-superheater heating surface . . . . 455 m^2
Circulation in evaporator 4-pass

A number of experiments have been carried out at the present time. The effects of interaction between sodium and water on failure of the heat-transfer tube have been studied. So has the effect of the composition of the gas blanket on the mechanism of the interaction, and the effect of the velocity and direction of the sodium flow on the temperature change at the point of contact of the reagents and on the propagation of the gaseous reaction products. The stability of the pipe bed of the evaporator when one of the pipes breaks and a large quantity of water passes into the sodium has been studied. The experiments were made on a model made of the design materials. The experimental test-bed constituted a closed sodium circulation circuit including a model of the evaporator, an electromagnetic pump, transport and drainage vessels, fittings, and conduit pipes.

In order to measure the pulsations in pressure at the point of breakage and in the gas space of the model, tensomanometers were used in combination with the appropriate amplification and supply systems and a loop oscillograph. The change in the temperature of the sodium at the point of contact and the temperature variation over the height of the interpipe space of the section was recorded with special low-inertia KhA microthermocouples.

Among the most important measurements, we also note the time variation in the position of the piston of the water dispenser in the course of injection. Five experiments were made in all. Up to 3 kg of water were fed into the sodium, the test volume of sodium being 100 liter. The injection time varied between 3 and 4 sec. The results were approximately the same in all the experiments.

At the moment of breakage, the pressure at the point of injection rose momentarily to 40 or 50 kg/cm^2; then there were a few pulsations, and the pressure fell. The flow of sodium through the model practically ceased, and the temperature at the injection point rose briefly to 700 or 800°C. The pressure in the gas cavity first rose, falling after the breakage of the safety membrane; the change in pressure was determined by the capacity of the reaction-product ejection system. In all the experiments, almost all the sodium enclosed between the injection point and the gas blanket flowed out into the ejection system.

There was not a single case of breakage in the neighboring tubes filled with water under a pressure of 50 to 60 kg/cm^2. The bending of the central and neighboring tubes was negligible. A characteristic graph giving the change of parameters in one of the experiments is shown in Fig. 4 and the form of the damage in Fig. 5.
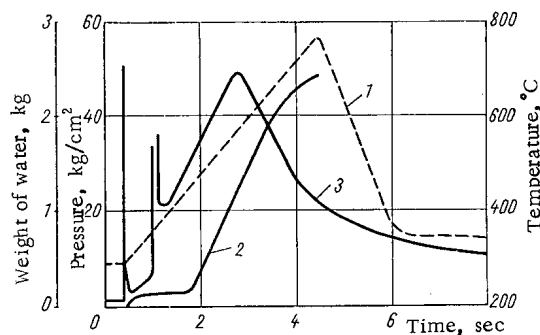

Fig. 4. Change in the principal parameters on injection of water into the sodium. 1) Temperature of sodium at the point of breakage; 2) weight of water passing into the sodium; 3) pressure at the breakage point.
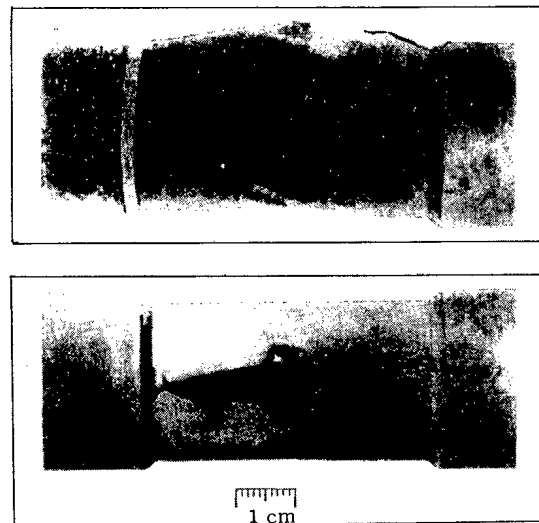

Fig. 5. Failure of the central tube.

18

The circulation characteristics of the Field tube were studied over a wide range of thermal loadings, and water-chemical tests of the evaporator elements were carried out. A special test system with a single Field channel was set up for this purpose.

A sodium test-bed of 3000 kW thermal power was set up and put into action in order to secure an experimental verification of the thermotechnological characteristics in the models of the evaporator and steam superheater. The models were full-scale structures as regards length, but had a number of heat-transfer channels corresponding to the power of the test system.

As a result of the experimental work it has so far been found that:

1) The experimental data on heat transfer and temperature distribution agree satisfactorily with computed data;

2) stable flow hydrodynamics in the Field tubes is obtained under a variety of operating conditions;

3) the separating systems of the evaporator model work reliably with respect to their output of steam of the required quality for two methods of extracting the steam-water mixture, namely, under the water level and directly into the steam space;

4) the individual components of the structure (the fitting of the tubes into the tube panels, the sealing, the welds, and so forth) operate satisfactorily. At present the models have operated for more than 2000 h, and experiments are continuing.

AUXILIARY SYSTEMS

The heat from the BN-350 reactor is eliminated or discharged by means of six parallel loops, of which five operate continuously and the sixth is held in reserve. Each loop of the first circuit has independent feed lines to the reactor and may be cut off from the rest of the system by slide valves.

The necessity and desirability of using a cut-off system is determined mainly by two considerations: first, the possibility of cutting out the loop and running off the sodium in it in case of any fault, and, secondly, the fact that there is then no need to enclose the whole primary circuit in a protective sheath in case of a break in the walls of the structure or the conduit pipes and tubes.

Only the body of the reactor and part of the piping (up to the slide valves) are enclosed in a casing filled with inert gas. Filling the space between the reactor body and casing with sodium does not lead to any break in the flow of circulating sodium or overheating of the core.

Sealing of the coupling rod of the principal slide valves is effected by means of solidified sodium cooled by a eutectic sodium-potassium alloy.

A characteristic feature of the construction of the slide valves is an arrangement by which their working components may be extracted for repair or replacement by remote control. This operation does not therefore necessitate cutting the conduits of the first circuit or going into the room in which it is situated; the operation may even by carried out without draining the sodium from the circuits, since the two slide valves are positioned approximately at the level of the upper part of the reactor. Access to the demountable joints is facilitated by built-in biological shielding as in the pump and intermediate heat exchanger.

The efficiency of the installation as a whole is ensured by a number of auxiliary systems. The most important of the auxiliary molten-metal systems include a system for purifying the sodium of the first and second circuits and indicating the oxide content, overflow tanks for the first and second circuits, and a system for preparing the coolant.

The filtration and oxide-indicating systems serve to determine the quantitiative sodium-oxide content in the coolant of the first and second circuits and also to purify the latter.

In the first circuit there are six cold traps. The number of working traps will depend on the degree of contamination of the sodium. As a rule, one or two traps are connected simultaneously; the trap-cooling system, however, is designed for four. In addition to this, two oxide indicators (of the plug-gage type) are provided; the sodium in these in air-cooled.

Each loop of the second circuit has its own independent system, including a cold trap and indicator. One cold trap is calculated for a sodium flow of 10 m³/h. The circuit traps are identical in construction
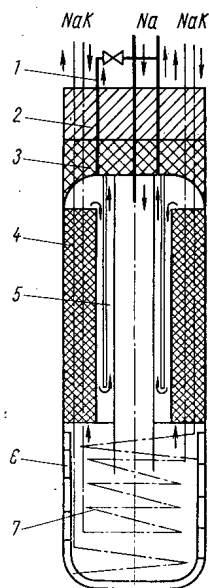
19

Fig. 6. Cold trap of the first circuit. 1) Bypass; 2) cast-iron shield; 3) thermal insulation; 4) filling(chips); 5) regenerator; 6) NaK-containing sleeve; 7) NaK-containing coil.

(Fig. 6) and constitute vertical cylindrical vessels about 6 m high and 1 m in diameter. These are placed in special electric furnaces and all feed lines to them are placed at the top. The first-circuit traps with their furnaces are arranged in a concrete shield. From above, the traps are closed with a layer of cast iron, ensuring access to the tubes should replacement be required.

The special sodium-potassium system carrying heat away from the cold traps includes two electromagnetic pumps rated at $150 \, m^3/h$ each and two air heat-exchangers. No reserve is provided in this system, and if any component of the system goes out of order some of the traps will be cut off.

An analogous but independent sodium-potassium system is provided for cooling the seals of the fittings and pumps. In this case, continuous trouble-free cooling is important, and 100% reserve equipment is therefore provided.

The overflow tanks of the first circuit (10 tanks at $50 \, m^3$ each) are designed for the overflow of sodium from the whole circuit. The tanks are connected in pairs. Each pair is placed in a separate box. In addition to this, in each box are two similar tanks constantly connected to the gas cavity of the reactor; thanks to these, the fluctuations of gas pressure in the reactor on changing the volume or temperature of the sodium are kept within tolerable limits.

The overflow tanks of the second circuit (four tanks at $50 \, m^3$ each) are designed for the simultaneous overflow of any two loops out of the six. The first and second circuits are filled from the overflow tanks by means of linear electro-magnetic pumps. The overflow of sodium from the circuits is free.

Means are provided in the BN-350 reactor for facilitating the repair and replacement of the sodium equipment of the principal circuits. The removable parts of the pumps, the heat-exchanger pipe beds, and the working parts of the principal slide valves are taken out of the circuit into pressurized vessels filled with an inert atmosphere. The pressurized vessels enable equipment to be replaced without draining the sodium from the circuit. A special sluice valve prevents the inner cavity of the circuit from coming into contact with the atmosphere in this process. The same pressurized equipment is used to take components into the washing system, in which any units taken from the circuit may be washed free from residual sodium (with water and steam), and if necessary treated with deactivating solutions. After such washing, the components are taken to the repair section.

ROLE OF CONDENSATE DECONTAMINATION IN
SINGLE CIRCUIT ATOMIC POWER STATIONS

T. Kh. Margulova

It is shown that the principal impurities in the supply water of single-circuit atomic-power stations (APS) are corrosion products. In view of the high solubility of these impurities in saturated steam, the efficiency of their removal with the scavenging water is relatively low, and decontamination of the whole condensate in ion-exchange filters becomes necessary. This condensate decontamination also ensures continuous deactivation of the condensate-supply tract and frees the circuit from hardness-producing salts passing into the condenser as a result of indrafts of the cooling water together with the corrosion of the condenser tubes. Of no small importance is the protective effect of condensate decontamination in any possible emergencies which may develop. Under condensate-decontamination conditions, the filtration velocities may be relatively high, and this demands filters of small dimensions.

The supply water for the reactors of single circuit APS comprises the condensate with the addition of desalinated water. Under these conditions the principal impurities are oxides formed in the circuit as a result of the corrosion of the structural materials. Also of no small importance are the hardness-producing salts arising from indrafts of cooling water in the condensers. In order to keep the concentration of these impurities at a level ensuring reliable operation of the active zone of the reactor, it is of prime importance to organize the water system in such a way that corrosion and indraft in the condensers may be reduced to a minimum. However, in view of the impossibility of stopping impurities from reaching the circuit altogether (at all events, after prolonged service), suitable means of withdrawing them from the circuit must be provided all the same. One such method is scavenging the circuit. For a single-circuit APS, this means the continuous removal of a proportion of the water (usually 1 to 2% but in rare cases 4%) to the purifying plant. However, analysis of the behavior of individual impurities in the technological circuit of the APS and an estimate of their acceptable concentrations leads to the conclusion that the scavenging method by itself is insufficient. For single-circuit APS this method must be supplemented by ion-exchange condensate decontamination for a 100% flow of condensate. Reasons for this requirement are set out below.

BEHAVIOR OF THE OXIDES OF CONSTRUCTION
MATERIALS IN THE CIRCUIT

It has been frequently noted in the boilers of ordinary thermal power stations that there is a great tendency for corrosion products to be carried away with the vapor rather than to be condensed in the scavenging water. An analogous situation occurs in single-circuit APS. Thus it has been pointed out, in connection with the water system of the Dresden APS, that scavenging the reactor only removes 20% of the iron oxides entering with the supply water. This means that a large proportion of the iron is carried out of the reactor with the saturated vapor. A large number of papers published over the past ten years by O. I. Martynova, D. G. Tskhvirashvili, and others, under the direction of Academician M. A. Styrikovich, on the solubility of various substances in saturated steam enable us to estimate the quantities of impurities passing into the steam. Figure 1 shows the so-called distribution ratio K as a function of the ratio of the densities of the water and the steam (ρ_w/ρ_s) for different impurities in the water, i.e., the ratio of the amounts of dissolved substances in the saturated steam and the boiler water. The behavior of the iron oxides is characterized by data for magnetite. It follows from Fig. 1 that the solubility of magnetite in steam is much greater than that of the other impurities, and it is considerable even at low pressures. At the same time, the solubility of magnetite is less dependent on pressure

---
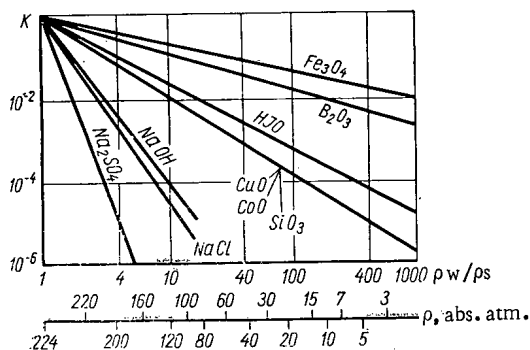
Fig. 1. Graph of distribution ratio of various impurities in the circuit water.

than that of any of the other impurities. At a pressure of 70 abs. atm. the value of K for magnetite is about 10%, i.e., it considerably exceeds the ordinary scavenging factors for the reactors of single-circuit APS.

The balance of any impurities for the steam-generating plant is

$$(100 + p) S_{s.w.} = (K + p) S_{sc.w.} \tag{1}$$

where p is the scavenging factor in % and $S_{s.w.}$ and $S_{sc.w.}$ are the concentrations of the impurity in the supply and scavenging water respectively.

Strictly speaking, for corrosion-product calculations, Eq. (1) should contain two or more terms; on the left-hand side there should be a term allowing for the arrival of oxides as a result of the corrosion of the construction materials in the reactor, and on the right-hand side there should be a term allowing for the loss of corrosion products associated with deposition inside the reactor. For a single-circuit APS, however, these terms are small in comparison with the principal terms in Eq. (1), and may therefore be neglected, especially in view of the fact that they are of similar magnitude and enter into opposite sides of the equation.

If we take the quantity of impurity carried in with the supply water as 100%, then the amount of this impurity carried away with the scavenging water is

$$\frac{p}{100+p} + \frac{S_{sc}}{S_{s.w.}} \cdot 100\%;$$

and with the dry saturated steam

$$\frac{K}{100+p} \cdot \frac{S_{sc}}{S_{s.w.}} \cdot 100\%.$$

The ratio of the impurities carried away by the scavenging water and by the saturated steam depends on the scavenging factor and K. The scavenging factor, however, varies very little, while the distribution ratios differ by an order of magnitude for different impurities (see Fig. 1). Hence for substances with a large value of K scavenging may not be an effective means of eliminating impurities. In order to illustrate this, Fig. 2 shows the ratio of the amounts of dissolved impurities carried away with the steam and the scavenging water for p = 1% and p = 2% on varying the distribution ratio K from 0 to 20%. It follows from Fig. 2 that, if K = p, as much impurity passes off with the steam as with the scavenging water. If K < p, then scavenging is the principle means of removing impurities. If, however, K > p, and especially if K ≫ p, then the impurity in question passes off principally with the saturated steam, and increasing (e.g., doubling) the scavenging factor makes comparatively little difference in the amount of the impurity removed from the circuit with the scavenging water. If as before we take a K of about 10% for Fe_3O_4 at 70 abs. atm., then for p = 2% only 18% of the impurity passes off with the water, and the other 82% remains in the steam! This means that, in order to secure efficient elimination of the corrosion products from the circuit (these products being in the truly dissolved state), the whole condensate flow must be treated (condensate decontamination must be calculated for a 100% steam rating).
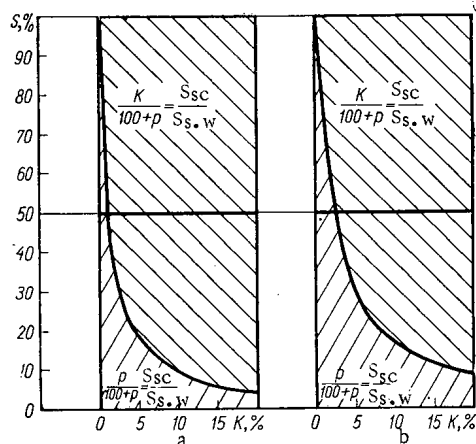
The solubility of the oxides of other construction materials and individual metals composing the alloys employed has been studied less extensively. However, existing data suggests that cobalt and zirconium oxides are carried out as well as silicon oxides. Hence the effective removal of these from the circuit also requires supplementing the reactor scavenging operation with 100% condensate decontamination, especially when we consider that cobalt and zirconium (and to a lesser extent iron) are carriers of activity under single-circuit

Fig. 2. Ratio of the amounts of dissolved impurities carried away with the steam and the scavenging water for p = 1% (a) and p = 2% (b) as a function of K.

22

APS conditions. Hence the removal of these elements from the part of the circuit in which the vapor is replaced by water is extremely important from the point of view of the continuous deactivation of the whole succeeding tract and that of ensuring its accessibility for use and repair.

The treatment of 100% of the condensate flow in ion-exchange filters does not eliminate the necessity of continuously scavenging the APC circuit. After condensate decontamination, the concentration of iron oxides in the supply water will rise again owing to the corrosion of the condensate-supply tract and may exceed the values corresponding to the truly dissolved state, so that a corrosion scum appears in the water. This is all the more likely in view of the fact that the solubility of iron oxides in water falls as temperature rises. The effective removal of this iron oxide scum, dangerous from the point of view of its possible "scaling-on" to the fuel-element cans, is only possible by means of scavenging water, and this constitutes the main purpose of continuous scavenging in the reactors of single-circuit APS.

INDRAFTS OF THE COOLING WATER IN THE CONDENSERS AND COMBATING THEM

The causes of indrafts of the cooling water may be of a technological character (leaky tube rolling, technological defects in the tube material), but may also arise in the course of use (failure of vacuum-tightness at the rolling points as a result of vibrations, corrosion cracking in the tube material). These factors mean that we cannot count on the creation of a condenser free from such indrafts. The smallest value of indraft guaranteed by the factories is $q = 0.005\%$ of the flow of steam through the condenser. For a powerful condenser with tens of thousands of tubes and 900 tons/h of steam passing through them, this corresponds to a transferred flow of 45 liters/h of cooling water. If we consider that it is almost impossible, with existing test methods, to observe such an indraft, so that it is very hard to discover the points of indraft, and the reactor has to be shut down or its power sharply reduced in order to remove an inaccessible indraft, it becomes clear how important it is to take precautions against indrafts and to eliminate their consequences. The first problem is solved by a number of constructional measures and the second by desalinating part or all of the condensate flow.

The constructural measures include: 1) use of corrosion-resistant alloys; 2) use of thick-walled tubes; 3) setting up of double tube panels; 4) setting up of the so-called salt compartments in regions near the tube panels and desalination of the condensate passing through these spaces (30 to 40% of the total flow); 5) smearing the rolling points with sealing pastes of the liquid Nairit (= Neoprene) type.

Thermal-power experience shows that a combination of the first and last measures is the most promising. The setting up of double tube panels complicates the manufacture and repair of the condensers and only removes the effects of indrafts at the rolling points. The same may be said of salt compartments. A study of the condensate quality in a condenser with salt compartments in the Lugansk Thermal Power Station (in μg/kg sodium) give the following results:

Condensate of salt compartments (flow 30 to 40%) after ion-exchange filters . . . . . 5 to 7
Main flow of condensate (60 to 70%) . . . . 65 to 70
Mixture of main condensate flow and desalinated condensate of the salt
    compartments. . . . . 50 to 60

Hence this method also fails to give a very high quality of condensate.

Considering the extremely well-developed surface of the tubes in condensers, it should be pointed out that an indraft associated with the corrosion of the tube material is entirely commensurate with an indraft at the rolling points, or may indeed exceed this, as shown by experimental results.

Regarding the corrosion of brass condenser tubes in the Melekesse single-circuit APS, there is a continuous flow of copper and zinc ions (associated with the dezincification of the brass) into the condensate. Experience in the use of double tube panels in this APS also shows that the removal of the effects of indraft at the rolling points cannot entirely eliminate the deleterious influence of indrafts.

All this makes desalination of the condensate of prime importance. Considerations of economy alone would suggest partial (rather than 100%) desalination of the condensate in regions near the rolling points (salt compartments). The flow of condensate, however, is still large, and this complicates the assembly of the plant and fails to reduce the dimensions of the system. It is therefore better to change over to 100% desalination of the condensate with increased filtration velocities. Thus for a condenser
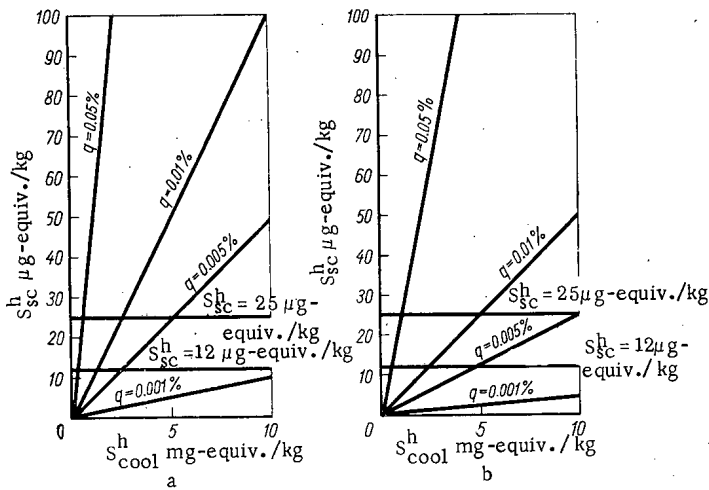
Fig. 3. Hardness of the water in the circuit as a function of the indraft in the condenser; a) p = 1%; b) p = 2%.

with a steam flow of 900 tons/h, at filtration velocities of 30 m/h, the filter diameter equals 6.2 m, while for filtration velocities of 120 m/h (quite acceptable for the condensate) the filter diameters are only 3.1 m. The indraft of cooling water in the condenser is also a source of silica, chlorine ions, and hardness-producing salts.

Limitation of the concentration of silica is only necessary when using superheated steam at high temperatures and pressures. Inadmissible concentrations of chlorine ions arise in the condensate when the indraft in the condenser leads to inadmissible concentrations of hardness-producing salts. Hence the influence of indrafts of cooling water on the water system of the reactor of a single-circuit APS is only a consequence of the influence of the hardness-producing salts. Heat-exchange conditions without either scaling or scum formation must be ensured in the reactor.

There can thus be no talk of phosphating the reactor water, i.e., the water system must be correction-free. Thus normalization and testing of the water system should be based on the hardness of the scavenging water of the reactor. It follows from Fig. 1 that we may neglect the solubility of the salts in the steam up to extremely high pressure (K = ~ 0). Hence scavenging is an effective method of removing hardness-producing salts from the circuit (see Fig. 2). The balance of impurities for hardness-producing salts is simpler:

$$(100 + p) S_{s.w} = p S_{sc}. \tag{2}$$

The impurity concentration of the supply water is given by the expression

$$S_{s.w} = \frac{q}{100} S_{cool}, \tag{3}$$

where S_{cool} is the impurity concentration in the cooling water of the condenser.

Figure 3 shows the results of calculating the hardness of the water in a reactor as a function of the admissible degrees of indraft in the condenser and scavenging of the reactor. The hardness of the cooling water is taken as the mean value for river water; desalination of the condensate is not carried out. Figure 3 also shows the admissible hardness of the water in the reactor corresponding to scale-free operation (12 μg-equiv./kg for constant use and 25 μg-equiv./kg for short term use). It follows from the figure that it is only permissible to omit desalination of the condensate (at any rate for cooling water with a hardness up to 100 μg-equiv./kg) for indrafts of the order of 0.001% in the condenser, which is certainly an unrealistic value for prolonged service. When the indrafts are 0.005% (even more if they are 0.01% or over) desalination of the condensate is essential.

Considering that it is impossible to guarantee that indraft should only at the rolling points, and that it probably arises at arbitrary points in the tubes (for example, slight corrosion cracks), we must be wary of desalinating only part of the flow of condensate. We must remember futhermore that the purity of the condensate is only tested periodically, and that between samplings there may be an increase in the indraft, not large enough to be reflected in the degree of vacuum, but dangerous from the point of view of reliable reactor operation. For example, an indraft of 0.05% is regarded as being the upper admissible limit from the thermotechnical point of view, but as Fig. 3 shows it is quite unacceptable for ensuring reliable operation of the reactor water system. This means that condensate decontamination with 100% flow of condensate fulfils yet another important function in protecting the reactor from possible emergency situations associated with damage to the condenser tubes.

Thus we may conclude from the present discussion that for single-circuit APS the setting up of ion-exchange filters for the total quantity of condensate is absolutely essential. This: 1) removes iron oxides and the oxides of other construction materials from the coolant; 2) ensures proper accessibility of the equipment of the condensate-supply tract; 3) removes hardness-producing salts arising from the

24

indraft of cooling water in the condenser and hence enables the scavenging of the reactor to be reduced without danger of scale deposition; 4) frees the condensate from copper and its oxides and also certain other metals (e.g., zinc) arising in the circuit as a result of the corrosion of the condenser tubes, and protects the reactor from possible emergency situations associated with condenser-tube damage.

The main purpose of scavenging the reactor of a single-circuit APS with 100% condensate decontamination is the removal of corrosion scum and the maintenance of the hardness of the reactor water at an acceptable level. In view of this the degree of scavenging may be somewhat reduced, thus achieving increased economy in the running of the installation.

25

STUDY OF THE ZONES OF DAMAGE CAUSED BY
FISSION FRAGMENTS OF HEAVY NUCLEI

V. K. Gorshkov, L. N. L'vov,
and P. A. Petrov

UDC 621.039.553:546.799.6

This study is based on the well-known anomalous fall in the evaporation rate of thin sources containing the isotope Cm^{244}. The anomaly is apparently due to local surface damage induced by fission fragments. The mean diameter of the local damage zones depends on the pressure of the medium containing the source; it lies between 0.1 and 1μ.

The irradiation of a solid by fission fragments of heavy nuclei produces local damage both inside the solid and on its surface. This is confirmed by electron-microscope examination of single crystals and polycrystalline material [1-3]. In order to explain the nature of this interaction, experimental measurement of the dimensions of the damaged zones as a function of the surrounding conditions is of interest.

In the present investigation, the zones of surface damage were studied by measuring the evaporation rate of atoms and molecules from the surface of a solid under the influence of fission fragments [4, 5]. It was found in [6] that thin sources (thickness less than 1μ) containing spontaneously evaporating isotopes of curium evaporated predominantly under the influence of the fission fragments along the surface of the source. Evaporation occurred from a region of relatively small radius (about 100 Å) around the track, the number of evaporated atoms per fragment being independent of the substance. Hence the evaporation should only be determined by the relief of the source surface. In other words, evaporation will be the greater, the more even the surface over the path of the fragment. Hence the character and extent of the surface damage induced by fission fragments may be judged from the variation in the evaporation rate.

ARRANGEMENT OF THE EXPERIMENTS

In all, five sources of different strengths (see table) consisting of a mixture of Cm^{244} and certain rare-earth elements were studied. The sources were prepared by evaporating an acetone-alcohol solution of the nitrates of the mixture in question and cellulose (photographic plate dissolved in amyl acetate), deposited on aluminum substrates, with subsequent annealing at about 500°C. This gave strong layers less than 0.1μ thick, which were almost unaltered on treatment with alcohol-moistened pads. The area of the active layer for all the sources was $0.12\,cm^2$, and the uniformity of the curium distribution was 5 to 8%.

Relative Strengths of Different Sources

Number of source	Relative strength of source
1	–
2	8.0
3	1.9
4	1.0
5	0.58

Note. By relative strength of the source we mean the number of fragments emitted from its surface per unit time.

We studied the time variation of the evaporation rate of the sources in vacuum (pressure of the order of 10^{-2} mm Hg), at atmospheric pressure, and also under the influence of fission fragments from an additional source. Some time after preparation, all the sources (except No. 2) were fixed in a special apparatus for measuring the degree of evaporation (Fig. 1) and placed in a vacuum chamber. The relative number of evaporated atoms was determined from the α-activity (due to the α-decay of the Cm^{244}) of the collectors, which were periodically replaced.

In the experiment at atmospheric pressure, after sources Nos. 3 and 4 had been taken out of the apparatus for a considerable time, it was difficult to measure the evaporation rate, owing to the low energy of the evaporated atoms; hence the
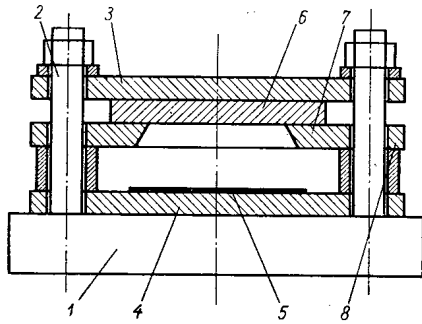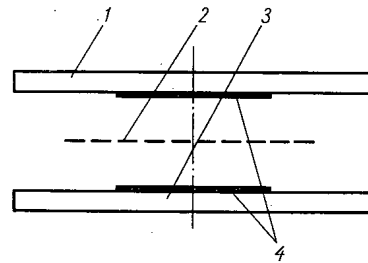
26

Fig. 1   Fig. 2

Fig. 1. Apparatus for measuring the evaporation of the sources: 1) base; 2) centering rod; 3) clamping plate; 4) source substrate; 5) active layer; 6) collector for evaporated atoms (aluminum foil 0.1 mm thick); 7) disc with standard aperture; 8) separating spacers.

Fig. 2. Layout of experiment involving the supplementary irradiation of source No. 1: 1) supplementary source; 2) Al_2O_3 film; 3) source No. 1; 4) active layers of sources.

change in the evaporation rate was deduced on the basis of measurements carried out in a vacuum before and after the experiment.

In the experiments involving prolonged irradiation of the source (Fig. 2) an Al_2O_3 film served to prevent the evaporated atoms from the supplementary source from striking the surface of source No. 1.

The relative strengths (see table) were measured by counting the number of fragments revealing traces on the surface of the glass after etching in hydrofluoric acid [7]. Periodic measurements showed that the strength remained constant during the whole experiment; this was because of the comparatively long half life of Cm^{244} ($T_{1/2} = 17.6$ years).

RESULTS

The time variation in the evaporation rate of sources Nos. 3 and 4 is shown by the curves in Fig. 3: AB, CD, EF, HI, KL, MN, PQ, correspond to vacuum measurements and DE, LM to measurements
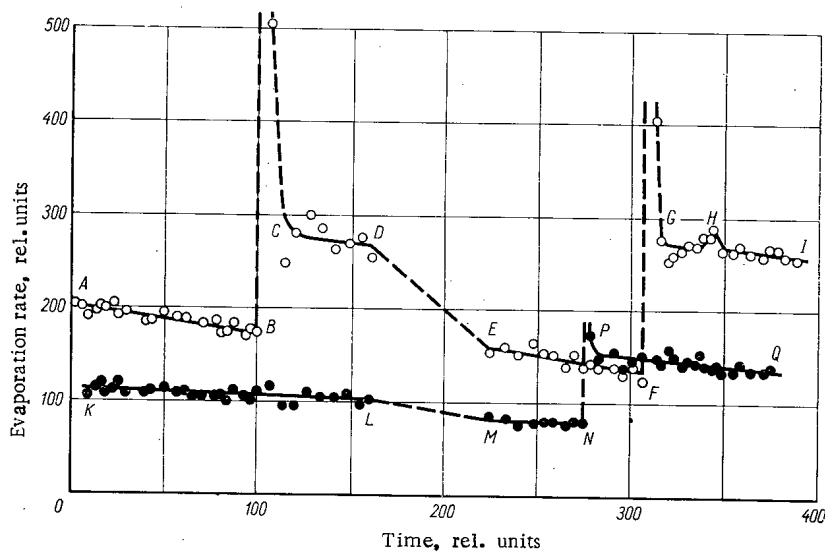

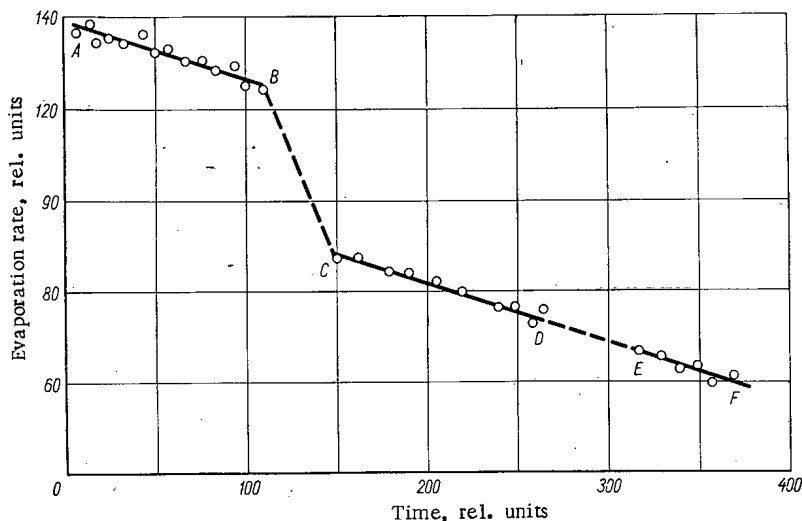Fig. 3. Fall in the evaporation of the sources with time. O) Source No. 3; O) source No. 4.

27

Fig. 4. Change in evaporation rate of source No. 1 under the
influence of fragments from an additional source.

at atmospheric pressure. Both sources show an anomalous fall in the evaporation rate as compared with that associated with the decay of Cm^{244}. The fall in the evaporation rate for sources Nos. 3, 4, and 5 (curve for latter not shown) during the experiments in a vacuum equals 17, 8, and 5% per 100 time units, respectively. These results agree satisfactorily with the relative source strengths (see table).

Despite the slight spread in the values on section CD and the very slight effect for source No. 4, the difference between the fall in the evaporation rate in segments DE and LM and that in the other segments is quite obvious. Calculations showed that the evaporation rate of both sources fell some three times more rapidly in air than in a vacuum.

At points B, F, N, and H, the sources were taken out of the vacuum system for some hours, after which their surfaces were smoothed slightly with a glass rod. After this treatment the evaporation rate rose (CD relative to AB and PQ relative to MN). On subsequent treatment of the surface after a short interval of time (point H) the evaporation rate changed very little.

A sharp change in the evaporation rate was also observed when the surface of source No. 1 was irradiated with fission fragments from an additional strong Cm^{244} source (see segment BC in Fig. 4).

The Cm^{244} isotope is principally α-active ($T_\alpha : T_{fiss} = 17.6 : 1.4.10^7$). In order to discover the role of the α-particles in this effect, in subsequent experiments (DE in Fig. 4) we replaced the Al_2O_3 film with aluminum foil μ thick; this completely absorbed the fission fragments but had little effect on the number and energy of the α-particles from the additional source. No relative change in the evaporation rate was observed in these experiments.

Source No. 2 was kept at atmospheric pressure throughout the experiments and thus received the maximum surface damage. Measurements made after the experiments revealed no fall in the evaporation rate.

DISCUSSION OF RESULTS

We may conclude from the experiments described that the anomalous fall in the evaporation rate of the sources with time is due to the effects of fission fragments from heavy nuclei.

The increase in the evaporation rate after smoothing the surface of the source and the absence of an anomalous effect in source No. 2 ("saturation") indicate the way in which the fragments act. The effect apparently reduces to local damage in the form of depressions or protuberances. The relative strength of the active layers and the low irradiation dose imparted to the surface by the fragments during the whole period of the experiments (as shown by calculations for sources No. 3 and 4) tend to favor the second mechanism.

28

Hence the pronounced overshoots on the curves (see segments BC, FG, and NP in Fig. 3) may be explained by the weak link between the very small particles formed as a result of the destruction of the mounds (protuberances) and the surface of the source. At the first instant of evacuation, the particles may be carried away by gas molecules. After this they become "vacuum-sintered" to the active layer.

It is not hard to show that the fall in the evaporation rate of the atoms resulting from the change in the surface relief does not depend on the nonuniformity of evaporation along the track of the fragment. This means that the extent of the fall in the evaporation rate corresponds to the proportion of the surface of the source damaged by the fragments. Thus by calculating the area of the surface damage during the whole experiment and determining the total number of fragments which have passed through the surface of the source we may calculate the mean diameter D of the local zone of damage per fragment.

On the basis of the data obtained for sources Nos. 3, 4, and 5 for experiments in a vacuum, D equals 0.1 to 0.2μ. This roughly ten times exceeds the mean diameter of the region of evaporation measured earlier [6] for the same sources. No clear explanation for this difference has yet been found. In the case of experiments at atmospheric pressure, the value of D equals approximately 1μ.

These values agree with the results obtained by bombarding a lithium fluoride crystal with fission fragments [3], where hillocks 0.1 to 1μ in diameter were formed by each fragment on the surface of the crystal.

Of particular interest is the variation in the observed anomaly with the degree of vacuum during the experiment. The increase in D for the experiments at atmospheric pressure may evidently be explained by the interaction of the active layer with gas molecules surrounding the source or penetrating into the thin layer. This should lead to the formation of protuberances on the surface of the source at the points at which the fragments pass through and to a variation in the extent of the damage with the degree of vacuum. We may suppose that the prolonged or intensive irradiation of a solid specimen similar to the active layer with fission fragments may constitute a cause of its swelling.

LITERATURE CITED

1. R. Price and R. Walker, Phys. Rev. Lett., 8, 217 (1962).
2. L. Chadderton et al. J. Appl. Phys., 34, 3090 (1963).
3. T. Knorr, J. Appl. Phys. 34, 2767 (1963).
4. F. S. Lapteva and B. V. Érshler, "Atomnaya Énergiya", No. 4, 63 (1956).
5. M. Rogers and J. Adom, J. Nucl. Materials, 6, 182 (1962).
6. V. K. Gorshkov and L. N. L'vov, "Atomnaya Énergiya", 20, 327 (1966).
7. R. Fleischer and P. Price, J. Appl. Phys., 34, 2903 (1963).

RADIATION STABILITY OF LOW–MELTING ORGANIC COOLANTS IN THE LIQUID AND SOLID PHASES

V. A. Khramchenkov, I. I. Chkheidze, Yu. N. Aleksenko, and N. Ya. Buben

UDC 541.15:621.039.534.7

The radical yields G_r in gas oil, hydroterphenyl, and monoisopropyldiphenyl were measured after their irradiation by electrons at —170°C, as were the yields of high-boiling products $G_{h.b}$ after irradiation of these same substances in a reactor at a temperature of 50°C. From a comparison of these quantities it follows that larger values of G_r correspond to larger values of $G_{h.b}$. It was shown that the calculated radiation yields of radicals in the liquid phase differ from the values measured in the solid phase by no more than four-fold. On this basis it is concluded that the radiation stability of organic coolants in the liquid phase can be predicted according to the radiation yield of radicals in the solid phase.

This work was conducted to determine whether the radiation yields of radicals obtained in the irradiation of low-melting organic coolants by electrons at low temperatures can give an idea of the radiation stability of these substances in the liquid phase. Moreover, a preliminary estimation of the radiation chemical stability of the compound in the solid phase [for example, by the electron-paramagnetic-resonance (EPR) method] was needed before tests could be conducted in a nuclear reactor, since such tests involve experimental difficulties and require substantial expenditures of time.

The changes that occur in a substance under the action of radiation are determined chiefly by two factors: in the first place, by the radiation stability of the molecules of the starting material (by the number of cleavages of chemical bonds per 100 eV of absorbed energy), and in the second place by the ability of the active particles formed (ions and radicals) to enter into the reactions with one another, as well as with molecules of the starting material. While at low temperatures, in the solid phase, the radiation chemical transformations are determined chiefly by the first factor, in the case of liquid–phase radiolysis, the second factor also plays an important role. It is known [1] that the formation and accumulation of high-boiling products during irradiation of organic coolants in a reactor entirely determine the changes in their thermophysical characteristics.

EXPERIMENTAL SECTION

Radiation stability in the solid and liquid phases was determined for three coolants which are now of practical importance: 1) monoisopropyldiphenyl, $T_{melt} = -40°C$; 2) hydrostabilized gas oil, representing a mixture of paraffin (35%), naphthenic (44%), and aromatic (21%) hydrocarbons, $T_{melt} = -60°C$; 3) hydroterphenyl, which is a mixture of incompletely hydrogenated terphenyls, $T_{melt} = -11°C$.

The low-temperature stability (—170°C) was determined according to the radiation yield of radicals G_r by the EPR method on the EPR-2 apparatus of the Institute of Chemical Physics mounted under a beam of 1.6 MeV electrons [2]. The dose rate was 250-400 Mrad/h; the total dose did not exceed 300 Mrad. The radiation yield of radicals was determined according to the initial slope of the curve of accumulation of radicals. The accuracy of the determination of G_r was about 20%.

To determine the stability of the coolants in the liquid phase, they were irradiated by mixed (n, γ) radiation at 50°C in evacuated and sealed quartz ampules. The irradiation intensity was 35 Mrad/h, and the total dose reached 7000 Mrad. The radiation chemical yield of the high-boiling product (HB products) was determined according to their content in the liquid phase with an accuracy of 5%. The HB products

were isolated by simple vacuum redistillation. Their molecular weights were determined by a cryoscopic method in freon-112, with an accuracy of 1%. The radiation chemical yield of the HB products was determined as the number of molecules of the starting material converted to HB products per 100 eV of absorbed energy.

RESULTS OF THE MEASUREMENTS

The results of the measurements are summarized in the table.

If M is the maximum molecular weight of the HB product, determined experimentally, while m is he molecular weight of the initial molecule, then $n = M/m$ is the number of monomer units in the molecule of the HB product. Then the yield of radicals in the liquid phase can be determined as $[G_r]_{liq} = (G_{h.b}/n) \cdot 2$. The table presents the molecular weights of the HB products, extrapolated to a zero value of the absorbed energy, for compounds 1-3. Since extrapolation of $G_{h.b}$ and M to zero dose of absorbed energy was impossible for the literature data, the table gives the maximum molecular weight of the HB product for compounds 4-11. It should be mentioned that in the estimates cited, the possible contribution of ionic-molecular processes and reactions with excited molecules, leading to the formation of HB products, is not taken into consideration.

As can be seen from Fig. 1, in the case of irradiation of gas oil, hydroterphenyl, and monoisopropyldiphenyl by electrons, the radical concentration increases as a linear function of the dose. In the irradiation of monoisopropyldiphenyl a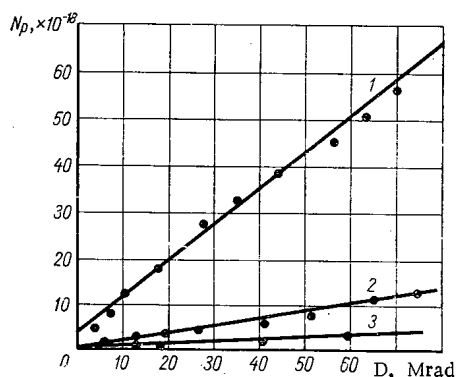nd hydroterphenyls in a nuclear reactor, the accumulation of HB products is also a linear function of the dose all the way up to 7000 and 4500 Mrad, respectively. In the case of gas oil, on the other hand, the rate of accumulation of HB products slows down as the dose increases (Fig. 2) [1]. Figure 3 presents the dependence of the molecular weight of the HB products isolated from irradiated coolants on the irradiation dose.

Fig. 1. Accumulation of radicals in electron irradiation at−170°C: 1) gas oil; 2) hydroterphenyl; 3) monoisopropyldiphenyl.

DISCUSSION OF RESULTS

As follows from a comparison of the values of G_r characterizing the radiation stability at low temperature, in the series monoisopropyldiphenyl — hydroterphenyl — gas oil the stability drops, which is due to the chemical nature of the substances. The yield of radicals in gas oil ($G_r = 1.3$) is close to the yield of the radicals in aliphatic compounds, while for monoisopropyldiphenyl and hydroterphenyls (G_r equal to 0.1 and 0.3, respectively), it is close to the yields of radicals in alkylated aromatic compounds [3, 4]. The radiation stability of these substances in the liquid phase, determined according to $G_{h.b}$

Comparison of Yields of HB products of Various Compounds with Yields of Radicals and Molecular Weights of HB Products

| Item No.	Compound	$[G_r]_{sol}$, T_{form} = −130 to −170°C	T_{form}, °C	m	M	n	$G_{h.b}$	$[G_r]_{sol}$ = $(G_{h.b}/n) \cdot 2$	$[G_r]_{liq} / [G_r]_{sol}$
1	Hydroterphenyls	0.3	50	221	480	2	0.46	0.46	1.5
2	Gas oil	1.3	50	199	420	2	2.9	2.9	2.2
3	Monoisopropyldiphenyl	0.1	50	198	420	2	0.4	0.4	4
4	Benzene	0.15[12]	30	78	530	7	0.75[11]	0.22	1.5
5	Toluene	0.22[4]	30	92	395	4	1.28[13]	0.64	3
6	Isopropylbenzene	0.35[4]	37	120	350	3	1.7[14]	1.13	3
7	Para-xylene	0.35	-80	110	230	2	0.43[15]	0.43	1
8	Para-xylene	0.35	20	110	300	3	1.10[15]	0.73	2
9	Para-xylene	0.35[4]	110	110	300	3	1.17[15]	0.77	2
10	Terphenyl (average for three isomers)	0.015[12]	30	230		−	2	0.05[16]	0.05	3
11	Terphenyls	0.015[12]	330	230		−	2	0.06[17]	0.06	1
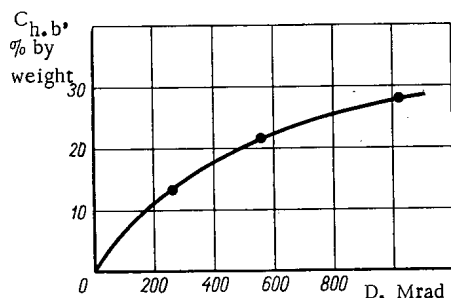
Fig. 2

Fig. 3

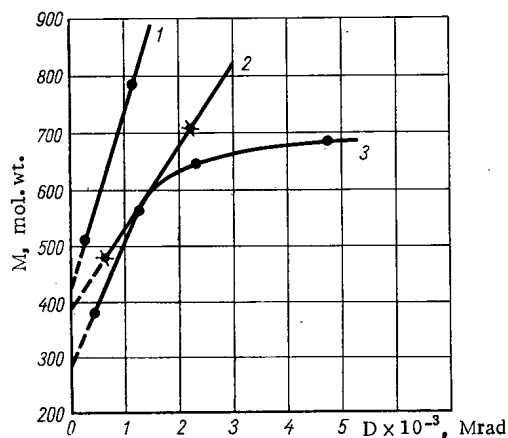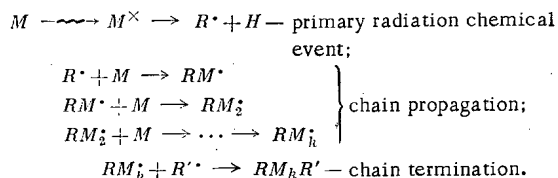Fig. 2. Dependence of the content of HB products in gas oil on the irradiation dose in the reactor at 50°C.

Fig. 3. Dependence of the molecular weight of HB products on the irradiation dose at 50°C: 1) gas oil; 2) monoisopropyldiphenyl; 3) hydroterphenyl.

(see table), also increases in the transition from monoisopropyldiphenyl and hydroterphenyl ($G_{h.b}$ equal to 0.35 and 0.46, respectively) to gas oil ($G_{h.b} = 2.9$).

A comparison of the values of G_r and $G_{h.b}$ shows that the yields of the HB products in the liquid phase are close to the yields of radicals in the solid phase, and that larger G_r corresponds to larger $G_{h.b}$. This correlation of the changes in the values G_r and $G_{h.b}$ for compounds of different classes permits us to assume that the initial yield of radicals in the liquid and solid phases is almost the same. Thus, on the basis of the radiation stability of the substance at low temperature, we can estimate the yields of HB products in the liquid phase.

We were interested in comparing the radiation yields of radicals in the solid phase, known from the literature, and the yields of HB products in the liquid phase (see table, compounds 4-11). The table presents these data, as well as the results of their comparison for the three coolants investigated and several individual aromatic compounds. In estimating the yields of radicals in the liquid phase according to the yield of HB products, it is necessary to take into consideration certain peculiarities of aromatic compounds. It is known that in the usual chemical reactions [5-7] and radiation chemical transformations [8], aromatic rings are strong acceptors of atoms and radicals arising in the course of this reaction. On this basis, it is proposed in [9, 10] that the formation of HB products occurs by successive addition of molecules of the starting material to the radical according to the scheme

$$M \longrightarrow M^X \longrightarrow R\cdot + H - \text{ primary radiation chemical event;}$$

$$\left.\begin{array}{l} R\cdot + M \longrightarrow RM\cdot \\ RM\cdot + M \longrightarrow RM_2^* \\ RM_2^* + M \longrightarrow \cdots \longrightarrow RM_h^* \end{array}\right\} \text{chain propagation;}$$

$$RM_h^* + R'\cdot \longrightarrow RM_h R' - \text{ chain termination.}$$

Thus, two radicals are consumed for the formation of a molecule of an HB product consisting of $n = k + 2$ units: one to initiate the chain, the other for its termination.

As can be seen from the data cited in the table, the ratio $[G_r]_{liq}/[G_r]_{sol}$ is 1-4, i.e., considering the extremely approximate nature of the calculation, in practice

$$[G_r]_{liq} \approx [G_r]_{sol}.$$

However, the fact that for all the cases cited $[G_r]_{liq} > [G_r]_{sol}$ evidently is an indication of the contribution of nonradical processes to the formation of the HB products. It may be that dimer products are formed both in the recombination of radicals, and in reactions of excited molecules.

32

LITERATURE CITED

1. Yu. N. Aleksenko et al., in the Collection: Investigations of the Use of Organic Coolant-Moderators in Energy Reactors [in Russian]. Moscow, Atomizdat, p. 78 (1964).
2. Yu. N. Molin et al., Pribory i Tekhnika Éksperimenta, No. 6, 73 (1960).
3. Yu. N. Molin et al., Kinetika i Kataliz, 2, 192 (1961).
4. Yu. N. Molin et al., Kinetika i Kataliz, 3, 674 (1962).
5. K. Geib and P. Harteck, Berichte, 66, 1815 (1933).
6. M. Levy and M. Szwarc, J. Amer. Chem. Soc., 77, 1949 (1955).
7. L. I. Avramenko et al., Izv. AN SSSR, Otd. Khim. Nauk, 11, 2079 (1962).
8. A. J. Swallow, Radiation Chemistry of Organic Compounds, Pergamon, N.Y. (1963).
9. S. Gordon, A. Van Dyken, and T. Doumani, J. Phys. Chem., 62, 20 (1958).
10. M. Eberhardt, J. Phys. Chem., 67, 2856 (1963).
11. W. Patrick and M. Burton, J. Amer. Chem. Soc., 76, 2626 (1954).
12. I. I. Chkheidze et al., Dokl. AN SSSR, 130, 1291 (1960).
13. R. Heutz and M. Burton, J. Amer. Chem. Soc., 73, 532 (1951).
14. R. Heutz, J. Phys. Chem., 66, 1622 (1962).
15. D. Verdin, J. Phys. Chem., 67, 1263 (1963).
16. E. Colichmann and R. Gercke, Nucleonics, 14, No. 7, 50 (1956).
17. E. Colichmann and R. Fisch, Nucleonics, 15, No. 2, 72 (1957).

DECOMPOSITION OF URANYL CHLORIDE AND ITS INTERACTION
WITH URANIUM DIOXIDE IN MOLTEN NaCl — KCl

M. V. Smirnov, V. E. Komarov,
and A. P. Koryushin

UDC 621.039.543.4

The thermal decomposition of uranyl chloride and its interaction with uranium dioxide in a chloride melt of NaCl — KCl was investigated. It was demonstrated that the decomposition products of uranyl chloride and the products of its interaction with uranium dioxide are uranium octoxide and tetrachloride. An explanation was given for the nonstoichiometry of the cathodic deposits of uranium dioxide produced in the electrolysis of chloride melts containing uranyl ions.

It is known that uranium dioxide can be used as a nuclear material for the preparation of fuel elements. One of the promising methods for producing the crystalline dioxide is the electrolysis of chloride melts containing uranyl ions; in this case a deposit whose density and stoichiometric composition are close to UO_2 is obtained at the cathode. Inasmuch as the process of electrolysis is carried out at comparatively high temperatures (450-850°C), the question of the thermal stability of uranyl chloride under these conditions, as well as that of the nature of the interaction of uranium dioxide with the electrolyte, must be resolved.

Wilks [1] believes that uranyl chloride dissolved in a molten mixture of sodium and potassium chlorides is partially decomposed into uranium octoxide and gaseous chlorine, while in [2] it was shown that the decomposition results in the formation of uranium dioxide and chlorine. The information on the interaction of uranium dioxide with a chloride melt containing uranyl ions is just as contradictory. Some authors [1] assert that uranium dioxide is enriched with oxygen in such melts and approaches the composition $UO_{2.02-2.23}$, while Adams [3] on the basis of spectral measurements and Stromatt [4] from an analysis of cathodic and anodic chronopotentiograms concluded that UO_2 interacts in molten chloride with UO_2Cl_2, resulting in the formation of a compound of pentavalent uranium UO_2Cl.

As was shown earlier [5], the electrode potential of uranium dioxide in molten chlorides of the alkali metals, containing uranyl ions, is more electronegative than the chloride reference electrode by ~0.6 V. This is evidence that the equilibrium pressure of chlorine above the melt will already be substantial (~ 10^{-6} atm). Consequently, if the partial pressure of chlorine in the gas phase is somehow reduced (evacuation of the cell, purging of chlorine with inert gas or its absorption by acid metals), then the reduction of hexavalent uranium to the lower valence forms may be expected in the melt. In this case, the redox potential of the system will decrease, which may be ascertained with the aid of an indicator electrode that is indifferent to the investigated melts. An analysis of the reduction products makes it possible to investigate the reactions that occur in this process.

The most stable oxygen compound of uranium at temperatures up to 1000°C is the octoxide [6]. It was of interest to determine how far this is correct for molten salts containing uranyl chloride and uranium dioxide. This work was devoted to a study of these questions. A molten equimolar mixture of sodium and potassium chlorides was investigated within the interval 750-850°C.

DESCRIPTION OF EXPERIMENT

A salt mixture of NaCl — KCl was prepared according to the method described in [5]. The molten salt was additionally purged with purified helium. The helium was freed of traces of water and oxygen by repeated passage over phosphoric anhydride and metallic calcium, heated to 780°C. The solution of uranyl chloride was prepared by chlorination of the octoxide, prepared from chemically pure uranyl carbonate, with gaseous chlorine in a molten mixture of NaCl and KCl. Uranium dioxide was produced at 750°C on a platinum cathode from an electrolyte containing 20% UO_2Cl_2, 10% UCl_4, and 70% NaCl — KCl.

34

According to the data of x-ray diffraction study, the cathodic deposit was identified as $UO_{2.01\pm0.01}$, and as a result of an investigation by a polarographic method, as $UO_{2.005}$.

The measurements were performed in a hermetic quartz instrument, the design of which was similar to the instrument used in [5]. Before the experiment the cell was evacuated, then filled with purified helium. For the absorption of chlorine in the gas phase, uranium or zirconium shavings were placed in a quartz crucible, which was fastened to a platinum holder. The indicator electrode was a platinum wire. The potential was measured relative to a chloride reference electrode. After the experiment the soluble portion of the salt was analyzed for total uranium and reduced uranium. The precipitate formed during the experiment was subjected to x-ray diffraction study, and the ratio of oxygen to uranium (contained in this deposit) was determined by a polarographic method.

A series of experiments was conducted in which we investigated the cathodic polarization of platinum electrodes in the original melt and in a melt exposed in direct contact with uranium dioxide or with a metallic absorber of chlorine (zirconium shavings) in the gas space of the cell. The method of investigation is described in [7]. In the case when the gas medium above the melt was exposed to a metallic absorber of chlorine, the current was turned on only after the potential of the polarized electrode returned to its original value (± 0.01 V).

RESULTS OF THE MEASUREMENTS AND DISCUSSION

Figure 1 shows the variation of the potential of the indicator electrode after the introduction of uranium dioxide into a melt containing uranyl chloride, or when the chlorine pressure in the gas phase above the melt decreased; in the latter case, chlorine was absorbed by the metallic uranium.

During the first period, when the melt did not contain uranium dioxide and was at equilibrium with the gas phase, the potential of the platinum remained practically unchanged. This is evidence of stability of uranyl chloride in molten NaCl — KCl. If during the experiment uranium dioxide was introduced into the melt (without disturbing the hermetic sealing of the cell), then the electrode potential dropped at first rather sharply, and then monotonically; moreover, its value was close to the equilibrium value for the dioxide in melts of this composition [5].

Analogous changes in the platinum potential were also observed in the case when metallic uranium was placed in the hot portion of the gas space of the cell. However, the electrode potential was somewhat more positive than in the first case, even in the case of a longer experiment. The slow change in the platinum potential in both cases is evidently due to the kinetic peculiarities of the systems, which were not investigated in this work.

During the experiments (both series), a black crystalline deposit precipitated onto the walls of the crucible with the melt. X-ray diffraction and polarographic analyses demonstrated that its composition depended upon the conditions of the experiment. In all the experiments it was determined as a phase intermediate between UO_2 and U_3O_8.

After exposure to zirconium dioxide or a gas phase containing metallic uranium or zirconium at the temperature of the experiment, the melts changed color from lemon yellow to grayish green. Chemical analysis demonstrated that such melts contain reduced forms of uranium. Their concentration reached 3-7% of the total amount of uranium in the melt.

The results of the polarization measurements are presented in Fig. 2. As can be seen (curve 1, Fig. 2), the deposition of the uranium dioxide on the cathode is preceded by a process characterized by
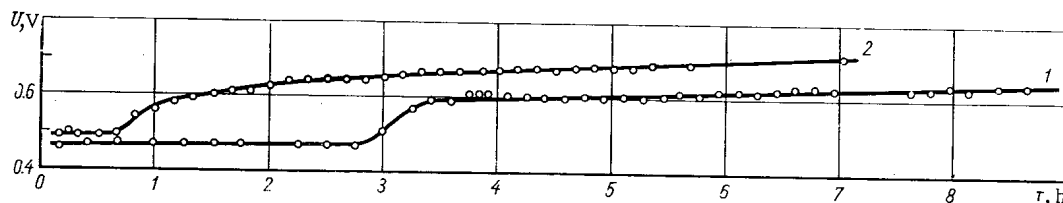

Fig. 1. Variation of the potential of a platinum electrode in the reduction of a NaCl — KCl melt, containing 7% by weight UO_2Cl_2, at 777°C: 1) without addition of UO_2; 2) with addition of UO_2.
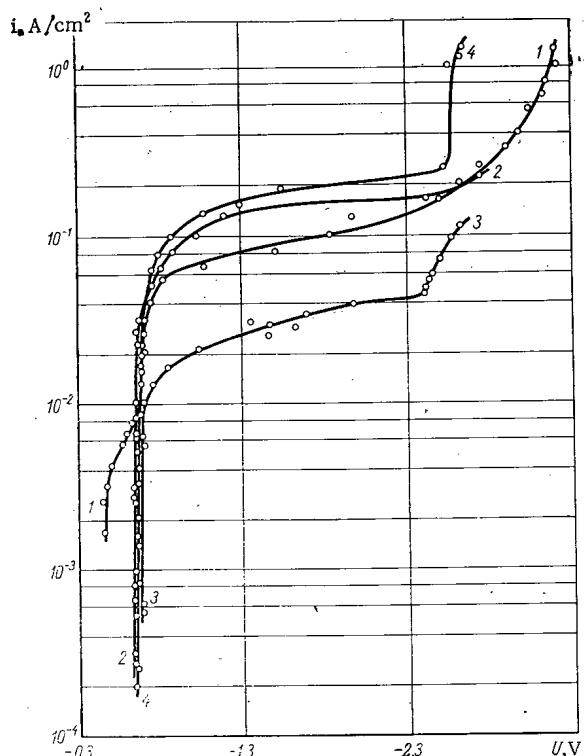
35

Fig. 2. Cathodic polarization of a platinum electrode in molten NaCl — KCl with initial UO_2Cl_2 content 7% by weight at 777°C: 1) UO_2Cl_2; 2) $UO_2Cl_2 + UO_2$; 3, 4) UO_2Cl_2 and $UO_2Cl_2 + UO_2$, respectively, kept in contact with a gas phase containing metallic zirconium.

Fig. 3. Oscillogram of the change in the potential of a platinum electrode after the current was turned off (the arrow indicates the wave of uranium).

a pronounced wave at a potential of –0.46 V. An analogous wave was observed in [7]. Moreover, it has been shown that it corresponds to charge exchange of the UO_2^{+2} ions to UO_2^+ [4]. With increasing current density, the electrode potential reached values corresponding to the equilibrium values for uranium dioxide under the conditions of this experiment. In those cases when uranium dioxide was introduced into the salt mixture NaCl — KCl — UO_2Cl_2, or metallic zirconium was introduced into the gas phase above the melt and held there for a long time, the melt was reduced, and the wave at —0.46 V did not appear (see curves 3 and 4 in Fig. 2). The initial platinum potential was close to the equilibrium value for uranium dioxide. With increasing current density, a sharp point of inflection was observed on the curves of φ versus log i, in the direction of an increase in the current, at potentials of -2.4 to -2.6 V. It was shown earlier [7] that at such potentials, metallic uranium is deposited at the cathode in chloride melts. Figure 3 presents as an example a turnoff oscillogram (the variation of the cathode potential after removal of the polarizing current). A portion corresponding to the dissolution of uranium at potentials close to equilibrium is clearly visible on it [8]. The data of these experiments indicate that one of the decomposition products of uranyl chloride in the melt is the uranium ion U^{+4}, since chloride compounds of uranium where its valence is higher than 4 are thermodynamically unstable at the temperatures of our experiments [9].

The experimental data obtained show that when chlorine is removed from the gas phase above chloride melts containing UO_2Cl_2, the following reaction may occur in the melts:
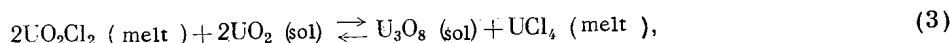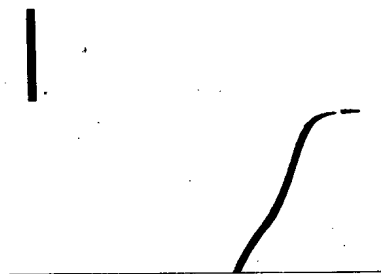
$$4UO_2Cl_2 \text{ (melt)} \rightleftarrows U_3O_8 \text{ (sol)} + UCl_4 \text{ (melt)} + 2Cl_2 \text{ (gas)}, \tag{1}$$
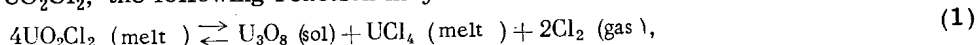
which, as follows from the thermodynamic calculation, is more probable than the reaction

$$UO_2Cl_2 \text{ (melt)} \rightleftarrows UO_2 \text{ (sol)} + Cl_2 \text{ (gas)}. \tag{2}$$
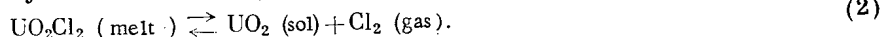
The deviation of the composition of the oxide deposits from U_3O_8 observed in our experiments is evidently due to the fact that the residual pressure of chlorine in the gas phase was below the equilibrium value according to reaction (1) and insured more profound reduction according to reaction (2).

The interaction of uranium dioxide with uranyl chloride melts may be described by the reaction

$$2UO_2Cl_2 \text{ (melt)} + 2UO_2 \text{ (sol)} \rightleftarrows U_3O_8 \text{ (sol)} + UCl_4 \text{ (melt)}, \tag{3}$$

the constant of which

$$\log K = 2.24 - \frac{5600}{T}$$

36

and is equal to $6 \cdot 10^{-4}$ at 750°C. This means that in a chloride melt at equilibrium with a mixture of uranium dioxide and uranium octoxide, the bulk of the uranium is in the hexavalent state. However, the concentration of tetravalent uranium also becomes appreciable.

It is quite possible that at the first stage of the reduction of UO_2Cl_2 through the gas phase and its interaction with UO_2 in chloride melts, pentavalent uranium is formed. However, under these conditions, when its concentration reaches the equilibrium value, it may be disproportionate to U_3O_8 and UCl_4. On the other hand, with the accumulation of the equilibrium concentration of uranium tetrachloride, the interaction of its dioxide with uranyl chloride practically ceases, since reaction (3) is reversible. Actually, in the electrolysis of a chloride melt of uranium tetrachloride, to which the octoxide was added, a deposit whose composition was close to UO_2 precipitated at the cathode.

The formation of uranium octoxide in uranium containing chloride melts may be one of the causes of the deviation of the cathodic deposit of the dioxide from the stoichiometric composition. Actually, as can be seen from Fig. 2 (curve 1), on the cathode together with the deposition of the dioxide, there is the process of charge exchange of UO_2^{+2} to UO_2^{+}, the fraction of which depends upon the cathodic current density. If there is no tetravalent uranium in the melt, then we should expect a disproportionation reaction:

$$4UO_2Cl_2 \,(\text{melt}) \rightleftarrows U_3O_8 \,(\text{sol}) + UCl_4 \,(\text{melt}). \qquad (4)$$
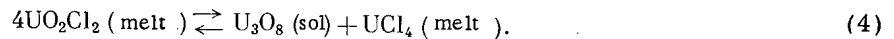
Evidently this reaction will occur until the equilibrium concentration of uranium tetrachloride for the given conditions has accumulated in the system.

LITERATURE CITED

1. R. Wilks, J. Nucl. Materials, 7, 157 (1962).
2. D. Wenz et al. Inorg. Chem., 7, 989 (1964).
3. M. Adams et al. J. Phys. Chem., 67, 1939 (1963).
4. R. Stromatt, J. Electrochem. Soc., 110, 107 (1963).
5. M. V. Smirnov and O. V. Skiba, Transactions of the Institute of Electrochemistry, Ural Affiliate, Academy of Sciences of the USSR [in Russian], No. 4, 3 (1963).
6. J. Katz and E. Rabinovich, The Chemistry of Uranium [Russian Translation], Moscow, Izv. Inostr. Lit., (1964).
7. M. V. Smirnov and I. V. Skiba, Transactions of the Institute of Electrochemistry, Ural, Affiliate, Academy of Sciences of the USSR [in Russian], No. 4, 17 (1963).
8. O. V. Skiba and M. V. Smirnov, Transactions of the Institute of Electrochemistry, Ural Affiliate, Academy of Sciences of the USSR [in Russian], No. 2, 3 (1961).
9. D. Hill et al. J. Electrochem. Soc., 107, 698 (1960).

MEASURING THE MEAN LIFETIME OF THERMAL
NEUTRONS FROM A SMALL SPECIMEN

V. V. Miller

UDC 539.125.525:550.3

The author describes a method of measuring the mean lifetime τ of thermal neutrons for specimens whose dimensions are commensurate with the thermal transport length. The method makes use of a pulsed neutron generator and is intended for determining τ for rocks by means of measurements on core samples. It can also be used to estimate the concentrations in rocks of elements with large thermal-neutron absorption cross sections.

At the present time, neutron methods are being widely adopted in nuclear geophysics in the Soviet Union and elsewhere [1-5]. For a quantitative interpretation of the results of these methods when used to estimate mineral concentrations, we must know the neutron characteristics of rocks, in particular the mean lifetimes τ of thermal neutrons.

In this connection the problem has arisen of determining τ from measurements on core samples taken from boreholes. The dimensions of these samples are of the order of a few centimeters, i.e., comparable with the thermal transport lengths of neutrons in rocks. The measurements must be made without breaking up the cores, because, owing to nonuniform distribution of elements with large absorption cross-sections for thermal neutrons, the macroscopic absorption cross section depends not only on the mean chemical composition but also on the shapes and sizes of the inhomogeneities, owing to the self-screening effect. For such large specimens we cannot use the usual methods to determine neutron cross sections in a beam of thermal neutrons, because it is difficult to allow for multiple scattering. On the other hand, the cores are too small for us to use the usual experimental methods of determing the neutron diffusion parameters of the substance. For example, in the method of "non-stationary diffusion" [6-8] the dimensions of the system must be more than 7-10 times the transport path lengths for thermal neutrons. For measurements by stationary methods we need an even greater quantity of material. Below we shall discuss one of the possible methods of finding τ when the specimen has dimensions of the same order as the thermal transport length.

THEORY

Principle of the Method.

The method is based on the disturbing effect of the specimen, when it is placed in a moderator of finite dimensions, on the logarithmic decrement of the thermal neutron density in a system irradiated by pulses of fast neutrons. If the dimensions of the moderator are sufficiently great, then, some time after a burst of neutrons, an equilibrium, nearly thermal, neutron spectrum is established in the system. For this reason, the absorption of neutrons in the specimen will be the same as if it were in an infinite medium.

Since the moderator flattens out the neutron field in the specimen, the latter's scattering properties have little effect on the logarithmic decrement of neutrons in the system. Therefore, for a given moderator, the logarithmic decrement varies mainly with the specimen's absorption properties. We measure this relation for standard specimens and construct a calibration curve, which we use to determine τ for our unknown specimens. The indeterminacy in their scattering properties will introduce additional errors in the measured value of τ. However, if the scattering properties of the standards are similar to those of the samples, this error will be small, and can be even further reduced by appropriate selection of the moderator dimensions.

The accuracy with which τ is found depends on the closeness of the relation between the logarithmic decrement of the neutron density and the value of τ, and also on the statistical accuracy with which the decrement is measured. The result is that there is an optimum moderator which enables us to measure τ with minimum error.

Selection of Moderator.

To choose an optimum moderator, we made a theorectical study of the problem of nonstationary diffusion of thermal neutrons in a system consisting of a spherical sample placed inside a spherical sheath (moderator). We found a solution for the thermal-neutron density in the form of a sum of harmonics which decrease exponentially with time; each harmonic has its own logarithmic decrement α_n. The values of α_n depend on the dimensions and neutron properties of the system. They are the roots of a transcendental equation, which was solved by means of a computer for the cases of moderators made of light and heavy water, graphite, and beryllium. In each case the neutron parameters and the sample dimensions, and also the moderator dimensions, were varied over wide ranges. We calculated the logarithmic decrements of the first three harmonics α_1, α_2, α_3. The calculations revealed the possibility of isolating the fundamental harmonic with logarithmic decrement α_1, for all the cases when the delay times are relatively short and α, depends slightly on the specimen's scattering properties: this dependence practically vanishes when $\tau_1 \approx 1/\alpha_1$ (where τ_1 is the mean lifetime of thermal neutrons in the medium under study). Analysis of the results enabled us to select a moderator which would yield optimally accurate determinations of τ_1. This was found to be a moderator made of light water or of a substance with similar neutron properties. With a specimen of radius 2 cm, the optimum moderator radius is ~6 cm. If we allow for the fact that the conditions of isolating the fundamental harmonic deteriorate with increasing moderator dimensions, we see that the optimum radius should be somewhat smaller.

EXPERIMENT

Experimental Apparatus.

The pulsed fast-neutron source was a neutron generator of the evacuated type. It consisted of a 100 keV linear deuteron accelerator. The mean yield of 14 MeV neutrons was 10^7 neutr/sec.

The recording equipment was a scintillation detector with an FÉU-24 photomultiplier, a preamplifier, pulse shaper, and an AI-256, 256-channel time analyzer. The scintillator was a powered mixture of boron and zinc sulfide in a flat cassette.
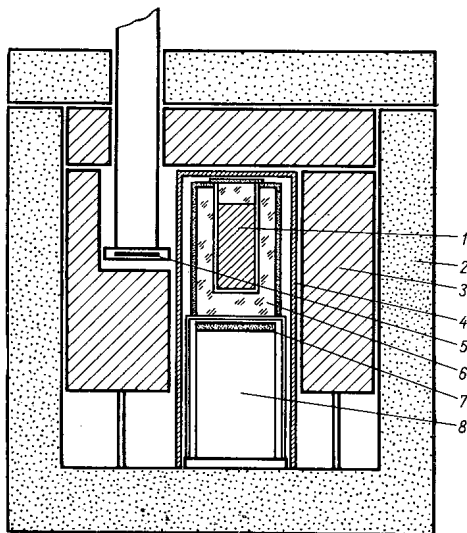

Figure 1 shows a general view of the equipment. The material and dimensions of the moderator were chosen in accordance with the calculated results on the choice of an optimum moderator. Since the cores were cylindrical, the moderator was also made cylindrical. The chosen moderator material was Plexiglas, which has neutron properties close to those of water. The diameter of the moderator was 8 cm and its height 12 cm. The diameter of the samples was 4 cm, and their height 8 cm. To increase the initial neutron density, the moderator was surrounded by a reflector, made of a mixture of paraffin and boron about 5 cm thick. The entire system with the neutron detector was enclosed by boron-cadmium screening.

Fig. 1. General view of equipment: 1) sample; 2) H_3BO_3; 3) paraffin + H_3BO_3; 4) cadmium; 5) target; 6) transparent plastic; 7) B + ZnS; 8) photomultiplier.

Measurement Procedure and Treatment of Experimental Results.

The pulse generator operated at 1000 Hz, the width of the ion pulse being 5 μsec. The channel width of the time analyzer was 4 μsec. The beginning of the measurements was delayed 60-200 μsec relative to the ion pulse. Figure 2 shows a characteristic n(t) curve obtained after subtracting
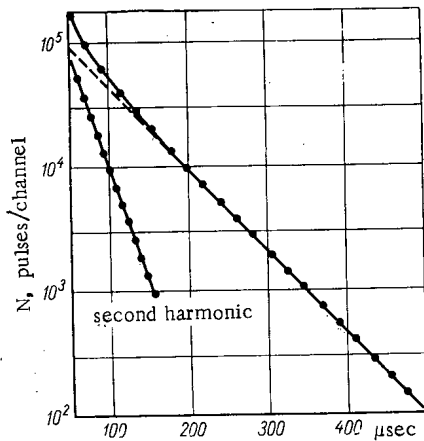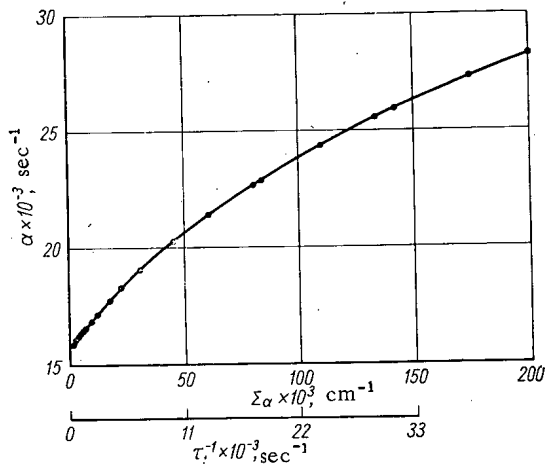
Fig. 2. Characteristic experimental curve of n versus t.

Fig. 3. Experimental calibration curve.

the background count. From 60 μsec onwards, this curve can be expressed as the sum of two exponentials:

$$n\,(t) = 1{,}8\mathrm{e}^{-16\cdot10^3 t} + 5{,}5\mathrm{e}^{-45\cdot10^3 t}$$

In this case the specimen characteristics were as follows: $\tau_1 = 3.10^{-3}$ sec, diffusion coefficient $D_1 = 5.5\cdot10^5\,\mathrm{cm}^2/\mathrm{sec}$. Here the amplitude of the second harmonic is three times greater than the amplitude of the first harmonic. The logarithmic decrements α_2 and α_1 stand in approximately the same ratio. At higher values of τ_1 the higher harmonics die out earlier. For $\tau_1 \leqq 100$ μsec, after 60 μsec practically only the fundamental is left. The amplitudes and logarithmic decrements of the higher harmonics vary markedly with D_1. When D_1 decreases, they make a smaller contribution for any given time t.

To determine α_1 from the experimental data, we estimated the effects of the higher harmonics and chose an interval on the (n, t) curve such that the error in it due to the higher harmonics would be half as great as the statistical error of α_1. The value of α_1 and its rms error were calculated by the usual statistical methods. The relative error in determining α_1 was 0.25-0.5%.

Calibration Curve.

To plot the calibration curve we prepared 30 standard specimens with values of τ_1 ranging from 23 to 38,000 μsec. They were made of a mixture of quartz sand with graphite and boric acid. The values of D_1 for the various specimens varied from $1.7\cdot10^5$ to $5.5\cdot10^5\,\mathrm{cm}^2/$ sec approximately. Figure 3 is the experimental graph of α_1 versus $1/\tau_1$. Within the experimental error, the values of α_1 for all the specimens characteristically lie on a single smooth curve, independent of D_1. The error in measuring α_1 was 0.4%.
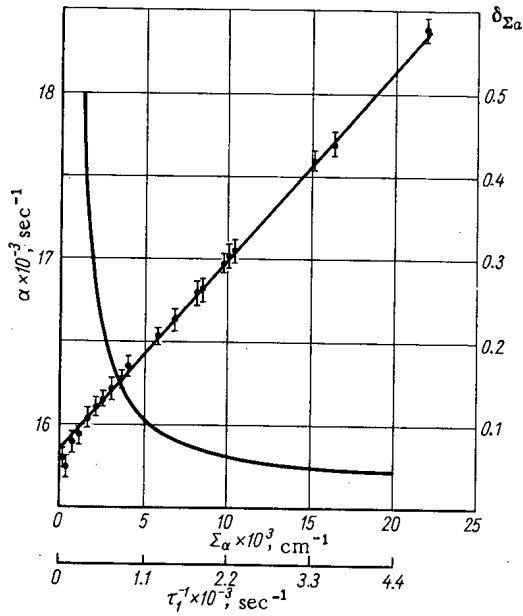
For measuring the neutron characteristics of rocks, the most interesting range of τ_1 is 200-3000 μsec. Figure 4 plots the results of measurements on the standard specimens in this range. It will be seen that in the range $\tau_1 \approx (200-3000)\cdot10^{-6}$ sec the experimental results are adequately represented by the linear relation

$$\alpha_1 = a + b\,(1/\tau_1).$$

On processing the data by the method of least squares we obtained

$$\left.\begin{aligned} a &= (15.86 \pm 0.03)\cdot10^3\ \mathrm{sec}^{-1}; \\ b &= 5.17 \pm 0.014. \end{aligned}\right\} \tag{1}$$

This treatment enables us to estimate the relative error of determination of τ_1 from the calibration curve when the standard error in an individual measurement of α_1 is σ:

$$\delta = \frac{1}{b}\sqrt{(\sigma_a^2 + \sigma^2)\,\tau_1^2 + \sigma_b^2}\,, \tag{2}$$

where σ_a and σ_b are the standard deviations of a and b. By (2) and (1) we plotted δ versus $1/\tau_1$. This curve is shown in Fig. 4. Here $\sigma^2 = 1.6\cdot10^3\ \mathrm{sec}^{-2}$, which corresponds to a relative error of about 0.3% in this interval. With this error in an individual measurement, the relative error of determination of τ_1 is 10% when $\tau_1 = 1$ μsec. It should be noted that (2) is not exact, as it was derived on the assumption that α_1 varies linearly with $1/\tau_1$. It can be used to estimate the error in a limited interval of τ_1 where the $(\alpha_1, 1/\tau_1)$ curve is nearly linear. Outside such an interval (2) is not valid.

40

Fig. 4. Calibration curve and relative error of determination of τ_1 ($\delta_{\tau_1} \equiv \delta_{\Sigma_a}$).
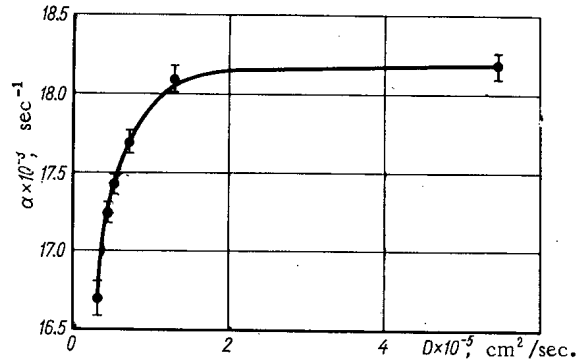

Fig. 5. Experimental graph of logarithmic decrement of fundamental harmonic of neutron density in specimen-moderator system versus scattering power of specimen.

Relation between α_1 and D_1.

Figure 5 plots the experimental α_1-D_1 curve. Specimens with various values of D_1 were prepared from mixtures of heavy and light water. All specimens had the same τ_1 (210 μsec), obtained by adding appropriate amounts of boric acid. The specimen with $D_1 = 5.5 \cdot 10^5$ cm^2/sec was prepared from quartz sand. From the graph it will be seen that in the range $D_1 \approx (1.7-5.5) \times 10^5$ cm^2/sec the variation of α_1 with D_1 is negligible within the experimental error. This explains why the α_1 values of all the standard specimens were found to lie on a single calibration curve.

Testing the Method.

We measured the values of τ_1 for several cores taken from oil wells in Tatariya and also measured τ_1 for samples of the material composing the models of the beds on which the neutron methods had been tested. We also made measurements on specimens with various cinnabar concentrations in quartz sand to estimate the available sensitivity and accuracy of determination of the concentration of cinnabar in a rock. The measurement results are given in Table 1; for comparison, this table also gives results calculated from chemical-analysis data.

In making the measurements, the cores were first extracted and machined to the dimensions of the standard specimens. For all the specimens we obtained satisfactory agreement between the experimental results and the chemical analysis data: the only exception was the specimen of Lyubertsy sand. This specimen may perhaps contain microimpurities of absorbent elements which were not detected in the chemical analysis.

The concentration of cinnabar uniformly distributed in SiO$_2$ was calculated from the formula

$$C = \frac{\Sigma_a - \Sigma_{a\,SiO_2}}{\Sigma_{a\,HgS} - \Sigma_{a\,SiO_2}} \cdot 100\%, \qquad (3)$$

where Σ_a are the measured values and Σ_{aSiO_2} and Σ_{aHgS} are values calculated from the neutron cross sections of the corresponding elements. Table 2 gives the concentrations calculated from (3) and those found experimentally. Here we also give the errors of determination of the concentrations.

With measurements of the given accuracy, the sensitivity to the cinnabar content of SiO$_2$ is about 0.05%.

TABLE 1. Values of τ for Various Specimens

Medium	$\Sigma_a, \times 10^3$ c.м$^{-1}$		τ_{exp} (μsec)
	Calculated	Experimental	
SiO$_2$+0.028% HgS	2.52	2.7±0.5	1680±330
SiO$_2$+0.056% HgS	2.93	3.0±0.5	1540±300
SiO$_2$+0.11% HgS	3.76	3.6±0.4	1260±150
SiO$_2$+0.22% HgS	5.42	5.8±0.5	780±70
SiO$_2$+0.5% HgS	10.4	9.8±0.7	460±50
Core No. 1(limestone)	5.95	6.0±0.7	760±80
Core No. 2(limestone)	6.3	5.7±0.7	800±100
Core No. 5(limestone)	6.3	6.0±0.7	760±80
Lyubertsy sand, ρ=1.64 g/cm^2	2.16	3.1±0.4	1460±170
Silicate brick, ρ = 1.9 g/cm^2	9.1	9.4±1	485±50

41

TABLE 2. Measured Cinnabar Contents of Various Specimens

True cinnabar concentration, %	Experimental values of cinnabar concentrations calculated from (3), %
0.028	0.03± 0.03
0.056	0.05± 0.03
0.11	0.09± 0.02
0.22	0.24± 0.03
0.55	0.51± 0.05

We made measurements on specimens of quartz sand in which boric acid and cinnabar were nonuniformly distributed. The boric acid was distributed as fine layers in the specimen (its mean concentration was one percent). From the measurements we obtained the following values for τ_1: with uniform distribution $\tau_1 = 336 \pm 12\,\mu$sec; for four layers $\tau_1 = 296 \pm 16\,\mu$sec; for two layers $\tau_1 = 500 \pm 20\,\mu$sec.

The cinnabar was distributed in the specimen in the form of variously sized grains. For 1-mm grains, the cinnabar concentration calculated from the concentration measurements was one half as great as the true value; for 2-mm grains it was one fifth of the true value.

These results indicate that nonuniform distribution of elements with large thermal-neutrons absorption cross sections has an effect on the measured values of τ_1 and C.

The above work was carried out at the All-Union Research Institute for Nuclear Geology and Geophysics under the direction of Yu. S. Shimelevich. The author would like to thank E. A. Selin for performing the numerical calculations with a "Strela" computer, and also N. M. Arbuzov and Yu. F. Baryshev who helped with the experimental work.

LITERATURE CITED

1. Symposium: "Nuclear Geophysics", ed. by F. A. Alekseev. Moscow, Gostoptekhizdat (1959).
2. Symposium: "Nuclear Geophysics in Mineral Prospecting". Moscow, Gostoptekhizdat (1960).
3. Radioactive Isotopes and Nuclear Radiations in the National Economy of the USSR. Proceedings of All-Union Conference (Riga, 12-16 April, 1960). Vol. IV, Moscow, Gosatomizdat (1961).
4. Proceedings of Conference on the Peaceful Uses of Atomic Energy (Tashkent, November 1959). Izd. UzSSR (1960).
5. Symposium: "Portable Neutron Generators". Gosatomizdat, Moscow (1962),
6. I. M. Frank, Trudy FIAN, XIV, 117 (1962).
7. A. V. Antonov et al. In: "Proceedings of International Conference on the Peaceful Uses of Atomic Energy (Geneva, 1955)". Reports of Soviet scientists. Vol. 5, Moscow, Izd. AN SSSR (1958).
8. A. V. Antonov et al. Report FM 68/54 to International Symposium on Radioactive Devices in Industry and Geophysics (Cracow, October 1965). Vienna, IAAE (MAGATÉ) (1966).

ABSTRACTS

ACCELERATOR TUBES FOR HEAVY-CURRENT MACHINES

E. A. Abramyan and V. A. Gaponov

UDC 621.386.2

The authors describe certain features of tubes for the acceleration of high-current beams of charged particles. To get a beam of small cross section inside the tube use is made of a system of strong-focusing permanent magnets made of oxide-barium or other alloys. The magnets are small and their gas emission is negligible and does not impair the vacuum, at least in continuously evacuated tubes.

The diagram shows the construction of the tube of an ÉLT-1.5 accelerator [1] in which electrons are accelerated to 1.5 MeV with currents of up to 100 Ma and beam diameters of ~5 mm. The mean current in the tube was then 17 mA, and the average power ~25 kW. The axial component H_z of the magnetic field of the lenses changes sign along the tube axis (see the figure). The lenses are permanent magnets 4 made of barium ferrite, with pole pieces 5 having an aperture of 16 mm; the axial component of the lens field reaches 750 G, while the field of the lens nearest the injector is less by a factor of 1.5. To shield the tube insulation, gas gaps, and other electrically charged components from radiation arising near the tube axis, the tube contains screens 6 and 7 made of an alloy containing 90% lead.

The body of the tube is a continuous insulated tube. Potential separation is effected by metal rings 8 and 9, fed by an ohmic divider. The possibility of getting a high electric gradient along a continuous insulated tube is governed by the degree of success in constructing the junctions between the metal rings and the insulator. Several variant versions of these junctions suitable for insulators of epoxy resin or ceramic are given.
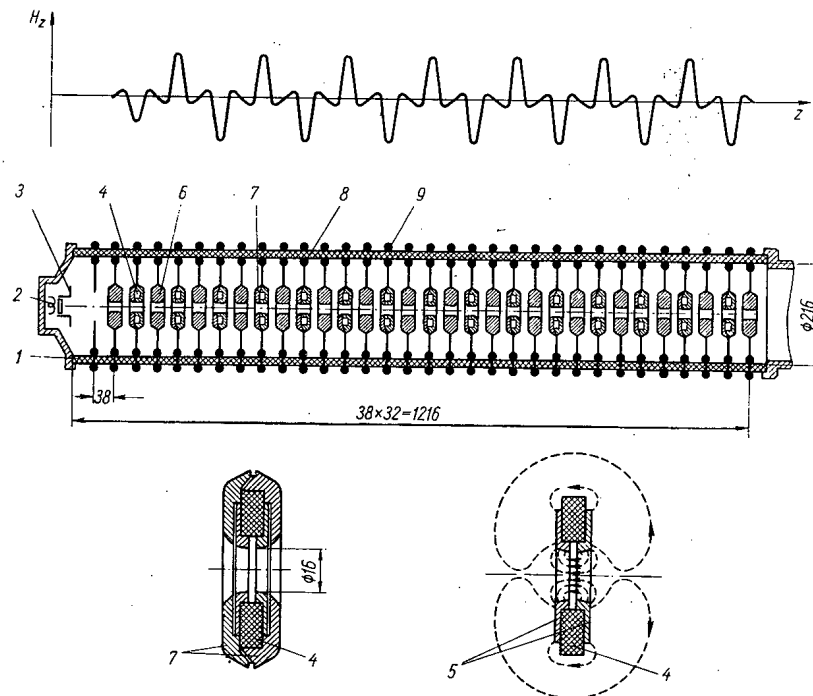
Fig. 1. Construction of tube of ÉLT-1.5 accelerator: 1) tube insulator; 2) injector; 3) injector control electrode; 4) focusing magnets; 5) magnet pole pieces; 6, 7) shielding screens; 8, 9) potential rings.

43

THE PROBLEM OF MAXIMUM REACTOR POWER

B. P. Kochurov and A. P. Rudik   UDC 621.039.50:621.039.517.5

The optimum distribution of fissionable material along a reactor channel $u(z)$ $(0 \leq z \leq H)$ to yield maximum power is determined subject to the heat-engineering restriction

$$p(x, u, v) \equiv ux^1 + \zeta x^3 - \varphi(z) + v = 0,$$

where $v \geq 0$, x^1 is the neutron density, $x^3 = \int_0^z ux^1 dz$, and $0 \leq u \leq u_0$. The parameter ζ depends on the geometry and on the thermal and physical properties of the materials; the function $\varphi(z)$ gives the maximum allowable temperature of the fuel or cladding and is supposed constant or monotonically decreasing.

In the one-group theory the vector $x = (x^1, x^2, x^3, x^4)$ is a solution of the system of equations

$$\dot{x}^1 = x^2; \quad \dot{x}^2 = -(ku-1)x^1; \quad \dot{x}^3 = ux^1; \quad \dot{x}^4 = 1, \quad \text{or} \quad \dot{x} = Ax + B.$$

The functional $W = \int_0^H ux^1 dz$ takes on its maximum value when the function $\mathscr{H} = \psi(Ax + B)$ is maximum with respect to the variables u and v at each point z, i.e., *

$$\frac{\partial \mathscr{H}}{\partial U} = \lambda \frac{\partial p}{\partial U} + \sum_i \nu_i \frac{\partial q_i}{\partial U}, \quad U = (u, v),$$

or

$$\lambda x^1 + \nu_1 - \nu_2 = x^1(1 + \psi_3 - k\psi_2), \quad \lambda \geqslant 0, \ \nu_1 \geqslant 0, \ \nu_2 \geqslant 0, \quad (1) \tag{1}$$

where $\lambda = 0$ for $v > 0$; $\nu_1 = 0$ and $\nu_2 = 0$ for $0 \leq u \leq u_0$. The function ψ must be continuous and satisfy the equation $\dot{\psi} = -\frac{\partial \mathscr{H}}{\partial x} + \lambda \frac{\partial p}{\partial x}$.

Analysis of condition (1) leads to the following result. If $\varphi(z)$ decreases rapidly enough, then $W = \varphi(H)/\zeta$, and at the reactor coolant outlet there must exist a region with $u = 0$ (in this case the conditions of transversality for ψ must be formulated in a special way so that $\psi_3(H) \leq 0$. If $\varphi(z)$ is constant or falls off sufficiently slowly, for example, $\max|\varphi(z)| \leq \varphi(z)\zeta(e^{\zeta H} - 1 - \zeta H)^{-1}$, the reactor is optimum when the regions $0 \leq z \leq h_1$ and $h_2 \leq z \leq H$ contain the maximum allowable concentration of uranium $u = u_0$ $(h_1 > H - h_2)$ while the central zone has a value given by the heat engineering limitation, i.e., $v = 0$. If φ is constant the ratio of the maximum power to the power corresponding to a uniform distribution of uranium lies within the limits $0 \leq (W_{max}/W_{uni}) \leq \frac{\pi}{2}$ depending on the values of ζ and u_0.

---

*Cf. L. S. Pontryagin et al. "Mathematical Theory of Optimum Processes," Moscow, Fizmatgiz, 1961, (Theorem 23).

A CORRECTION TO THE SPHERICAL-HARMONICS METHOD
FOR SOLVING THE TRANSPORT EQUATION

V. A. Zharkov, V. P. Terent'ev,
and T. P. Zorina

UDC 621.039.50

A solution of the one-velocity transport equation in spherical geometry by a modification of the spherical-harmonics method is discussed. Even in the lower P_N^{mod} approximations the accuracy is appreciably greater than in the ordinary P_N approximation. The results may be used to solve problems related to the behavior of localized absorbers in neutron fields.

The essence of the modification consists in taking into account the effects of the higher harmonics in the expansion of the solution in Legendre polynominals – the harmonics which are discarded in a given P_N approximation. A correction factor is introduced based on the use of a fictitious source of the form

$$U_N^{Fict}(r,\mu) = f_N(r) P_{N+1}(\mu),$$

Fig. 1

Fig. 2
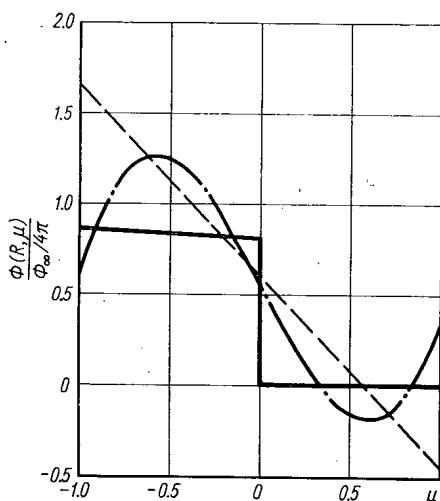
Fig. 1. The angular distribution of the neutron flux $\Phi(R,\mu)$ at the surface of a sphere placed in graphite (Φ_∞ is the value of the unperturbed neutron flux; negative values of μ correspond to directions into the sphere) – – – – ordinary P_1 approximation; – · – · ordinary P_3 approximation; —— modified P_1 approximation (on the scale used it is identical with the curve obtained in the modified P_3 approximation).
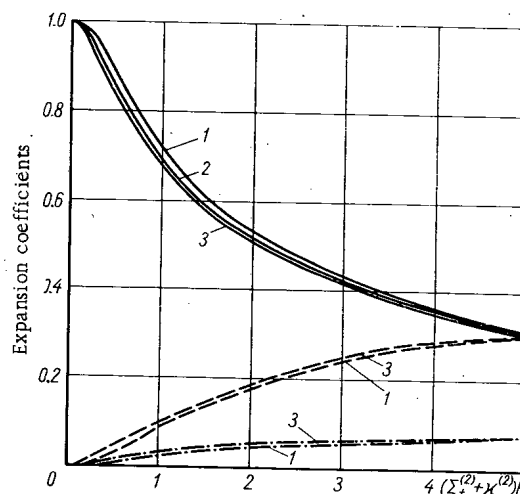
Fig. 2. Expansion coefficients of the function $\Phi(R,\mu)$ in a power series for a spherical absorber placed in graphite:

$$\text{——} \quad -\frac{\Phi(R,-1)}{\dfrac{\Phi_\infty}{4\pi}}; \quad \text{– – – –} \quad -\frac{\dfrac{\partial \Phi}{\partial \mu}(R,-1)}{\Phi(R,-1)};$$

$$\text{– · – · –} \quad -\frac{\dfrac{1}{2}\cdot\dfrac{\partial^2 \Phi}{\partial \mu^2}(R,-1)}{\Phi(R,-1)}; \quad 1-\Sigma_a^{(1)}=1 \text{ cm}^{-1}$$

$$2-\Sigma_a^{(1)}=3 \text{ cm}^{-1}; \ 3-\Sigma_a^{(1)}=\infty;$$

$$\varkappa = \sqrt{3\Sigma_a(\Sigma_a+\Sigma_{tr})}.$$

Subscript (1) refers to the absorber and subscript (2) to the surrounding medium; Σ_a and Σ_{tr} are respectively the macroscopic absorption and transport cross sections.

where r is the distance from the center of symmetry, μ the cosine of the angle between the direction from the center of symmetry and the direction of motion of the neutron:

$$f_N(r) = \frac{N+1}{2} \cdot \frac{d}{dr} \varphi_N(r) - \frac{N(N+1)}{2} \cdot \frac{\varphi_N(r)}{r},$$

where $\varphi_N(r)$ is the N$^{\underline{th}}$ expansion coefficient of the angular flux in terms of Legendre polynominals determined by solving the transport equation in the ordinary P_N approximation, and P_{N+1} is the Legendre polynominal of order N + 1.

A solution is investigated which is a superposition of an ordinary solution in the P_N approximation and of a solution corresponding to the fictitious source. The latter is given by the relation

$$\Phi^{(U_N)}(r, \mu) = \int_0^\infty \exp\left[-\int_0^l \Sigma_t \left(\sqrt{r^2 + y^2 - 2ry\mu}\right) dy \right] f_N\left(\sqrt{r^2 + l^2 - 2rl\mu}\right) P_{N+1}\left(\frac{r\mu - l}{\sqrt{r^2 + l^2 - 2rl\mu}} \right) dl,$$

where Σ_t is the total macroscopic cross section.

Angular distributions of the neutron flux for spherical absorbers having various absorption and scattering cross sections placed in various diffusion media were calculated on a BÉSM - 2 computer. It was found that the error in the angular distribution of the neutron flux at the surface of an absorber amounted to a few percent in the modified P_1 - approximation, and that the calculational procedure was rather simple and did not require a large amount of machine time.

Figure 1 shows the angular distribution of the neutron flux at the surface of a sphere of radius 1 cm with $\Sigma_t = \infty$ placed in graphite.

An approximate analytic expression, in the form of a Taylor series in powers of $\mu + 1$ about the point $\Phi(R, -1)$, for the inwardly directed angular neutron flux $\Phi(R,\mu)$ on the surface of an absorber is presented and discussed.

Figure 2 shows the coefficients in the expansion of the angular neutron flux in a power series for a spherical specimen in graphite.

The modification of the spherical-harmonics method developed in this article may also be used for systems with any geometry.

ACTIVATION OF SPHERICAL SPECIMENS IN A
THERMAL NEUTRON FIELD

V. A. Zharkov and V. P. Terentév

UDC 539.172.4

The problem of neutron-induced activity has many important practical applications: the production of radioactive isotopes in nuclear reactors, activation analysis, the measurement of neutron fluxes, etc. The main difficulty in calculating the activity of specimens irradiated in a diffusion medium has to do with the description of the perturbation of the neutron flux incident on the specimen. The theory of neutron activation for foils, which correctly takes into account the effect of the perturbation of the flux, has been worked out in considerable detail, see e.g., [1]. However, an analogous theory for "three-dimensional" specimens such as spheres or cylinders, while of great practical interest, cannot be regarded as complete.
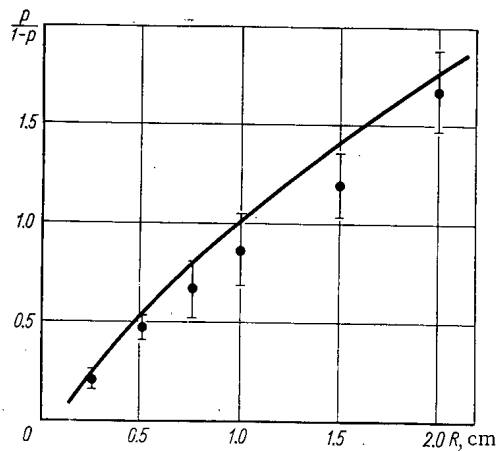
Fig. 1. The quantity p/(1-p) as a function of the radius of the specimen, R, for water. ——) analytic expression; •) Monte-Carlo method.

Relations are obtained in the present article for calculating the activity of three-dimensional specimens irradiated by thermal neutrons, taking into account both the effect of self-shielding and the effect of the perturbation of the flux by the specimen: for example, a sphere. The effect of the flux perturbation is described in terms of the probability of back-scattering, calculated by the Monte-Carlo method, and also on the basis of a solution of the transport equation using the modified spherical-harmonics method [2].

It is shown that the relation for the number of neutrons captured per unit time, Q, by a three-dimensional specimen irradiated by thermal neutrons in a diffusion medium may, within a few percent, be written in the form

$$Q = \frac{\Phi S}{4} \Psi H,$$

where Φ is the unpertubed neutron flux, S the surface area of the specimen, Ψ the probability, averaged over the Maxwellian spectrum, of the absorption of neutrons in the specimen for isotropic incidence, taking into account self-shielding, and H the flux perturbation coefficient (H = $1/[1+\psi \, p/(1 - p)]$), p the probability of back-scattering, that is, the average probability that a neutron emitted isotropically from the specimen will return to the surface of the sphere after a series of collisions in the diffusion medium. The probability of back-scattering was calculated by the Monte-Carlo method for several directions of emission from the surfaces of spherical specimens of various radii irradiated in water. These data gave the probability, p, for isotropic emission. Values of the function Ψ which do not depend on the properties of the diffusion medium have been tabulated for specimens with absorption cross sections obeying the 1/v law. All numerical calculations were performed on a BÉSM - 2 computer.

A combination of the modified spherical-harmonics method and the back-scattering probability method is used to obtain an analytic expression for the function p/(1 - p) in ordinary water, heavy water, and graphite. The values of p/(1 - p) calculated by the Monte-Carlo method and from the analytic solution are in good agreement (cf. Fig. 1).

The buildup of activity with time for a specimen whose absorption cross section obeys the 1/v law is also discussed.

LITERATURE CITED

1. R. Ritchie and H. Eldridge, Nucl. Sci. and Engn., 8, 300 (1960).
2. V. A. Zharkov, V. P. Terent'ev, and T. P. Zorina, present issue, p. 45.

47

GENERALIZATION OF THE ALBEDO METHOD

P. Wertesz   UDC 621.039.51.12

Albedo boundary conditions for a layer* are considered as integral operators of general form. The kernels of these operators are Green functions for the transport equation, i.e., if $\Phi^{\pm}(r, v, \Omega, v_0, \Omega_0)$ in the layer (r^+, r^-) satisfy the transport equation with the boundary conditions

$$\Phi^{\pm}(r_{B_0}^{\pm}, v, \Omega) = \delta(v-v_0)\,\delta(\Omega-\Omega_0), \quad \pm \pi_{B_0}\Omega > 0;$$

$$\Phi^{\pm}(r_{B_0}^{\mp}, v, \Omega) = 0, \quad \pm \pi_{B_0}\Omega < 0$$

where π_{B_0} is the normal to the boundary surface,

$$\Phi^{\pm}(r_{B_0}^{\pm}, v, \Omega) = B^{\pm}(v_0 \to v, \Omega_0 \to \Omega, d), \quad \pm \pi_{B_0}\Omega > 0;$$

$$\Phi^{\pm}(r_{B_0}^{\mp}, v, \Omega) = T^{\pm}(v_0 \to v, \Omega_0 \to \Omega, d), \quad \pm \pi_{B_0}\Omega < 0,$$

where $B^{\pm}(d)$ and $T^{\pm}(d)$ are reflection or transmission operators of layer d. If the layer d surrounds some medium, the boundary conditions for this medium may be written in the form

$$\varphi(r^{\pm}, v, \Omega) = \int dv' \int d\Omega' B^{\pm}(v' \to v, \Omega' \to \Omega, d)\,\varphi(r^{\pm}, v', \Omega'), \tag{1}$$

where $\pm \pi_{B_0}\Omega' > 0$, $\pm \pi_{B_0}\Omega < 0$.

The neutron distribution at the outside of the layer has the form

$$\varphi(r^{\mp}, v, \Omega) = \int dv' \int d\Omega' T^{\pm}(v' \to v, \Omega' \to \Omega, d)\,\varphi(r^{\pm}, v', \Omega') \text{ for } \pm \pi_{B_0}\Omega' > 0 \text{ and } \pm \pi_{B_0}\Omega > 0. \tag{2}$$

If the layer contains a neutron source $S(r, v, \Omega)$, to Eqs. (1) and (2) must be added the terms

$$\int dv' \int d\Omega' \int d\tau G^{\pm}(v' \to v, \Omega' \to \Omega, r, d)\,S(r, v', \Omega'),$$

where $G^{\pm}$ is the Green function for the transport equation with homogeneous boundary conditions. This operator may be called the source operator.

Formulas are presented for the addition of operators, i.e., the operators for a layer $d_1 + d_2$ are found in terms of the operators for the individual adjacent layers d_1 and d_2. It is shown that source operators may be expressed in terms of reflection and transmission operators.

For convenience in calculating, the operators are given in matrix form. The multigroup representation is used and expansions are made in terms of orthogonal spherical functions in the variables Ω and Ω'.

The results of the present work may be applied to the development of a computational method which is most effective in calculating multilayer systems. The generality of the formulation allows the use of any approximations in one layer independently of the others, since they are related only by the albedo operators. The method of obtaining these operators does not play an essential role.

In conclusion an example is presented of the analytical determination of the one-velocity albedo operators for a two-medium slab lattice by using the albedo operators for the component media.

---

*Cf. V. V. Orlov, "Neutron Physics," [in Russian], Moscow, Gosatomizdat, 1961, p.179.

LETTERS TO THE EDITOR

PARAMETRIC INSTABILITY ACCOMPANYING INTERACTION
OF A MODULATED BEAM WITH A PLASMA

V. D. Shapiro   UDC 533.9

Fainberg and Shapiro [1] showed the possibility of partial elimination of beam instability by density modulation of the beam. In this letter I consider another type of instability associated with parametric resonance. This instability arises from the interaction of a modulated beam with a plasma in the case when twice the modulation wavelength is a multiple of the plasma wavelength $2\pi (v_0/\omega_0)$.

As before [1], I shall consider the case when in the stationary state the beam is broken up into bunches with compensated charge, moving with constant velocity v_0 along the z axis. In this case, the beam particle density is given by the equations

$$n_0(\xi) = \begin{cases} n_{0B} & \text{when } sl < \xi < sl + a; \\ 0 & \text{when } sl + a < \xi < (s+1)\,l, \ s = 0 \pm 1 \ldots \end{cases} \tag{1}$$

Here N_{0B} is the constant particle density in a bunch, $\xi = z - v_0 t$, a is the length of a bunch, and l is the distance between bunches. To investigate the parametric instability of one-dimensional Langmuir oscillations in a plasma-bunches system, as the initial equation I shall use that given in [2] for the electric field of the oscillations. In a frame of reference moving with the bunches, this equation becomes

$$\left(i\omega + v_0 \frac{d}{d\xi} \right)^2 D + \frac{\omega_0^2}{\varepsilon^B(\xi, \omega)} D = 0, \tag{2}$$

where $D = \varepsilon^B E$ (E is the electric field of the oscillations); $\varepsilon^B(\xi, \omega) = 1 - (\omega_1^2(\xi)/\omega^2)$ is the dielectric constant of the beam in a frame of reference moving with its particles; ω is the frequency of oscillations in this system; $\omega_1(\xi) = \left(\frac{4\pi e^2 n_0(\xi)}{m} \right)^{1/2}$ and $\omega_0 = \left(\frac{4\pi e^2 \rho_0}{m} \right)^{1/2}$ are the Langmuir frequencies of the beam and plasma, respectively. Let us consider the case when

$$\frac{a}{l} \cdot \frac{\omega_B^2}{\omega^2 - \omega_B^2} \ll 1, \quad \left(\omega_B^2 = \frac{4\pi e^2 n_{0B}}{m} \right) \tag{3}$$

while for all $n \neq 0$, $f_{n,\omega} \ll f_{0,\omega}$ ($f_{n,\omega}$ are the Fourier coefficients of the expansion of $\frac{1}{\varepsilon^B} : \frac{1}{\varepsilon^B(\xi, \omega)} = \sum f_{n,\omega} e^{i n k_0 \xi}, \ k_0 = \frac{2\pi}{l}$). In this case, the solution of (2) is

$$D = A_+ \exp(i k_+ \xi) + A_- \exp(i k_- \xi). \tag{4}$$

Here

$$k_\pm = -\frac{\omega}{v_0} \pm \frac{\omega_0}{v_0} \sqrt{f_0} = -\frac{\omega}{v_0} \pm \frac{\omega_0}{v_0} \left(1 + \frac{a}{2l} \times \frac{\omega_B^2}{\omega^2 - \omega_B^2} \right); \tag{4'}$$

$A_\pm$ is a slowly varying function of ξ. As usual, parametric instability arises when

$$k_+ = k_- + n k_0 + \Delta; \quad \frac{|\Delta|}{k_0} \ll 1, \tag{5}$$

where n is an integer. Then for $A_\pm$ from (2) we find the following system of equations:

$$\begin{aligned} \frac{dA_+}{d\xi} + \frac{\omega_0^2 f_n}{2 i v_0 (\omega + k_+ v_0)} A_- \exp(-i\Delta\xi) &= 0; \\ \frac{dA_-}{d\xi} + \frac{\omega_0^2 f_n^*}{2 i v_0 (\omega + k_- v_0)} A_+ \exp(i\Delta\xi) &= 0. \end{aligned} \right\} \tag{6}$$

Hence $A_\pm = \text{const} \exp\left(i\varkappa\xi \mp \frac{i}{2}\Delta\xi \right)$, where for $a \ll 1$ we find $\varkappa$ from the equation

$$\varkappa^2 = -\frac{\omega_0^2}{4 v_0^2} \cdot \frac{|f_n|^2}{f_0} + \frac{\Delta^2}{4} = -\frac{\omega_0^2}{4 v_0^2} \cdot \frac{a^2}{l^2} \cdot \frac{\omega_B^4}{(\omega^2 - \omega_B^2)^2} + \frac{1}{4}\left[2\frac{\omega_0}{v_0}\left(1 + \frac{a}{2l} \cdot \frac{\omega_B^2}{\omega^2 - \omega_B^2} \right) - n k_0 \right]^2. \tag{7}$$

Let us examine the problem of excitation of oscillations with given wave number k. Since $k = k_\pm \mp \frac{\Delta}{2} + \varkappa$, therefore, by using (4') and (5), we obtain the following relation between ω and k:

$$\left(k + \frac{\omega}{v_0} - \varkappa \right)^2 = \left[\frac{\omega_0}{v_0}\left(1 + \frac{a}{2l} \cdot \frac{\omega_B^2}{\omega^2 - \omega_B^2} \right) - \frac{\Delta}{2} \right]^2 = \frac{n^2 k_0^2}{4}. \tag{8}$$
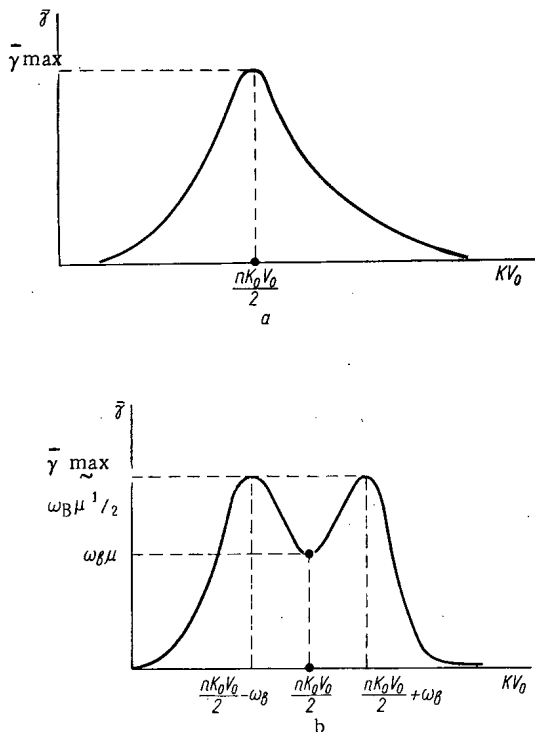
49

Fig.1. Maximum value of increment in instability region versus detuning

$$k - \frac{n}{2} k_0 = \frac{\omega_B^{2/3}\omega_0^{1/3}}{v_0} \xi;$$

a) $\mu = \frac{\omega_0 a}{\omega_B l} \gg 1$;   b) $\mu \ll 1$.

For the frequency in the laboratory system we obtain

$$\omega_1 = \omega + kv_0 = \frac{nk_0v_0}{2} + \varkappa v_0. \tag{8'}$$

Finding $\varkappa$ from (8'), with the help of (7) we obtain the dispersion equation:

$$\left(\omega_1 - \frac{n}{2} k_0 v_0\right)^2 = \left(\omega_0 - \frac{n}{2} k_0 v_0\right)^2$$
$$+ \frac{a}{l} \omega_0 \left(\omega_0 - \frac{n}{2} k_0 v_0\right) \frac{\omega_B^2}{(\omega_1 - kv_0)^2 - \omega_B^2}. \tag{9}$$

Equation (9) can also be derived from the more general dispersion equation in [1] if in the latter we assume

$$\left|\omega_0 - \frac{n}{2} k_0 v_0\right| \ll k_0 v_0, \left|\omega_1 - \frac{n}{2} k_0 v_0\right| \ll k_0 v_0 \text{ and neglect thermal}$$
motion in the bunches.

For sufficient detuning, $\left|\omega_0 - \frac{n}{2} k_0 v_0\right| \gg Jm\omega$, from (9) follows the formulas for the spectrum and increments of the beam instability given in [1, 2]. In the present letter I investigate the case of small detuning

$$\left|\omega_0 - \frac{n}{2} k_0 v_0\right| \leqslant Jm\omega, \text{ when the instability is associated}$$
with parametric resonance. Introducing the dimensionless quantities

$$\xi = \frac{\left(k - \frac{n}{2} k_0\right) v_0}{\omega_B^{2/3}\omega_0^{1/3}}, \quad \eta = \frac{\omega_1 - \frac{n}{2} k_0 v_0}{\omega_B^{2/3}\omega_0^{1/3}}, \quad \delta = 1 - \frac{n}{2} \frac{k_0 v_0}{\omega_0},$$

into (9), we can rewrite it in the following form:

$$\eta^2 = \left(\frac{\omega_0}{\omega_B}\right)^{4/3} \delta^2 + \frac{a}{l} \left(\frac{\omega_0}{\omega_B}\right)^{2/3} \frac{\delta}{(\xi - \eta)^2 - \left(\frac{\omega_B}{\omega_0}\right)^{2/3}}. \tag{10}$$

At exact resonance $\delta = 0$, there is no instability $\left(\eta = 0, \eta = \xi \pm \left(\frac{\omega_B}{\omega_0}\right)^{1/3}\right)$. Let us consider how the increment varies with the detuning δ. First let us consider large values of $k - \frac{n}{2} k_0$, where $\xi \gg |\eta|$, which corresponds to $|\omega L - kv_0| Jm\omega$. In this case, (10) yields an equation for η:

$$\eta^2 = \left[\left(\frac{\omega_0}{\omega_B}\right)^{2/3} \delta + \frac{a}{2l} \frac{1}{\xi^2 - \left(\frac{\omega_B}{\omega_0}\right)^{2/3}}\right]^2 - \frac{a^2}{4l^2} \frac{1}{\left[\xi^2 - \left(\frac{\omega_B}{\omega_0}\right)^{2/3}\right]^2}. \tag{11}$$

Hence it follows that in these conditions instability arises even at small detuning:

$$-\frac{a}{l} \frac{\left(\frac{\omega_B}{\omega_0}\right)^{2/3}}{\xi^2 - \left(\frac{\omega_B}{\omega_0}\right)^{2/3}} < \delta < 0. \tag{12}$$

The maximum value of the increment in the region of instability is

$$\bar{\gamma} = \frac{a}{2l} \cdot \omega_B^{2/3}\omega_0^{1/3} \frac{1}{\xi^2 - \left(\frac{\omega_B}{\omega_0}\right)^{2/3}}. \tag{12'}$$

As ξ decreases, the increment $\bar{\gamma}$ increases, but at small ξ equation (11) is inapplicable, because the condition $|\eta| \ll \xi$ is violated. For small ξ the solution essentially depends on the parameter

$\mu = \frac{\omega_0 a}{\omega_B l}$, which characterizes the degree of nonuniformity in the density distribution in the beam.

When $\mu \gg 1$, $\bar{\gamma}$ attains its maximum value when $\xi = 0$ (see Fig.1). Assuming $\xi = 0$ in (9), we find that there are two regions of instability

$$0 < \delta < \frac{a}{l}, \tag{13}$$

50

in which $\bar{\gamma}$ attains its maximum value when

$$\delta = \left(\frac{a}{2l}\right)^{1/3} \left(\frac{\omega_B}{\omega_0}\right)^{2/3} \text{ and is}$$

$$\bar{\gamma}\,\text{max} = \left(\frac{a}{2l}\right)^{1/3} \omega_B^{2/3}\omega_0^{1/3} \tag{13'}$$

and

$$-\left(\frac{4a}{l}\right)^{1/3} \cdot \left(\frac{\omega_B}{\omega_0}\right)^{2/3} < \delta < 0,$$

in which the maximum increment $\bar{\gamma}$ is of the same order:

$$\bar{\gamma} = \frac{1}{2}\left(\frac{a}{l}\right)^{1/3} \omega_B^{2/3}\omega_0^{1/3} \left[\text{when } \delta = -\left(\frac{a}{l}\right)^{1/3}\left(\frac{\omega_B}{\omega_0}\right)^{2/3}\right]. \tag{14}$$

When $\mu \ll 1$, resonance becomes significant when $\xi = \pm\left(\frac{\omega_B}{\omega_0}\right)^{1/3}$, which corresponds to $\left(k - \frac{n}{2}k_0\right)v_0 = \pm\omega_B$.* When $\xi = \pm\left(\frac{\omega_B}{\omega_0}\right)^{1/3}, |\eta| \ll \xi$, we obtain from (9) a cubic equation for η:

$$\eta^3 - \left(\frac{\omega_0}{\omega_B}\right)^{1/3}\delta^2\eta + \frac{a}{2l}\cdot\frac{\omega_0}{\omega_B}\delta = 0, \tag{15}$$

whence if follows that in this case instability will arise when

$$-\frac{3^{3/2}}{2}\mu^{1/2}\frac{\omega_B}{\omega_0} < \delta < \frac{3^{3/2}}{2}\mu^{1/2}\frac{\omega_B}{\omega_0}. \tag{16}$$

The maximum value of the increment in the instability region is equal in order of magnitude to:

$$\bar{\gamma}\,\text{max} \approx \omega_B\mu^{1/2} = \left(\frac{a}{l}\right)^{1/3}\mu^{1/6}\omega_B^{2/3}\omega_0^{1/3}. \tag{16'}$$

As ξ decreases further, $\bar{\gamma}$ decreases (see Fig. 1b), and when $\xi = 0$, from (9) we obtain the following relations for the width of the instability region and the maximum increment in it:

$$0 < \delta < \frac{\omega_B}{\omega_0}\mu; \quad \bar{\gamma} = \frac{\mu}{2}\omega_B \left(\text{when } \delta = \frac{\mu}{2}\frac{\omega_B}{\omega_0}\right). \tag{17}$$

The maximum value of the increment in the oscillations due to parametric instability, given by (13') in the case when $\mu \gg 1$ and by (16') in the case when $\mu \ll 1$, is of the same order as the maximum increment for beam instability in [1, 2]. This value is attained with sufficient detuning $\delta \sim \frac{\gamma\text{max}}{\omega_0}$. With less detuning the increment is less, and the instability develops more slowly than in the nonresonance cases discussed in [1, 2].

The author thanks Ya. B. Fainberg and V. I. Kurilko for helpful discussion.

LITERATURE CITED

1. Ya. B. Fainberg and V. D. Shapiro, Atomnaya Énergiya, 19, 336 (1965).
2. V. D. Shapiro, ZhTF, 36, No. 2 (1967).

---

*When $\mu \gg 1$, there is no resonance when $\xi = \pm\left(\frac{\omega_B}{\omega_0}\right)^{1/3}$, because for such ξ, Im $\eta \sim \left(\frac{a}{l}\right)^{1/3} \gg \left(\frac{\omega_B}{\omega_0}\right)^{1/3}$.

51

A SEMISTATISTICAL METHOD FOR MEASURING THE EFFECTIVE DELAYED-NEUTRON FRACTION

A. I. Mogil'ner, G. P. Krivelev,   UDC 621.039.512:621.039.514
E. K. Malyshev, S. A. Morozov, and D. M. Shvetsov

Values of the reactivity measured by studying the time behavior of a reactor are obtained in units of the effective delayed-neutron fraction β_{eff}. Calculations predict the reactivity in absolute units. The calculations and the experimental data are usually compared by using the calculated value of $\gamma = \beta_{eff}/\beta$, the ratio of the importance of the delayed neutrons for the given reactor to the known quantity β. Unfortunately, detailed information on the energy spectrum of delayed neutrons is frequently lacking, and it is impossible to make a reliable calculation of γ, particularly for reactors with beryllium or heavy water moderators in which the threshold reaction (n, 2n) may have a pronounced and not easily calculated effect on the importance of the delayed neutrons. Therefore the experimental determination of the effective yield of delayed neutrons is an important problem of reactor physics which must be solved, on the one hand, to determine the absolute reactivity, and on the other hand, to test the theoretical methods and constants.

Existing methods for determining the absolute reactivity and the related quantity β_{eff} are applicable to a very restricted class of reactors. For example, [1] describes a method for determining the absolute reactivity based on the replacing of core material by material which absorbs neutrons but does not undergo fission. The main problem in this method is the selection of an appropriate material, and while it can be solved, more or less, for thermal reactors, the situation is appreciably more complicated for reactors having a harder neutron spectrum. Experiments using this method are described in [2-4]. Boron was used as an absorbing material, since its absorption cross section in the thermal region is similar to the absorption cross section of uranium. Kaplan and Henry [3] performed a similar experiment on a reactor with a neutron spectrum harder than thermal. They had to modify the method somewhat in order to select cross sections in the epithermal region properly.

A statistical method for determining β_{eff} proposed in [5] requires precision apparatus and extensive measurements. However, the accuracy of the results presented in [5] seems unjustifiably high.

PRINCIPLES OF THE METHOD

The method is based on a comparison of the results of measuring the absolute reactor power F in two ways, one of which is statistical. If the reactor is correctly described by a point monenergetic model, it is possible to obtain from statistical measurements the absolute power F [6], but with some uncertainty, since the effective delayed-neutron fraction β_{eff} is not always well-known. The experimentally measured quantity is essentially the product $F\beta_{eff}^2$. Any independent measurement of F makes it possible to determine β_{eff}. For example, let us consider one possible experiment for determining β_{eff}.

It is well-known that for frequencies $f \gg \lambda_{max}/2\pi$, where λ_{max} is the maximum decay constant of the delayed-neutron precursors, the spectral density of the current noise from an ionization chamber placed in a reactor is described by [7].

$$S(f) = 2q^2\varepsilon F\left[1 + \frac{\overline{\nu(\nu-1)}}{\overline{\nu}^2} \frac{\varepsilon}{\beta_{eff}^2(1+\Delta)^2} \frac{\alpha^2}{(2\pi f)^2+\alpha^2}\right], \tag{1}$$

where q is the charge in the detector per neutron absorbed, ε the efficiency of the detector expressed in counts per fission in the reactor, $\Delta = (1 - k_{eff})/\beta_{eff}$, $\alpha = [1-k_{eff}(1-\beta_{eff})]l$, where l is the prompt-neutron lifetime in the reactor, ν the number of neutrons produced per fission, and f the frequency in Hz. From Eq. (1) it is seen that the spectral density has two characteristic values: in the high-frequency region $(f \gg \alpha/2\pi)$
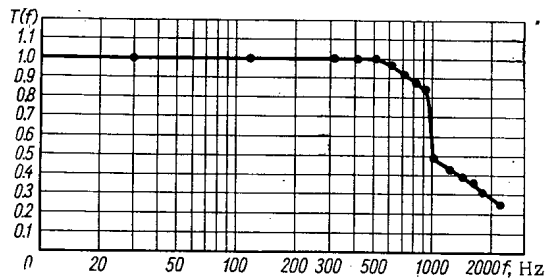
$$S(\infty) = 2q^2\varepsilon F \tag{2}$$

52

Fig. 1. Frequency response curve of the detector.

and in the low-frequency region ($\lambda_{max}/2\pi \ll f \ll \alpha/2\pi$)

$$S(0) = 2q^2\varepsilon F \left[1 + \frac{\overline{\nu(\nu-1)}}{\overline{\nu^2}} \cdot \frac{\varepsilon}{\beta^2_{eff}(1+\Delta)^2} \right]. \qquad (3)$$

Taking into account the fact that the average detector current is

$$\overline{J} = \varepsilon q F, \qquad (4)$$

we obtain

$$F = \frac{2}{\beta^2_{eff}(1+\Delta)^2} \cdot \frac{\overline{\nu(\nu-1)}}{\overline{\nu^2}} \cdot \frac{\overline{J}^2}{S(0) - S(\infty)}. \qquad (5)$$

Equation (5) was used in [8] to measure F on the assumption that β_{eff} was known. However, if the absolute power F (fissions/sec) is known from any other non-statistical measurements, this expression may be used to determine β_{eff}:

$$\beta_{eff} = \frac{1}{1+\Delta} \sqrt{\frac{2}{F} \cdot \frac{\overline{\nu(\nu-1)}}{\overline{\nu^2}} \cdot \frac{\overline{J}^2}{S(0)-S(\infty)}}. \qquad (6)$$

We note that absolute measurements of the ionization current and its fluctuations are not required, since only their ratio enters [6]. Values of $(\overline{\nu^2}-\nu)/\overline{\nu^2}$ for various fissionable isotopes are reasonably well-known [9].

EXPERIMENT

The described method was used to determine β_{eff} for one of the variations of the PF - 4 reactor [10]. As has already been pointed out, the main formula (1) is based on the point monoenergetic model of reactor kinetics. This model is a good approximation for many reactors. To test its applicability to the reactor under study, the quantity $\alpha_0 = \beta_{eff}/1$ was measured by two methods: the frequency method and the boron-poisoning method. The agreement of the experimental results ($\alpha_0 = 640$ sec^{-1}) shows that the assumed approximation is applicable.

As may be seen from Eq. (1), high accuracy requires high counter efficiency, otherwise the difference S(0) – S(∞) will be close to zero. Two He^3-filled corona counters were used as a detector. To increase the efficiency they were connected in parallel. The voltage on the wires was lower than the striking potential of the corona, so that the counters operated close to the ionization-chamber region.

It is very important to know the frequency response of the detector. This function was studied by measuring the noise spectrum of the current when the counters were irradiated by the neutrons from a Po - Be source. Since the frequency spectrum of the source is "white," the spectral density of the fluctuations of the ionization current is proportional to square of the absolute value of the detector transfer function. The measured frequency dependence T(f) is shown in Fig. 1.

Special experiments showed that a strict proportionality between ionization current and neutron flux was maintained while measurements were being taken.

Current fluctuations were analyzed with a spectrum analyzer containing filters arranged in a twin-T network in a feedback circuit. After passing through the filters, the noise enters a linear detector through a full-wave bridge and then passes to a smoothing circuit. A linear rather than a square-law detector could be used, since the current fluctuations have a normal distribution. In this case,

$$S(f) = \frac{\overline{|\Delta J(f)|^2}}{\Delta f} = \frac{\pi}{2} \cdot \frac{\overline{|\Delta J(f)|^2}}{\Delta f}. \qquad (7)$$

The analyzer contained three filters; one of them was tuned to high (f $\gg \alpha/2\pi$) frequencies and two to low (f $\ll \alpha/2\pi$) frequencies. The resonant frequencies and the energy passbands of the filters were

f_{res}, Hz	Δf, Hz
4.4	2.47 ± 0.057
7.45	3.04 ± 0.041
760	295 ± 9

The spectral density was measured simultaneously at all the indicated frequencies. An ÉPP - 09 automatic potentiometer was used as an output meter.
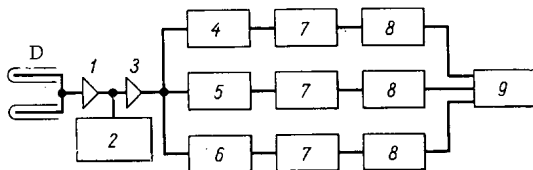
53

Fig. 2. Block diagram of measuring apparatus: D) detector; 1) cathode follower; 2) average chamber-current meter; 3) low-frequency amplifier; 4-6) filters 1, 2, and 3, respectively; 7) linear detectors; 8) smoothing circuits; 9) recorder.

A block diagram of the apparatus is shown in Fig. 2. The detector current from the cathode follower passes through a low frequency amplifier and then to the frequency analyzer. The magnitude of the direct current component is determined by the potential across the load resistor of the cathode follower.

The relative subcriticality of the reactor, Δ, was found from the position of a control rod, which had been previously calibrated in terms of the reactor period. The actual reactor power was determined independently by using an absolute-counting chamber with a known amount of U^{235}. The absolute power was calculated by the formula

$$F = \frac{M}{m} \cdot \frac{n(r_0)}{k(r_0)}, \tag{8}$$

where M is the weight of uranium in the reactor core, m the weight of uranium in the chamber, and $n(r_0)$ the counting rate with the detector placed at point r_0. The ratio of local to average power density at point r_0 is defined as

$$k(r_0) = \frac{n(r_0)}{\bar{n}}, \tag{9}$$

where $\bar{n}$ is the counting rate averaged over the core

$$\bar{n} = \frac{1}{V} \int_V n(r)\, dr. \tag{10}$$

The ratio of local to average power density was found by numerical integration of the experimental curves over the core volume V.

The absolute-counting chamber was a spherical ionization chamber with an outer-electrode diameter of 15 mm and an inner-electrode diameter of 5 mm. A layer of uranium compound having the same isotopic composition as the core material was deposited on a hemisphere of the inner electrode. The working volume of the chamber was filled with a mixture of A + 2% N_2 at a pressure of 1.5 tech. atm. For minimum neutron absorption the outer electrode was made of two aluminum hemispheres and placed in a steel tube 0.2 mm thick. The amount of uranium in the chamber (48.4×10^{-3} mg) was determined by comparing the absolute α activity of the material in the chamber with the specific α activity of a known weight of the preparation.

ERROR ANALYSIS

The error in the determination of β_{eff} is due mainly to the errors in measuring the current J, the difference $S(0) - S(\infty)$, and the power F. The error in the determination of the relative subcriticality has a negligible effect on the final result when $1 - k_{eff} \ll \beta_{eff}$.

Since all these errors are statistical in nature and may be considered independent, the relative error in the determination of β_{eff} is equal to

$$\frac{\sigma(\beta_{eff})}{\beta_{eff}} = \sqrt{\left(\frac{\sigma(\bar{J})^2}{\bar{J}}\right)^2 + \left(\frac{\sigma[S(0) - S(\infty)]}{2[S(0) - S(\infty)]}\right)^2 + \left(\frac{\sigma(F)}{2F}\right)^2}, \tag{11}$$

where the σ's are the mean-square errors of the corresponding quantities. The error in the determination of the direct-current component of the current J is about 2% and is due largely to inaccuracies of instrument calibrations. The errors in the measurement of the spectral densities are determined by the calibration errors of the filters, and taking into account the two low-pass filters, amount to 1.2% for S(0) and 3% for S(∞). Since in the experiment $S(\infty) \approx 1/3\ S(0)$, the error in S(0) - S($\infty$) is 2.4%.

The error in the measurement of F arises from the errors in determining the amount of material in the chamber m (2.6%), the amount of fuel M (2.6%), and the ratio of local to average power density $k(r_0)$ (2.8%).

54

Results of the Experimental Determination of β_{eff} for the PF-4 Reactor

Δ	$\bar{J}$	$S(0)$	$S(\infty)$	F, fissions/sec	β_{eff}
0.074	0.242	$0.1375 \cdot 10^{-6}$	$0.0442 \cdot 10^{-6}$	$1.623 \cdot 10^{10}$	$0.733 \cdot 10^{-2}$
0.085	0.209	$0.1190 \cdot 10^{-6}$	$0.0394 \cdot 10^{-6}$	$1.417 \cdot 10^{10}$	$0.716 \cdot 10^{-2}$
0.105	0.175	$0.0925 \cdot 10^{-6}$	$0.0324 \cdot 10^{-6}$	$1.160 \cdot 10^{10}$	$0.757 \cdot 10^{-2}$

Since the efficiency of the absolute-counting chamber is low, two fission chambers whose efficiencies had been compared with that of the absolute-counting chamber were also used. The accuracy of this comparison was about 1%. Thus the total error in the determination of F was 4.5%.

It is clear from Eq. (11) – and this is one of the advantages of the present method — that only half the error in the difference of the spectral densities and in the power appears as an error in β_{eff}. As a result, the error in the measurement of β_{eff} is 3.2%.

All told, three sets of measurements were performed on three different subcritical reactor configurations. The data obtained are presented in the table. The values of the current and of the spectral densities are given in relative units.

During the experiment the detectors were located in the reflector. The fission chambers were placed at positions in the core such that a displacement of the control rod left the value of the ratio of local to average power density, practically unchanged at 1.25 ± 2.8%.

The average value of β_{eff} for all the experiments was 0.74×10^{-2}. The standard deviation of the results of the individual measurements was 1.6%. Taking into account the errors that have been discussed

$$\beta_{eff} = 0.74 \cdot 10^{-2} \pm 3.6\%.$$

If we take $\beta = 0.64 \times 10^{-2} \pm 3.1\%$ [11], the relative importance of the delayed neutrons in the reactor investigated is

$$\gamma = \frac{\beta_{eff}}{\beta} = 1.16 \pm 4.8\%.$$

Thus our method for determining β_{eff} is more-widely applicable than the method of replacing fissionable material by an equivalent absorber. Since statistical methods may be successfully applied to the measurement of the parameters of a wide variety of thermal and fast reactors, and since in most cases the point monoenergetic model gives a good description of the experiments, this method may be expected to apply to reactors of many types. In certain cases the statistical study of something other than frequency may turn out to be preferable. The quantity F may be determined by any independent method which does not require knowledge of β_{eff}.

LITERATURE CITED

1. F. Hoffman, "The Science and Engineering of Nuclear Power," [Russian translation], Vol. 2, Moscow, IL, p. 106 (1950).
2. T. Raune et al, Trans. Amer. Nucl. Soc. 1, 142 (1958).
3. R. Perez-Belles et al, Nucl. Sci. and Engn. 12, 505 (1962).
4. T. Raune, Nucleonics 20, 94 (1962).
5. R. Karam, Trans. Amer. Nucl. Soc. 7, 248 (1964).
6. A. I. Mogil'ner and D. M. Shvetsov, Atomnaya Énergiya, 20, 117 (1966).
7. C. Cohn, Nucl. Sci. and Engn, 7, 472 (1960).
8. R. Schröder, Nukleonik, 4, 227 (1962).
9. J. Terrel, Phys. Rev, 108, 783 (1957).
10. A. I. Leipunskii et al, "The Physics of Fast and Intermediate Reactors" Vol. 1, SM 18/80, IAEA, Vienna, p. 326 (1962).
11. G. Keepin et al, Phys. Rev. 101, 1044 (1957).

HEAT TRANSFER IN FREE-CONVECTION

SODIUM BOILING

V. I. Deev, G. P. Dubrovskii,

L. S. Kokorev, I. I. Novikov, and V. I. Petrovichev

UDC 621.039.517

Various authors [1-4] have described experiments on heat transfer for sodium boiling in a large vessel under pressures on the order of 10^5 N/m^2 or less. In [3, 5] it was shown that the boiling of sodium at low pressures has specific characteristics. In particular, Subbotin et al. [3] found that the boiling process displays instability. Owing to the lack of experimental work on heat transfer for boiling sodium, it has not yet proved possible to establish definite limits for this instability or to elucidate the effects of various factors (thermal load, pressure, state of heating surface and its shape, dimensions, position, material, boundary conditions, etc.) on heat transfer in this case. Because of this, the theoretical relations proposed by various authors [2-4, 6] for heat transfer for boiling liquid metals under free-convection conditions should be regarded as first approximations.

The present authors have attempted to study the heat transfer accompanying the boiling of sodium in a large vessel over wide ranges of pressure and thermal load, and to obtain some detailed information on the boiling process.

The sodium was boiled at the surface of a plane horizontal disk with a diameter of 28 mm, made of Kh18N10T steel, immersed in a large volume of liquid. This disk was heated by electron bombardment. We measured the power conveyed to the disk and its temperature at three cross sections at different heights, the temperatures of the liquid and vapor, the temperature differences between the heat-emitting wall and the liquid, and the vapor pressure. The temperatures were measured with platinum-rhodium-platinum thermocouples. The emfs of the thermocouples were recorded on paper tape by means of a high-speed automatic potentiometer (ÉPP-09) with a 2-mV scale, and they were also recorded by a PMS-48 potentiometer. The sodium vapor pressure was measured by a compensation method. In determining the heat-transfer coefficient, the flux was calculated from the electric power input and monitored by the temperature differential at the working zone.

Before beginning the experiments with the sodium, we made preliminary heat-transfer measurements on boiling distilled water. The results for water agreed with the generally recommended formulas. The sodium used was freed from oxides in a circulation loop with a cold trap.

We studied heat exchange for sodium boiling under pressures between $5 \cdot 10^2$ and $7.5 \cdot 10^4$ N/m^2 with thermal loads between $9 \cdot 10^4$ and $2 \cdot 10^6$ W/m^2. Analysis of the experimental results revealed that we were dealing with different types of heat extraction. At low pressures ($p \approx 6 \cdot 10^2$ N/m^2) the sodium did not boil at the heated surface, and throughout the range of thermal loads ($1.4 \cdot 10^5$ - $1.3 \cdot 10^6$ W/m^2) heat extraction was by natural convection. Between $4 \cdot 10^3$ and $2 \cdot 10^4$ N/m^2, the boiling was unstable. We observed marked fluctuations in the temperature of the heat-emitting wall, some of which reached $\pm$ 25°C. By analyzing the recordings of the temperatures of the liquid and the heat-exchange surface, we found that these fluctuations were due to alternations between natural convection and boiling, and also to irregularities in the boiling process itself. At $p \approx 2 \cdot 10^4$ N/m^2 we observed a transition to stable boiling at the hot surface, which was characterized by slight fluctuations ($\pm$ 1-2°C) in the wall temperature and stable heat exchange with respect to time.

Figure 1 shows the heat-transfer data for boiling sodium. The points joined by dashed lines represent the two extreme values of the heat-transfer coefficient for those conditions under which the heat exchange varied greatly with time. At $6.1 \cdot 10^4$ N/m^2 the heat-transfer coefficient increases continuously with increasing heat flux up to $q \approx 9 \cdot 10^5$ W/m^2: the relation can be expressed as $\alpha \sim q^{1/3}$. When $q > 9 \cdot 10^5$ W/m^2 the heat-transfer coefficient increases much more slowly. The α-q curve is similar for
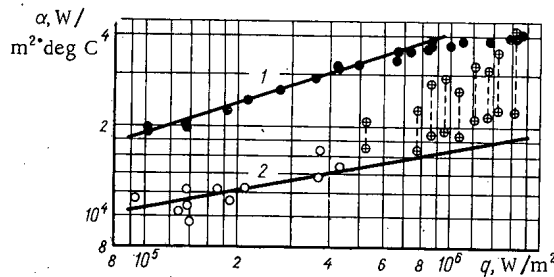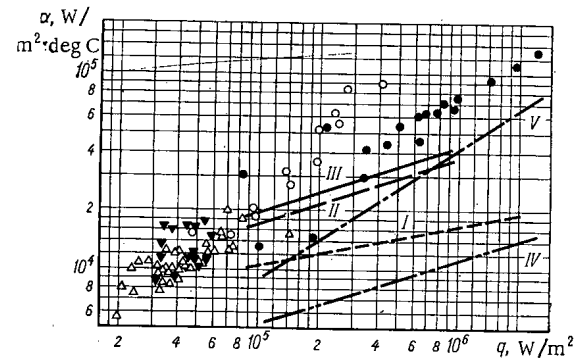
56

Fig. 1

Fig. 2

Fig. 1. Heat-transfer coefficient versus heat flux. $\bigcirc$, $\oplus$) $p = 5 \cdot 10^3$ N/m²; $\bullet$) $p = 6.1 \cdot 10^4$ N/m². (1) $\alpha = 136\, q^{1/3}\, p^{0.1}$; (2) natural convection (present authors' data).

Fig. 2. Heat-transfer for sodium boiling in large vessel. $\bigcirc$, $\bullet$) [1, 2] respectively, horizontal tubes; $\triangle$, $\blacktriangledown$) [4], horizontal and vertical tubes, respectively; II, III) data by present authors ($p = 2 \cdot 10^4$ N/m², $p = 7.5 \cdot 10^4$ N/m², respectively); V) [3]; I, IV) data of present authors and [3], respectively, natural convection.

all the pressures studied greater than $2 \cdot 10^4$ N/m² and for thermal loads of $9 \cdot 10^4 - 9 \cdot 10^5$ W/m² is satisfactorily represented by the equation

$$\alpha = 136 q^{1/3} p^{0,1},$$

where α, q and p are in International System units. At $5 \cdot 10^3$ N/m² the rate of heat exchange varies from the level corresponding to heat transfer by free convection (see Fig. 1, Curve 2) to a level corresponding to stable heat extraction. The data on heat transfer by free convection of sodium were obtained with excess argon pressure above the metal surface and at temperatures up to 840°C.

Figure 2 compares our results with those of other authors. The range of possible heat-transfer coefficients (including the region of unstable heat transfer) found in our experiments is bounded by lines I and III. At low thermal loads ($q < 10^5$ W/m²) this region includes the data of [1, 2, 4]. There is a marked discrepancy between our results and those of Lyon [1] at $q > 10^5$ W/m², and also between our results and those of Noyes [2] for $q > 3 \cdot 10^5$ W/m². For high thermal loads, the results of Subbotin [3] agree with our experimental data, but at low thermal loads his heat-exchange coefficient is lower than ours.

Subbotin et al. [3] obtained a curve $\alpha \sim q^{2/3}$ for the heat-transfer coefficient versus the thermal load that is close to the relation for ordinary nonmetallic liquids $\alpha \sim q^{0.7}$. However, for boiling sodium the exponent of q can take another value: this may be due to features of sodium boiling at low pressures, mainly the distribution of vapor-formation centers. In addition, in the heat transfer of boiling sodium an important part must clearly be played by free convection, which can make an appreciable contribution to heat transfer for boiling liquid metals, owing to their high thermal conductivities.

LITERATURE CITED

1. R. Lyon et al. Chem. Engng. Progr. Sympos. Series, 51, No. 17, 41 (1955).
2. R. Noyes, Trans. ASME, Ser. C., 85, 125 (1963).
3. V. I. Subbotin et al. Report No. 328 submitted by the USSR to the Third International Conference on the Peaceful Uses of Atomic Energy (Geneva, 1964).
4. V. M. Borishanskii et al. Atomnaya Énergiya, 19, 191 (1965).
5. V. I. Deev and A. N. Solov'ev, Inzh.-fiz. zh., VII, No. 6, 8 (1964).
6. D. A. Labuntsov, Teploénergetika, No. 5, 76 (1960).

EXPERIMENTAL STUDY OF ACCELERATION
OF AN EMERGENCY-SHUTDOWN ROD

R. R. Ionaitis and L. I. Kolganova   UDC 621.039.566.8

An emergency shutdown rod is located outside the core, but if emergency conditions arise it enters the core within a certain given time.

According to the kinematic system of emergency-shutdown [1], the rod can move upstream, in a stationary liquid, or downstream (in a closed or open loop).

There are practically no published data on the acceleration of the rod in its channel, with the exception of some data in [2] and [3].

To study the acceleration of the rod we constructed a test rig comprising an experimental channel with a head and shock-absorber and a hydraulic circuit (Fig. 1). Rod 1 is retained in its raised position by means of electromagnetic catch 2 or, during exchange of rods, by manually controlled stop 3. Sleeve 4 ensures smooth guidance of the rod into the channel, whose internal diameter is 33-68 mm. Valves 5-7 control the motion of the rod. Branch pipe 8 is for scavenging the rig. Inductive transducers 9 and photoelectric transducer 10 determine the position of the magnetic upper end of the rod during its fall. At the head and shock-absorber and at other places in the port and loop there are pressure gauges 11.

The internal diameter of the test port is 36 mm and its height is 19 mm. The rod, with a diameter of 30 mm and a length of 0.5-10 m, consists of smooth aluminum or steel pieces 0.1-1.8 m long, with four different types of joints (Fig. 2).

The table shows the valve positions required for any given type of descent of the rod. The valves were capable of quantitative as well as qualitative control (i.e., the four stated types of descent). Thus by adjusting valve No. 6 we could vary the resistance of the closed loop (see curves 1-7, Fig. 3).

The distances between the inductive transducers for the rod position were as follows (transducers 0 and 1 are indicated in Fig. 1 by the number 9):

Fig. 1. Head of experimental channel and hydraulic circuit.

Transducer No.	0—1	1—2	2—3	3—4	4—5	...	19—20
Distance, m . .	0.53	0.27	0.72	0.68	1.00	...	1.00

Each time the rod was dropped we measured the times of passage past the datum points by recording the pulses from the inductive transducers on film with an MPO-2 loop oscillograph, and we also measured the flow rates of liquid through the channel in either direction by recording the signal from the DM-6 transducer on the oscillograph film.
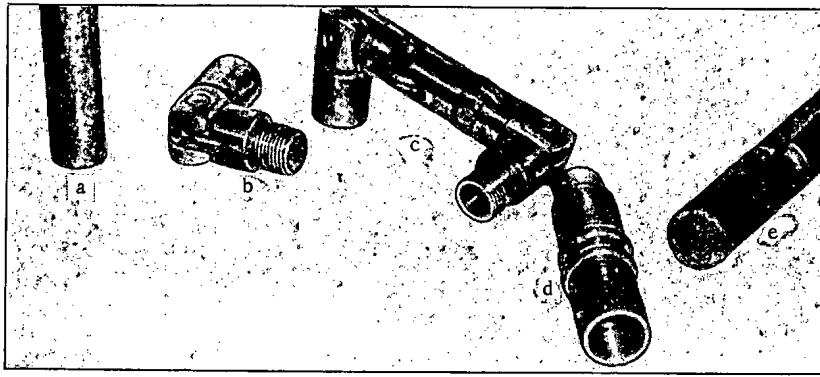
Fig. 2. Parts of rod: a) smooth insert; b, c, d, e) joints.

TABLE 1. Positions of Valves During Experiments

Mode No.	Type of descent	Position of valves		
		No. 5.	No. 6	No. 7
1	Upstream	Open	Closed	Open
2	In stationary water	Closed	"	Closed
3	In closed loop	"	Open	"
4	In closed loop initially upstream	Open	"	Open

In addition, by means of DD-10 pressure gauges and an ID-2I converter, we measured the pressure drop on the rod and the temperature. The tests were made in cold water (to 45°C). The clock frequency was 50 Hz.

We varied the following parameters: travel of rod, s, from 0 to 18 m; velocity of rod in water, w, from about 0 to 3.8 m/sec; length of rod, 1, from 0.55 to 9.55 m; length of hydraulic loop (including channel), l_K, from 45 to 55 m; relative density of material of rod, ρ/ρ_{liq}, from 2.8 to 7.7 (where ρ is the density of the rod and ρ_{liq} that of the liquid); weight of rod, G, from 2.1 to 40 kg; and ratio of force on rod to its weight in the liquid, P/G_{liq}, from 0.6 to 1. The force on the rod was reduced by the initial counter-current (see table).

When the rod descended in air, the experimental points lay almost exactly on the parabola

$$s = \frac{1}{2} g t^2.$$

As an example, Fig. 3 shows the initial motion of the rod, w, and of the liquid in the channel, w_K. In most cases the rod was dropped twice or sometimes three times (e.g., No. 3). The results showed satisfactory agreement, whether the descents were in rapid sequence or separated by several months.

We found that when the motion had become steady the velocity of the rod oscillated with a frequency which increased with the velocity itself. The amplitude of oscillation decreases when air is carefully removed from the loop, and, on the other hand, increases when air is added to the loop (see curves 7 and 7A in Fig. 3).

To convert these experimental curves to dimensionless form, it is most convenient to take as scales the velocity of the rod in steady motion, * w_y, and the characteristics (time, path) corresponding to free fall of a body.

We shall define the parameter W as

$$W = w/w_y,$$

_____
* The characteristics of steady motion are given in [4].
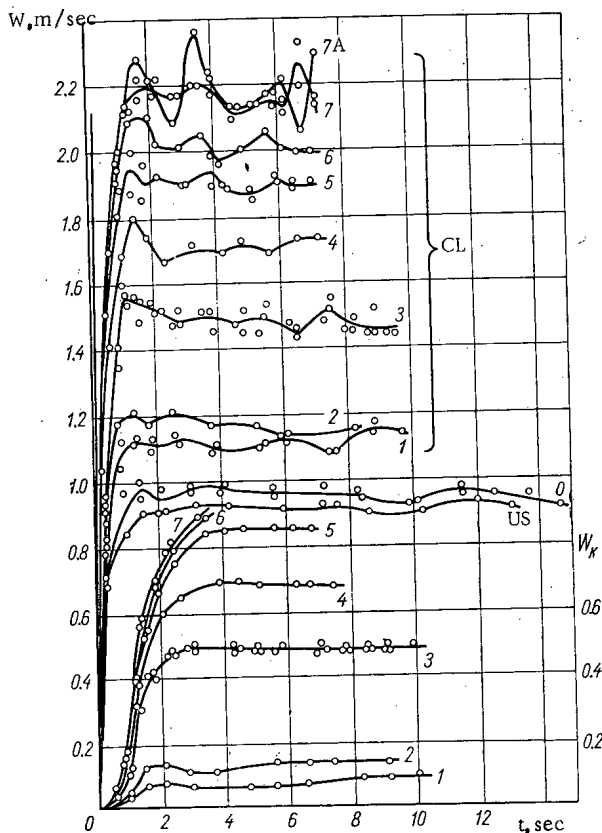
Fig. 3. Examples of experimental graphs of velocities w of rod and w_K of liquid in loop versus time t. Numbers on curves correspond to positions of valve No. 6 (see Fig. 1), which controls the resistance of the closed loop. US) upstream; O) stationary water; CL) closed loop; A) air.

and the parameter

$$T = t/t_g,$$

where $t_g = w_y/g$ is the time required to attain velocity w_y when moving according to the law of free fall with acceleration g.

Similarly, we also define a quantity S:

$$S = s/s_g,$$

where $s_g = w_y^2/g$ is the distance which would be traveled by a body in a time $t_g = w_y/g$ when moving with velocity w_y. Then the dimensionless velocity W of the rod, the time T, and both the path S traveled by the rod are expressed in terms of the dimensionless quantities as follows:

$$W = \frac{w}{w_y} ; \qquad T = \frac{tg}{w_y} ; \qquad S = \frac{sg}{w_y^2} . \qquad (1)$$

As a result of conversion to dimensionless form, the family of dimensional curves for the descent of one rod (see Fig. 3) are reduced to a single curve (see curve W in Fig. 4).

Figure 4 shows a sample experimental curve of the dimensionless path S versus the dimensionless time T, and five variants of the ratio of the length of the loop to that of the rod, l_K/l, and also the (W, T) curve for one of these variants.

For descent of a body in air in an infinite space, the correct formulas are W = tanh T and S = ln cosh T.

Our experiments (see Fig. 4) show that for a rod falling in a channel containing a liquid, the valid formulas are the analogous ones

$$W = \text{th } \delta T; \qquad (2)$$

$$S = \frac{1}{\delta} \ln \text{ch } \delta T, \qquad (3)$$

where δ is a coefficient varying with the ratio of the density of the liquid to that of the rod, ρ_{liq}/ρ, the ratio of the length of the channel to that of the rod, l_K/l, and the ratio of the initial driving force on the rod to its weight in the liquid, P/G_{liq}. These simplexes can be converted to the complex

$$\delta = \frac{1 - \dfrac{\rho_{liq}}{\rho}}{1 + \dfrac{l_K}{l} \cdot \dfrac{\rho_{liq}}{\rho}} \cdot \frac{P}{G_{liq}} . \qquad (4)$$

For comparison, Fig. 5 gives the acceleration calculated from (4) and that determined experimentally. It will be seen that (4) gives the lower bound of the value of δ.

Thus our investigation gives the principal laws and some incidental effects in the acceleration of an emergency shutdown rod. The simple, fairly accurate formulas which we propose can be used to calculate the law of motion of an emergency-shutdown rod moving in a liquid (formulas (2)-(4)), or for processing experimental data (formula (1)).
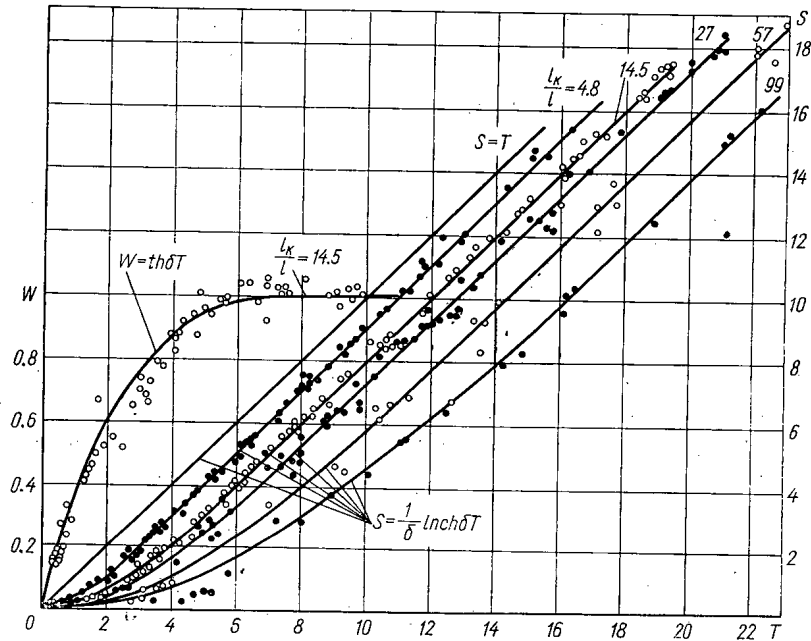
Fig. 4. Examples of dimensionless curves of acceleration of rod
$(\rho_{liq}/\rho = 0.13)$.
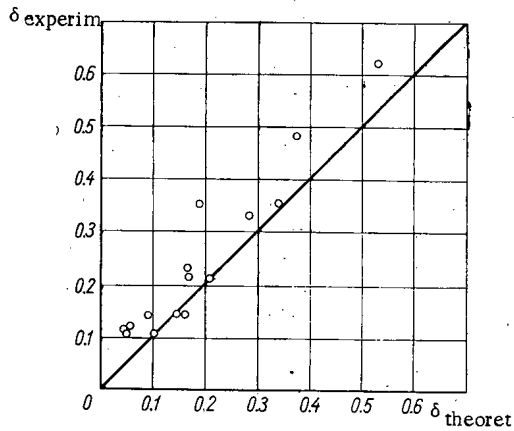
Fig. 5. Experimental and theoretical re-
sults compared in terms of coefficient δ.

LITERATURE CITED

1. A. F. Popov, Control Systems for Nuclear Reactors, [in Russian], Moscow-Leningrad, Gosenergoizdat, (1961).
2. E. Clements et al, Nucl. Sci. and Engng, 18, 205 (1964).
3. R. N. Karpov et al, Driving Gears for the Control Organs of Power Reactors for Ships, [in Russian], Leningrad, Sudostroenie, p. 33 (1965).
4. R. R. Ionaitis, Atomnaya Énergiya, 18, 422 (1965).

SOME CRITERIA OF THE SPEED OF NEUTRON-ACTIVATION ANALYSIS

E. R. Kartashev, O. K. Nikolaenko,
I. D. Danil'chenko, R. G. Gambaryan,
A. S. Shtan', and N. N. Bobrov-Egorov

UDC 543.53

In the well-known formula for induced activity A [1] we find certain characteristics which are constant for any given isotope (the activation cross section σ_{act}, the content p of the isotope in the natural mixture of the element, Avogadro's number N_A, and the atomic weight of the element A_{el}). Thus we obtain the expression

$$A = f \sigma_{rel} \, m \, S. \tag{1}$$

Here f is the neutron-flux density, $\sigma_{rel} = \dfrac{\sigma_{act} N_A p}{A_{el}}$ is the activation cross section per gram of element (the specific activation cross section), m is the mass of the element, and $S = [1 - \exp(-\dfrac{0.693 t_{irr}}{T_{1/2}})]$

Rapidity Characteristics of Neutron Activation Analysis for Certain Elements

Element (stable isotope)	Nuclear reaction	Product nucleus	$T_{1/2}$	σ_{rel}, cm^2/g	F_R, $cm^2/g \cdot sec$
Boron, B^{11}	n, γ	B^{12}	0.027 sec	$2.2 \cdot 10^{-3}$	$8.3 \cdot 10^{-2}$
Carbon, C^{12}	n, p	B^{12}	0.027 sec	$8.4 \cdot 10^{-4}$	$3.1 \cdot 10^{-2}$
Indium, In^{115}	n, γ	In^{116}	13 sec	$2.6 \cdot 10^{-1}$	$2.0 \cdot 10^{-2}$
Rhodium, Rh^{103}	n, γ	Rh^{104m}	42 sec	$8.2 \cdot 10^{-1}$	$1.9 \cdot 10^{-2}$
Silver, Ag^{109}	n, γ	Ag^{110}	24.2 sec	$3.1 \cdot 10^{-1}$	$1.3 \cdot 10^{-2}$
Dysprosium, Dy^{164}	n, γ	Dy^{165}	1.3 min	$5.3 \cdot 10^{-1}$	$6.8 \cdot 10^{-3}$
Scandium, Sc^{45}	n, γ	Sc^{46}	20 sec	$1.3 \cdot 10^{-1}$	$6.7 \cdot 10^{-3}$
Zirconium, Zr^{90}	n, n γ	Zr^{90m}	0.83 sec	$5.0 \cdot 10^{-3}$	$6.0 \cdot 10^{-3}$
Hafnium, Hf^{178}	n, γ	Hf^{179m}	19 sec	$7.5 \cdot 10^{-2}$	$3.8 \cdot 10^{-3}$
Iridium, Ir^{191}	n, γ	Ir^{192}	1.4 min	$3.1 \cdot 10^{-1}$	$3.7 \cdot 10^{-3}$
Tungsten, W^{182}	n, γ	W^{183}	5.5 sec	$1.7 \cdot 10^{-2}$	$3.1 \cdot 10^{-3}$
Lithium, Li^{7}	n, γ	Li^{8}	0.85 sec	$2.7 \cdot 10^{-3}$	$3.1 \cdot 10^{-3}$
Silver, Ag^{107}	n, γ	Ag^{108}	2.3 min	$1.3 \cdot 10^{-1}$	$9.3 \cdot 10^{-4}$
Beryllium, Be^{9}	n, α	He^{6}	0.82 sec	$6.7 \cdot 10^{-4}$	$8.1 \cdot 10^{-4}$
Sodium, Na^{23}	n, α	F^{20}	11 sec	$5.8 \cdot 10^{-3}$	$5.3 \cdot 10^{-4}$
Gold, Au^{197}	n, n γ	Au^{197m}	7.3 sec	$3.7 \cdot 10^{-3}$	$5.0 \cdot 10^{-4}$
Selenium, Se^{76}	n, γ	Se^{77}	18 sec	$4.8 \cdot 10^{-3}$	$2.7 \cdot 10^{-4}$
Cobalt, Co^{59}	n, γ	Co^{60m}	10.4 min	$1.6 \cdot 10^{-1}$	$2.6 \cdot 10^{-4}$
Dysprosium, Dy^{164}	n, γ	Dy^{165m}	139 min	$5.3 \cdot 10^{-1}$	$2.6 \cdot 10^{-4}$
Rhodium, Rh^{103}	n, γ	Rh^{104}	4.4 min	$7.0 \cdot 10^{-2}$	$2.6 \cdot 10^{-4}$
Indium, In^{115}	n, γ	In^{116m}	54.2 min	$7.8 \cdot 10^{-1}$	$2.4 \cdot 10^{-4}$
Beryllium, Be^{9}	n, p	Li^{9}	0.17 sec	$4.0 \ 10^{-5}$	$2.4 \cdot 10^{-4}$
Vanadium, V^{51}	n, γ	V^{52}	3.76 min	$5.3 \cdot 10^{-2}$	$2.3 \cdot 10^{-4}$
Oxygen, O^{16}	n, p	N^{16}	7.35 sec	$1.5 \cdot 10^{-3}$	$2.0 \cdot 10^{-4}$
Fluorine, F^{19}	n, p	O^{19}	29.4 sec	$4.3 \cdot 10^{-1}$	$1.4 \cdot 10^{-4}$
Yttrium, Y^{89}	n, n γ	Y^{89m}	16 sec	$2.0 \cdot 10^{-3}$	$1.2 \cdot 10^{-4}$
Cerium, Ce^{140}	n, 2n	Ce^{139m}	55 sec	$4.6 \cdot 10^{-3}$	$8.3 \cdot 10^{-5}$
Europium, Eu^{151}	n, γ	Eu^{152m}	9.2 h	2.6	$8.0 \cdot 10^{-5}$
Fluorine, F^{19}	n, α	N^{16}	7.35 sec	$5.4 \cdot 10^{-4}$	$7.3 \cdot 10^{-5}$
Chlorine, Cl^{37}	n, α	P^{34}	12.4 sec	$1.9 \cdot 10^{-4}$	$6.4 \cdot 10^{-5}$
Lead, Pb^{207}	n, n γ	Pb^{207m}	0.82 sec	$5.2 \cdot 10^{-5}$	$6.4 \cdot 10^{-5}$

TABLE Continued

Element (stable isotope)	Nuclear reaction	Product nucleus	$T_{1/2}$	σ_{rel}, cm^2/g	F_R, cm^2/g·sec
Lithium, Li^6	n, p	He^6	0.82 sec	$4.4 \cdot 10^{-5}$	$5.3 \cdot 10^{-5}$
Praseodynium, Pr^{141}	n, 2n	Pr^{140}	3.4 min	$8.9 \cdot 10^{-3}$	$4.4 \cdot 10^{-5}$
Aluminum, Al^{27}	n, γ	Al^{28}	2.27 min	$4.7 \cdot 10^{-3}$	$3.4 \cdot 10^{-5}$
Silicon, Si^{28}	n, p	Al^{28}	2.27 min	$4.4 \cdot 10^{-3}$	$3.2 \cdot 10^{-5}$
Bromide, Br^{79}	n, γ	Br^{80}	18 min	$3.2 \cdot 10^{-2}$	$3.0 \cdot 10^{-5}$
Fluorine, F^{19}	n, γ	F^{20}	11 sec	$2.8 \cdot 10^{-4}$	$2.6 \cdot 10^{-5}$
Barium, Ba^{138}	n, 2n	Ba^{137m}	2.6 min	$3.9 \cdot 10^{-3}$	$2.5 \cdot 10^{-5}$
Sodium, Na^{23}	n, p	Ne^{23}	40 sec	$8.8 \cdot 10^{-4}$	$2.2 \cdot 10^{-5}$
Rhodium, Rh^{103}	n, α	Tc^{100}	15.8 sec	$3.5 \cdot 10^{-4}$	$2.2 \cdot 10^{-5}$
Phosphorus, P^{31}	n, α	Al^{28}	2.27 min	$2.9 \cdot 10^{-3}$	$2.1 \cdot 10^{-5}$
Chlorine, Cl^{38}	n, γ	Cl^{28m}	1 sec	$2.1 \cdot 10^{-5}$	$2.1 \cdot 10^{-5}$
Iodine, I^{127}	n, γ	I^{128}	25 min	$2.6 \cdot 10^{-2}$	$1.8 \cdot 10^{-5}$
Copper, Cu^{65}	n, γ	Cu^{66}	5.1 min	$5.3 \cdot 10^{-3}$	$1.7 \cdot 10^{-5}$
Silver, Ag^{109}	n, 2n	Ag^{108}	2.3 min	$2.2 \cdot 10^{-3}$	$1.6 \cdot 10^{-5}$
Niobium, Nb^{93}	n, γ	Nb^{94m}	6.6 min	$6.5 \cdot 10^{-3}$	$1.6 \cdot 10^{-5}$
Manganese, Mn^{55}	n, γ	Mn^{56}	2.6 h	$1.5 \cdot 10^{-1}$	$1.6 \cdot 10^{-5}$
Bromine, Br^{79}	n, 2n	Br^{78}	6.4 min	$4.2 \cdot 10^{-3}$	$1.1 \cdot 10^{-5}$
Antimony, Sb^{123}	n, 2n	Sb^{122m}	3.5 min	$2.1 \cdot 10^{-3}$	$1.0 \cdot 10^{-5}$

is the saturation factor, where t_{irr} is the irradiation time, and $T_{1/2}$ is the half-life of the isotope formed.

The specific activation cross section σ_{rel} [2] does not include the time characteristics, and therefore we cannot assess the activation capacities of elements by comparing their σ_{rel} values if activation saturation is not attained.

If $t_{irr} \ll T_{1/2}$, the expression for the induced activity can be written in the form

$$A = \frac{0.693 \, f \, \sigma_{rel} \, m \, t_{irr}}{T_{1/2}} = 0.693 \, f \, m \, F_R t_{irr} \,. \qquad (2)$$

We suggest that F_R should be called the rapidity factor, as it characterizes the rapidity of activity induction. The term "index of quality", introduced by Coldwell and Mills [3] for an analogous characteristic, is less fortunate.

By compiling a table in which isotopes are arranged in decreasing order of F_R we can pick out the elements which are most suitable for rapid activation analysis.

In the table we give isotopes with $F_R \geq 1 \cdot 10^{-5}$ cm^2/g·sec [for thermal and fast (14 MeV) neutrons], and also the values of σ_{rel} for these isotopes. The elements at the beginning of the table have the best characteristics for rapid activation analysis (other conditions being equal).

The values of σ_{rel} and F_R can be used to make a preliminary estimate of the induced activity of components for analysis or impurity elements by means of (1) and (2). In specific calculations of the expected rapidity, allowance must be made for the for the yields of γ quanta and β particles, since σ_{rel} and F_R do not contain these characteristics.

LITERATURE CITED

1. D. Taylor, Neutron Emission and Activation Analysis, [Russian translation], Moscow, Atomizdat, (1965).
2. D. I. Leipunskaya and Z. E. Gauer, Coll: "Nuclear Geophysics" [in Russian], Moscow, Gostoptekhizdat, p. 238 (1959).
3. R. Coldwell and W. Mills, Nucl. Instrum. and Methods, 5, 312 (1959).

CHOICE OF IRRADIATOR FOR TREATMENT OF LOOSE MATERIAL

A. V. Bibergal' and V. N. Primak-Mirolyubov   UDC 621.039.83

Irradiation treatment is finding increasing application in agriculture. Various institutes [1, 2] have demonstrated the effectiveness of irradiating the seeds of various crops before sowing, potatoes and onions before storage, grain and grain products to destroy or sterilize insect pests, and so forth.

The best way of performing irradiation is to move the material continuously through the irradiator. This permits the most compact radiation shielding and highest productivity. However, it is most advantageous to move the material through the irradiator not by gravity flow but by forced flow. This method minimizes losses due to abnormal irradiation which occur when the plant is started and stopped and also ensures the greatest constancy and uniformity of motion of the material in the irradiator.

Despite the fact that forced flow permits simultaneous mixing, it is very desirable to get an adequate degree of uniformity of the dose field in the cross-sectional plane of the irradiated stream. On the other hand, variations in the dose rate along the flow path have no effect, because each object in turn traverses the various doses and the total energy absorption will be the same for all the objects.

One of the most popular irradiator configurations is the cylindrical. The greater the relative length of the irradiator (the ratio of the half-length to the radius, L/R), the greater the relative productivity. This follows from an elementary analysis of the relation between the working volume with permissible radiation nonuniformity and the relative length, L/R. The higher this quantity, the greater the permissible cross section of the flow of objects, i.e., the greater the productivity for a given irradiation nonuniformity.

However, the radiative efficiency of a cylindrical irradiator is relatively low (5-9 %). Therefore it is important to improve the productivity of the irradiator without abandoning forced flow of the objects: for this purpose it is convenient to have an additional linear source along the axis of the cylindrical irradiator. This retains the possibility of building a conveyor for forced motion of objects inside the irradiator.

The dose rate given by a linear source in air at any point p in its central cross-sectional plane is

$$P_{p \cdot 1} = \frac{2k_\gamma q}{nR} \text{arctg} \left(\frac{L}{R} \cdot \frac{1}{n} \right),$$

where nR is the distance of point p from the center as a fraction of the radius of the cylinder, $q = Q_c/2L$ (where Q_c is the total activity of the central linear source), and L is half the length of the cylindrical irradiator.

Let Q be the total activity and Q_s the activity of the sources on the cylindrical surface; then we have

$$Q = Q_s + Q_c.$$

Putting $Q_c = \delta Q$ and $Q_s = (1 - \delta)Q$, for the linear source we obtain

$$P_{p \cdot 1} = \frac{k_\gamma Q}{R^2} \cdot \frac{\delta}{n} \cdot \frac{1}{L/R} \text{arctg} \left(\frac{L}{R} \cdot \frac{1}{n} \right). \tag{1}$$

For a cylindrical surface in air we find

$$P_{p \cdot c} = \frac{4k_\gamma R q \pi}{R(1+n)} F(\varphi, k^2) = \frac{k_\gamma Q}{R^2} \cdot \frac{1-\delta}{1+n} \cdot \frac{1}{L/R} F(\varphi k^2). \tag{2}$$

Here $F(\varphi, k^2)$ is an elliptical integral of the first kind. Here

$$\varphi_0 = \text{arctg} \frac{1}{R(1-n)}; \qquad k^2 = \frac{4n}{(1+n)^2}.$$

64
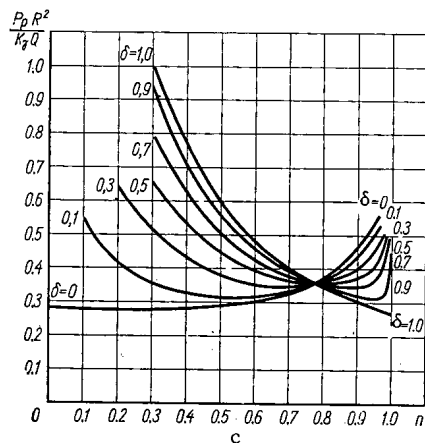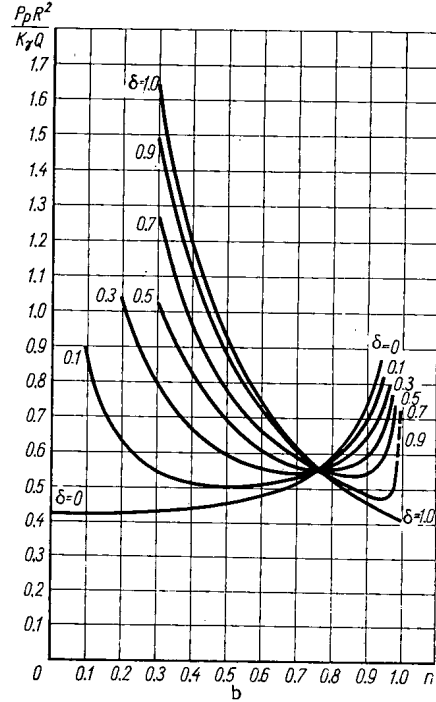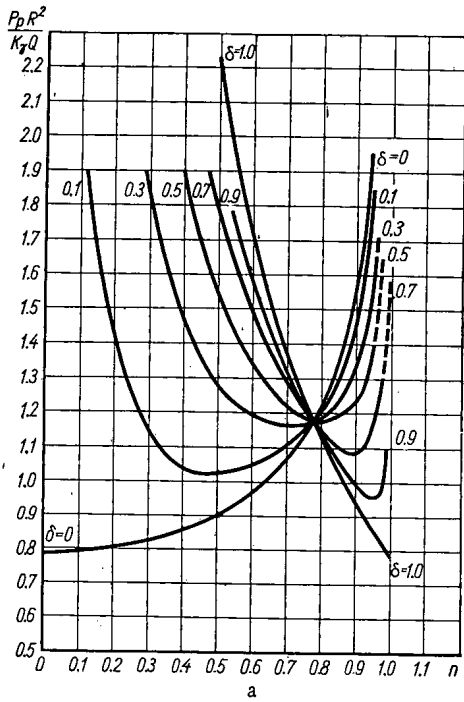
Fig. 1. Relative dose rate $\dfrac{P_p R^2}{k \gamma Q}$, plotted versus distance from central source, expressed as a fraction of the radius, for various values of δ. (a) L/R = 1; (b) L/R = 3; (c) L/R = 5.

Thus the dose rate in the central plane perpendicular to the axis of the cylinder will vary with the distance from the center, expressed as a fraction n of the radius of the cylindrical irradiator, according to the law

$$\frac{P_p R^2}{k_\gamma Q} = \frac{1}{L/R} \left[\frac{\delta}{n} \operatorname{arctg} \left(\frac{L}{R} \cdot \frac{1}{n} \right) + \frac{1-\delta}{1+n} F\left(\varphi,\, k^2\right) \right] . \qquad (3)$$

On the left-hand side we have the dose rate $P_p = P_{p.c} + P_{p.1}$ at point p divided by a multiplier which is constant for the given irradiator, $\dfrac{k \gamma Q}{R^2}$, and on the right-hand side we have a quantity which, for given L/R, depends only on δ and n.

Let us construct a family of curves, for various values of δ, as functions of n. Figures 1, a, b, c, are the curves of the dose rate along the radius of the cylinder (central plane) for various ratios between the activities of the linear and cylindrical sources, for three irradiators (L/R = 1, L/R = 3, L/R = 5).

We see that the dose rate has a minimum whose position depends on the activity distribution δ. If we are given the limiting permissible degree of irradiation nonuniformity, say ± 20%, then the minimum of $P_p R^2 / k \gamma Q$ is equal to 80% of the mean value, and the upper limit can be taken as approximately 140% of the minimum value, as the maximum permissible dose rate.

Drawing a line at the level of 140% of the minimum on the curve for a given value of δ, we get two maximum permissible dose rates — one close to the axis, the other near to the cylindrical surface. The interval between these values characterizes the width of the ring in which objects will receive a dose within given limits.

The area of this ring, $S = \pi R^2 (n_{max}^2 - n_{min}^2)$, characterizes the productivity of the irradiator for the given degree of nonuniformity.
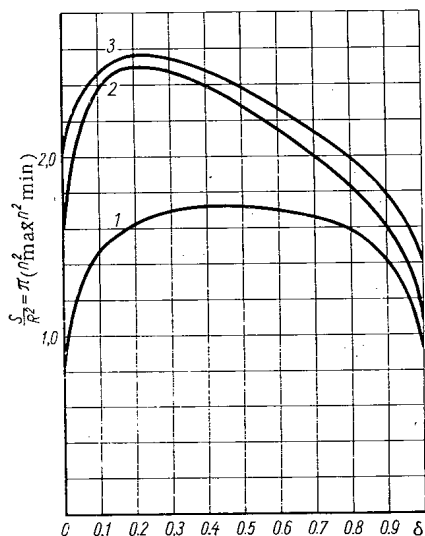
Fig. 2. Relative area, S/R^2, of ring with given uniformity of dose rate, plotted versus δ. (1) For ring-shaped irradiator; (2) for irradiator with $L/R = 1$; (3) for irradiators with $L/R = 3$ and $L/R = 5$.

Figure 2 plots the relative ring area S/R^2 versus δ. These curves reveal the following facts:

1. As L/R increases, the area increases somewhat, but when $L/R = 3$ or more it varies little. For comparison we give the graph of the relative ring area versus δ for an irradiator in which 2L is reduced to a minimum (a ring source), and which has a point source in the center. The variation of the field of such an irradiator along a radius is given by the expression

$$\frac{P_p R^2}{k_\gamma Q} = \left(\frac{\delta}{n^2} + \frac{1-\delta}{1+n^2} \right).$$

2. The relative area of the ring of moving objects is greatest when δ lies in the range 0.1-0.5. In this case the gain in productivity over the linear source alone is more than 200%, while that over the cylindrical source alone is about 165% [according to the curve for $L/R = 1$ (see Fig. 2)].

In addition, distribution of part of the total activity along the central axis of a cylindrical irradiator improves the efficiency of the irradiator.

For this type of irradiator, and for an irradiator in the form of a linear source surrounded by a layer of substance with unit density, the efficiency can be estimated as follows. As seen from Figure 1b, for an irradiator with $L/R = 3$, $\delta = 0.5$, and permissible nonuniformity ± 20%, the layer of substance can be (R(0.97 − 0.44)= 0.53 R, i.e., more than half of the radius of the cylindrical irradiator. This layer will therefore be situated almost up against the cylindrical surface. Taking R ≈ 20 cm, we find that more than 30% of the radiative energy of the central linear source will be usefully absorbed in the objects.

We can thus estimate the efficiency, taking $\eta = [(1 - \delta)\eta_c + 30\delta]\% = 100\ (0.5 \cdot 0.07 + 0.15)\% = 18.5\%$. In actual fact the efficiency will be even higher, because oblique rays are absorbed more strongly. For a linear source alone with R = 20 cm, the permissible layer thickness will not exceed R(1 − 0.75) = 0.25 R, i.e., 5 cm (see Fig. 1, b, $\delta = 1.0$). This layer of water-equivalent tissue absorbs about 10-12% of the radiation, i.e., the efficiency of an irradiator with only a linear source will be less than that of the suggested complex irradiator. When we consider the cylindrical irradiator alone, as already stated, its efficiency is found to be 5-9%, i.e., on the average one-third as great as the former. This estimate of the efficiency is merely qualitative, because it does not take account of dead angle along the axis of the linear source, in which there are no irradiated objects. Despite the qualitative nature of this estimate, it is clear that our suggested irradiator is also advantageous from the efficiency aspect.

LITERATURE CITED

1. Proceeding of Tashkent Conference on the Peaceful Uses of Atomic Energy, [in Russian], (Tashkent, 1959), Vol. 2, Tashkent, Izd. AN UzSSR (1960).
2. A. V. Bibergal' et al., Isotope γ-ray Equipment [in Russian], Moscow, Gosatomizdat (1960).

CORRELATION BETWEEN THE CONCENTRATIONS OF NATURAL AND FISSION-FRAGMENT RADIOACTIVE AEROSOLS IN THE SURFACE ATMOSPHERIC LAYER

A. É. Shem'i-zade

UDC 541.182.3:551.577.7

Investigations have shown that during a period of intense fallout of nuclear-fission fragments a correlation can be observed between their concentration in the surface layer and the concentration of radon-decay daughter products. Specimens of radioactive aerosols were collected by aspiration with FPP-15 filtering material. The diameter of the operating part of the filter was 42 mm, and the filtration rate was about 8 liters/min·cm². The volume of air passing through the filter was monitored with a gas meter and found to be 4000 liters. The air samples were taken at a height of 1.5 m above ground level.

An Sr^{90}-Y^{90} specimen was used as the standard for calibrating the radiometric apparatus used for measuring the rate of β decay in the naturally radioactive aerosol samples. The recording efficiency for the MST-17 counter was found to be 0.12; the average value of the relative square error of the radon-decay-product activity measurements was no more than 6%.

The relative method used for determining the recording efficiency is not suitable for calculating the activity of a mixture of fresh nuclear-fission products, since the spectrum of β-particle energies is not known a priori. Even when the composition of the fission-product mixture has been identified, it is not always possible to prepare a suitable control specimen.

A method for calculating the efficiency of recording of ionizing radiation is well known [1, 2]; it consists in calculating a number of corrections, which require a knowledge of the thickness of a layer which will attenuate the β radiation by 50%. The value we found for this was 60.6 ± 6.6 mg cm². The calculated value of measurement efficiency in this case was 0.40. The relative square error did not exceed 7.5%.

The specific activity of the emanation decay products was calculated by the formula

$$A' = 10.6 \cdot 10^{-15} \frac{n \varkappa_\beta}{\varepsilon'_{eff}} \text{ Ci/liter} \tag{1}$$

obtained for the experimentally determined value of the effective half-life of the emanation daughter products (35 min).

The specific activity of the fission-fragment products was calculated by means of the formula

$$A'' = \frac{n \varkappa_\beta}{\varepsilon''_{eff} V 2.22 \cdot 10^{12}} \text{ Ci/liter} \tag{2}$$

Here n is the counting rate in pulses/min; ε'_{eff} and ε''_{eff} are the recording efficiency values for the natural and fission-fragment activity, respectively; V is the volume of filtered air; $\varkappa_\beta$ is the absorption coefficient of β particles by the filter material.

The figure shows a correlation graph obtained by comparing the daily data on the concentration of β active aerosols of natural and fission-fragment origin for February-April, 1962. The value of the correlation coefficient

$$r = \frac{\Sigma (x_i - \bar{x})(y_i - \bar{y})}{V \Sigma (x_i - \bar{x})^2 \Sigma (y_i - \bar{y})^2} ,$$

calculated from the values of x and y shown in the figure, was found to be 0.780.

The change in the concentration of naturally radioactive aerosols in the air results from changes in a number of meteorological factors [3]. It may be assumed that some of these have an identical effect on the concentration of fission fragments in the surface atmospheric layer. Thus, increased turbulence in the surface layer may reduce not only the specific activity of radon and its daughter products but

67
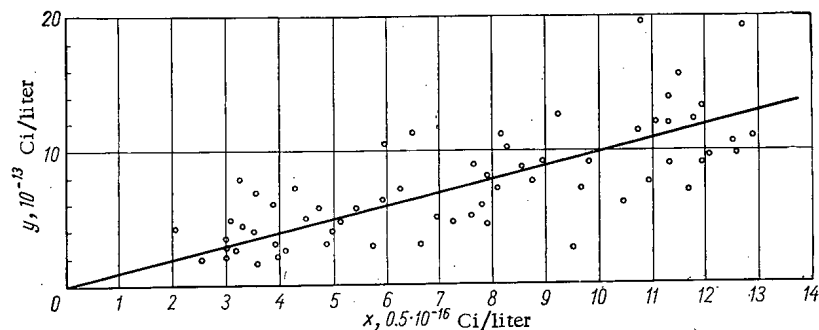
Fig. 1. Correlation graph for the concentration of natural and fission-fragment β-active aerosols.

also that of the fission fragments if their concentration has a negative gradient. The reverse relationship may exist between atmospheric turbulence and contamination with nuclear-fission fragments if the altitude gradient of fission-fragment concentration is positive, and this may explain the large deviation of some of the points in the figure.

The condition of the earth's surface, in turn, must affect the concentration of fragments in the atmosphere near the ground, since aerosol particles which have been deposited on dry soil may be lifted back into the atmosphere even by a slight wind [1]. It is known that the rate of release of radon from the surface of dry soil is faster than the rate from the surface of wet soil, and consequently this factor is also common to the two types of activity.

During the latest cases of world-wide fallout, no correlation was found between the volume concentrations of activity from natural and fission-fragment sources. Thus, in the summer of 1963 (July-August), the correlation coefficient was 0.184 for 30 pairs of values of the quantities under consideration. For February, 1964, the correlation coefficient was 0.171. It may be that this lack of any marked correlation during the latest world-wide fallout cases results from a general decrease in the concentration of fission-fragments in the atmosphere. The change in the dispersity of aerosols carrying radioactive products of nuclear fission may also affect the nature of their behavior during the latest stratospheric fallouts.

LITERATURE CITED

1. V. V. Bochkarev et al., Measurement of the Activity of Beta and Gamma Radiation Sources [in Russian], Moscow, Izd. AN SSSR (1953).
2. W. Price, Nuclear Radiation Detection, [Russian translation], Moscow, IL, (1960).
3. A. É. Shem'i-zade, Proceedings of the Scientific Conference Celebrating the Thirtieth Anniversary of the Institute. Collection of Scientific Works of the Uzbek Scientific Research Institute of Hygiene, Tashkent, Meditsina (1965).
4. B. I. Styro et al., Atomnaya Énergiya, 15, 339 (1963).

MEASUREMENT OF BACKGROUND EXPOSURE TO POPULATION
OF USSR CITIES, 1964-1965 PERIOD

I. A. Bochvar, A. A. Moiseev,
T. I. Prosina, and V. V. Yakubik

UDC 614.8;539.12.08

The program of measurement of annual doses of background external exposure of small groups of the population of some cities in the USSR was continued through the 1964-1965 period. The measurements were conducted with the aid of IKS personnal dosimeters, which use thermoluminescent aluminophosphate glass [1]. The experimental procedure was the same as earlier. Ten citizens from each city were instructed to carry dosimeters continuously on their persons for periods of 387 to 507 days, beginning with June 1964. After that period the dosimeters were collected and readings were taken. The error in individual dose determinations did not exceed ± 20%, with an additional error of ± 4 mrad. Results calculated for a one-year period are tabulated and compared with earlier data [2].

The doses obtained for 28 cities in the USSR fluctuated within the 50-150 mrad/year range. In seven cases out of 270, there were significant excesses over the averages, running as high as 570 mrad. These results are not tabulated. It is known that in two cases the subjects carrying dosimeters were exposed to x-rays during medical tests.

On the average, the external exposure dose throughout the USSR was approximately 90 mrad/year, which was in agreement with previous results.

External Background Exposure Doses to Population of Several Cities in the USSR

City	Exposure, days	Dose, mrad/year			Average dose in second half of 1963, mrad/year
		minimum	maximum	average	
Alma-Ata	387	120±28	200±44	160±10	110±18
Astrakhan	387	50±14	110±26	80±6	90±17
Ashkhabad	387	70±18	120±28	105±7	90±19
Baku	395	70±18	90±22	75±2	60±18
Vilnyus	387	90±22	140±32	100±6	70±22
Vladivostok	395	60±16	80±20	75±2	100±14
Dushanbe	507	100±24	170±40	130±6	—
Erevan	434	60±16	90±22	75±5	90±14
Irkutsk	398	70±18	140±32	110±7	120±22
Kiev	395	80±20	120±28	95±4	100±22
Kishinev	423	50±14	70±18	60±2	90±15
Leningrad	387	80±20	140±32	120±8	90±23
Lvov	387	80±20	120±28	100±4	110±21
Minsk	398	70±18	140±32	100±7	90±17
Moscow	398	70±18	110±26	90±5	—
Murmansk	387	90±22	150±34	110±10	130±26
Novosibirsk	507	60±16	90±22	80±3	100±11
Orenburg	387	60±16	110±26	80±4	50±16
Petropavlovsk-Kamchatskii	387	60±16	130±30	90±8	90±13
Riga	398	70±18	140±32	110±11	110±17
Sevastopol	427	30±10	60±16	45±3	40±12
Sochi	434	50±14	110±26	70±7	110±30
Tashkent	395	80±20	160±36	120±7	100±25
Tallin	387	60±16	120±28	90±5	110±22
Tbilisi	398	80±20	100±24	90±2	110±21
Khabarovsk	427	50±14	120±28	75±8	90±22
Chita	398	70±18	120±28	110±6	100±23
Yakutsk	427	50±14	100±24	70±6	70±21

LITERATURE CITED

1. I. A. Bochvar et al., Atomnaya Énergiya, 15, 48 (1963).
2. I. A. Bochvar et al., Atomnaya Énergiya, 19, 311 (1966).

RELATIVE NATURAL RADIOACTIVITY OF FÉU-49 PHOTOMULTIPLIERS

Yu. V. Sivintsev, V. A. Kanareikin,
and L. N. Serdyuk

UDC 539.107.43

In the radiometry of trace quantities of radioactive materials, the sensitivity of the detecting instrument is severely limited by naturally radioactive impurities in the materials of which it is made. In particular, a significant part of the background in scintillation counters may be due to the naturally radioactive isotope K^{40} present in the NaI(Tl) crystal, in the glass of its container, and in the photomultiplier envelope.
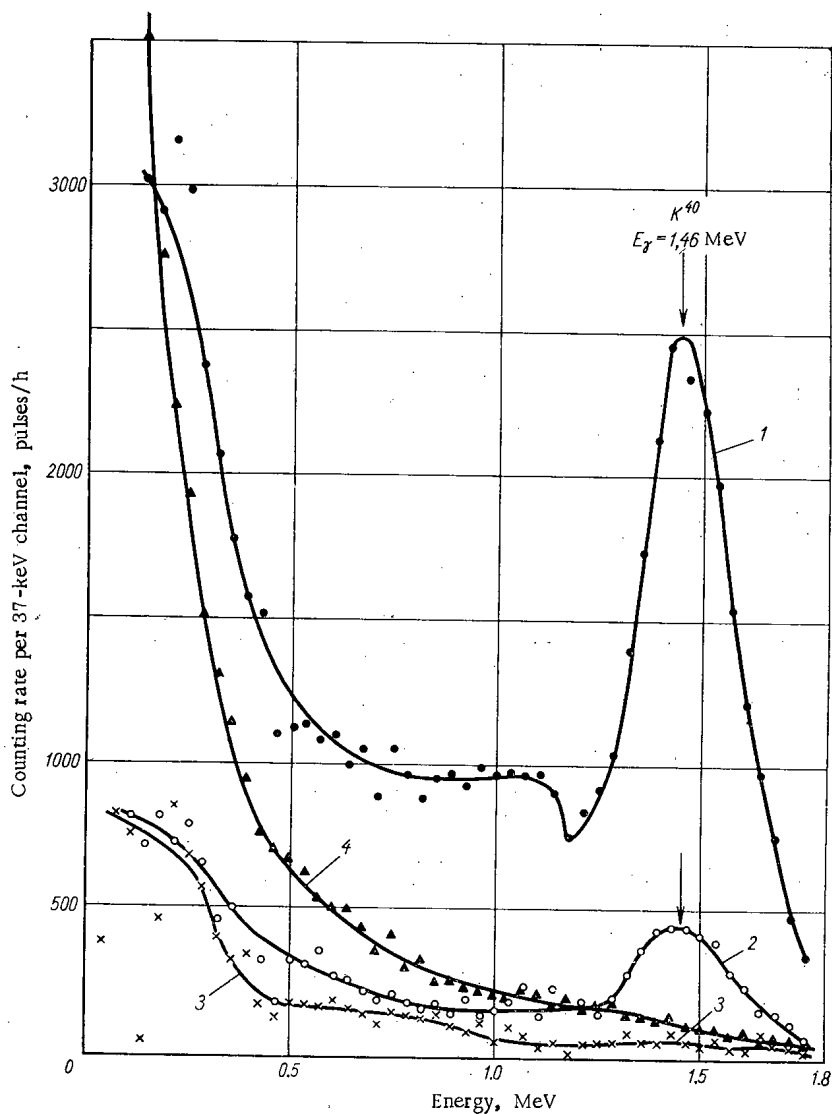
Fig. 1. Spectrograms of first series of measurements of the natural radioactivity of photomultipliers (after subtracting the (instrument background): 1) FÉU-49A No. 03; 2) FÉU-49B, No. 8179; 3) FÉU-44, No. 1410; 4) instrument background.

71

TABLE 1. Results of First Series of Instrument Background Measurements of Factory FÉU-49s.

Designation	Total counting rate in 37-1795-keV energy range		Counting rate for K^{40} in 1240-1795-keV energy range	
	Pulses/h	Relative units	Pulses/h	Relative units
Designation, -44, No. 1410	8580	1.00	790	1.00
Designation-49A, Experimental FEU-49A, No. 03	73670	8.59	22260	28.2
Designation-49, No. 7206	18060	2.21	4160	5.27
Designation-49B, No. 8048	17480	2.04	4100	5.18
Designation-49B No. 8179	15410	1.79	4320	5.47
Designation-49, No. 8186	17360	2.03	4060	5.15
Designation-49 No. 8190	18480	2.26	4260	5.39
Designation-49, No. 8191	16080	1.89	3560	4.50
Designation-49, No. 8245	14480	1.69	4100	5.18
Designation-49, No. 8247	16360	1.90	3580	4.53
Designation-49, No. 8258	14410	1.68	4310	5.46
Designation-49, No. 8263	17000	1.98	4320	5.47
Instrument background	74420	8.67	3600	4.56

TABLE 2. Results of Second Series of Measurements of Background Factory FÉU-49s (November 1965) *

Designation	Total counting rate in 74-1795-keV energy range		Counting rate for K^{40} in 1240-1795-keV energy range	
	Pulses/h	Relative units	Pulses/h	Relative units
Designation-44, No.1410	6200	1.00	480	1.00
Designation-49, No.1113	5440	0.88	520	1.08
Designation-49, No.1116	5290	0.85	420	0.88
Designation-49, No.1144	4330	0.70	400	0.83
Designation-49, No.1163	6280	1.01	440	0.92
Designation-49, No.9203	5780	0.93	500	1.04
Designation-49, No.9231	7010	1.13	600	1.25
Instrument background	35700	5.76	1890	3.94

*For technical reasons, the second series of measurements, made in November, 1965, used a different sensor with an NaI(Tl) crystal 140 mm in diameter and 50 mm thick. The background counting rate of this detector was 35,700 pulses/h for the 74-1795-keV energy range.

In connection with the problem of measuring the natural radioactivity of the human body, investigations were made of the reduction in the background counting rate of an NaI(Tl) scintillation counter shielded by large thicknesses of steel (20 cm) [1]. The result obtained (7450 pulses/hour per kg of scintillator) was due, in particular, to the use of an FÉU-44 (FÉU-2B), the envelopes of which are made of potassium-free glass (3C-5Na or C-49-1 brand).

However, the use of such photomultipliers, whose envelope has a convex front face, requires the use of light guides to maintain optical contact with the NaI(Tl) crystals. This seriously impairs the resolution of the spectrometric instruments.

In the design of the FÉU-49, which has a large diameter and a flat photocathode [2], it was considered important to determine the degree of radioactive purity for possible use in high-sensitivity radiometric and spectrometric equipment.

The measurements were made in a "steel chamber" measuring 2 × 2 × 2 m and surrounded on all sides by steel shielding 20 cm thick. For measuring the instrument background, we used as our γ-ray detector the sensor of a spectrometer previously installed in the steel chamber [3]. The instrument consisted of a sodium iodide crystal 200 mm in diameter and 50 mm thick, in a Duralumin container with a quartz window, an FÉU-44 in an envelope of potassium-free glass (the same brand as the glass in the FÉU-49 photomultipliers being tested), and a conical plexiglas light guide connecting them. Optical contact between the surfaces of the crystal, the light guide, and the FÉU was provided by lubricating them with mineral oil. The pulses from the preamplifier of the sensor were transmitted through a cable about 10 m long to an ADA-50D 50-channel pulse-height analyzer.

In the background measurements the FÉU-49 under investigation was placed with the photocathode down on the crystal of the aforementioned sensor, which was mounted in a vertical position with the

72
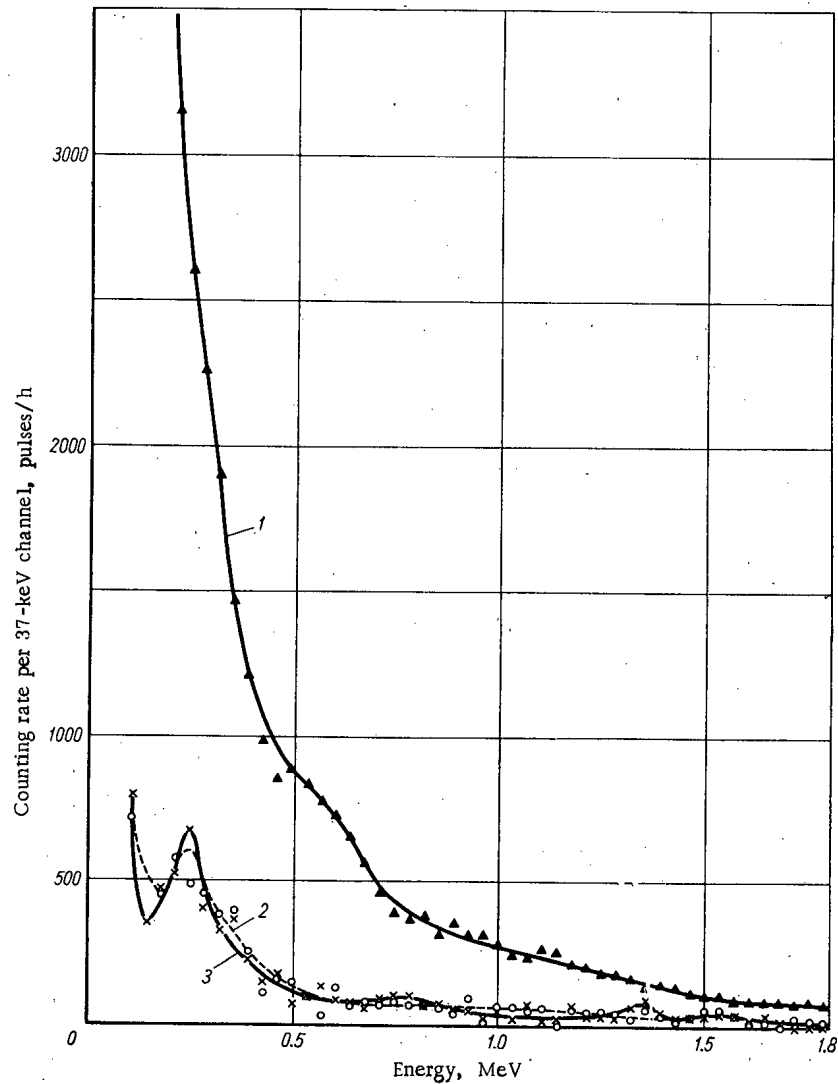
Fig. 2. Spectrograms of second series of measurements of natural activity of photomultipliers (2, 3 show data after the instrument background has been subtracted): 1) Instrument background; 2) FÉU-49, No. 1116; 3) FÉU-44, No. 1410.

crystal upward. From the number of pulses recorded per hour in each channel (the channels were 37 keV wide) we subtracted the background of the empty chamber, which had been measured separately. The background counting rate resulting from the activity of the photomultiplier being tested was found by adding the readings of channels 2-49 (37-1795 keV).

As a measure of the quantitative estimate of the potassium content in the glass of the photomultiplier, we used the counting rate (pulses/hour) at the photopeak found for the recording of K^{40} γ quanta (with energies of 1.46 MeV) in channels 34-49 (1240-1795 keV). In order to obtain the relative values in the same geometry, we used an FÉU-49A in an envelope of potassium glass (brand ZS-5K or C-49-2) and an FÉU-44 in an envelope of potassium-free glass of the aforementioned brand. The counting rate of the latter FÉU was taken to be 1.00.

The results of the corresponding measurements, made in October, 1964, are shown in Table 1 and Fig. 1.

On the basis of these measurements, the K^{40} content of the FÉU-49s manufactured in October 1965 was reduced to a level close to the level of the FÉU-44 used as a standard. The data of Table 2 indicate that the average counting rates resulting from the K^{40} in the FÉU-49 and in the FÉU-44 are equal.

73

The following conclusions may be drawn from the data of the first series of measurements:

1) The potassium content in the envelopes of the FÉU-49s which were manufactured at the factory in August, 1964, using potassium-free glass, was reduced (for the average of 10 sample FÉU-49s) by a factor of 5.4 in comparison with the experimental FÉU-49A which had an envelope of potassium glass.

2) The factory's FÉU-49's still contain measurable amounts of potassium, and therefore their instrument background in the region of the recorded photopeak of the K^{40} γ quanta is 5.2 times as great, on the average, as the corresponding readings for the FÉU-44, which has an envelope made of potassium-free glass of the same brand.

From comparison of the data on the chemical composition of C-49-1 and C-49-2 molybdenum glasses we were able to conclude that the sodium glass is completely free of potassium and has a higher general purity. Thus, the presence of potassium in the factory's FÉU-49s may be due to several different causes:

1) Some components used in the assembly of the FÉU-49 contain large amounts of naturally and artificially radioactive substances (in comparison with the background).

2) The original raw material used for the C-49-1 glass at the factory was contaminated with naturally or artificially radioactive substances with a higher radioactivity than the background.

3) The original raw material is relatively free of radioactive impurities, but the glass made from it contains potassium which entered the melt from the walls of the crucible (such a process has been observed in the manufacture of especially pure single crystals of sodium iodide [1]).

In order to find the true cause and to reduce the K^{40} content still further, the manufacturing plant has worked out measures designed to eliminate the latter two causes. A comparison of the spectrograms of the second series of measurements (Fig. 2) indicates that the residual background in the two photomultipliers is due to similar radioactive materials.

As a result of the above work, it was found that using the factory's FÉU-49 in scintillation counters with NaI(Tl) shielded with a very thick (20 cm) layer of steel makes it possible to reduce the background counting rate to 6000–8000 pulses/h per kg of scintillator.

LITERATURE CITED

1. Yu. V. Sivintsev et al., In the book "Proceedings of the Fifth Scientific and Technical Conference on Nuclear Radioelectronics" [in Russian], Vol. III, Moscow, Gosatomizdat, p. 138 (1963).
2. G. S. Vil'dgrube, N. N. Danilenko and A. I. Razumovskaya, Pribory i tekhnika éksperimenta, 6, No. 4, 74 (1961).
3. Yu. V. Sivintsev et al., Atomnaya Énergiya, 18, 141 (1965).

NEWS OF SCIENCE AND TECHNOLOGY

UKRAINE'S SECOND CONFERENCE ON ORDERING OF ATOMS AND ITS EFFECT ON PROPERTIES OF ALLOYS

V. I. Ryzhkov and B. I. Nikolin

The second conference on ordering of atoms and the effect of this ordering on the properties of alloys was held in Kiev, May 31 through June 7, 1966. The conference revealed that Soviet metal physicists have completed a good deal of interesting experimental studies of ordered alloys and development of underlying theory in the time elapsed since the first conference was held.

About 90 reports were delivered at the conference, which was attended by 230 delegates. The papers could be grouped under the headings: theory of atomic ordering in alloys, effect of different factors on ordering, effect of ordering on the major properties of alloys, experimental measurement of degree of ordering in alloys, ordering kinetics, plus five review papers.

V. I. Iveronova and A. A. Katsnel'son discussed different types of close-order effects: statistical close order, short-range stratification effects, short-range order in domains and at lattice defects. The report discussed the relationship between short-range order and certain physical properties of alloys. A. A. Smirnov gave an account of recent work at the Institute of Metal Physics of the Academy of Sciences of the Ukrainian SS^R on theoretical investigation of atomic ordering and spin ordering processes in complex alloys. Ya. P. Selisskii analyzed research findings on ordering in ternary alloys with face-centered and body-centered cubic lattices. L. I. Vasil'eva and A. N. Orlova briefly described basic concepts on dislocations and plastic flow in ordered alloys.

Statistical theory on ordered alloys and theoretical determination of the possible structures of ordered phases received close attention.

Theoretical results on the effect of pressure on ordering of atoms in alloys were presented. Some of the papers dealt with phenomena occurring on antiphase boundaries in ordered alloys.

Neutron diffraction studies of Ni — Mn alloys revealed a tetragonal lattice structure, and a study of Fe — Cr alloys of stoichiometric composition Fe_3Cr showed chromium segregation. Neutron diffraction was employed in a study of ordering in the alloy Ni_3Fe labeled with Ni^{62}. Ordering effects of neutron bombardment were found in the alloy Ni_3Mn, and information was also reported on radiation effects on diffusion processes in ordered alloys.

Some papers discussed the effect of molybdenum and chromium added to Fe—Al alloys on ordering, the effect of certain kinds of deformations on ordering, and the effect of ordering on hardening, plasticity, and failure stress in certain alloys (Ni_3Mn, Ni_3Fe), on magnetic anisotropy, hysteresis, magnetization, and diffusion in alloys, and particularly on the rate of hydrogen penetration into Ni—Mn, Ni—Fe, and Fe—Co alloys.

The reports stimulated interest in the possible use of the Mössbauer spectrum to monitor the ordering process, as well as interest in the electrical resistivity of modulated structures and in ordering kinetics in Fe—Ni, Mo—Ni, and Mg—Cd alloys.

BRIEF COMMUNICATIONS

CONFERENCE OF COMECON SPECIALISTS

The Permanent Commission on the Uses of Atomic Energy for Peaceful Purposes of the Council for Economic Mutual Aid convened a conference of specialists from COMECON member nations, June 7-11, 1966, to discuss standardization in the packaging and shipping of radioactive materials. Specialists from Bulgaria, the German Democratic Republic, Poland, Rumania, the USSR, and Czechoslovakia took part.

The conference discussed classification and defining of packages, crates, casks, etc., and basic variables and general technical specifications relating to them.

Different containers and packaging units are currently in use in different countries, and even within the confines of a single country, for shipping radioactive materials.

In the USSR, products with hard β radiation and the accompanying γ bremsstrahlung are shipped in TsR type or KIZ-41 type containers with lead insert lining. Gamma sources are shipped in lead containers of different designs. Sample sources are shipped in wooden or plastic cases enclosed in wooden boxes, and these boxes are not mass produced. The containers and shipping packages used for radioactive materials feature a wide variety of designations and classification symbols, and some have no identification at all.

This state of affairs certainly illustrates the need for unification and standardization of packages and containers for radioactive materials.

The main point under discussion in the draft recommendations on standardization of shipping packages for radioactive substances was reduction in the number of types of containers and packages, design improvements, and improvements in performance and external appearance.

The purpose of the standardization is also to bring about conditions facilitating centralized quantity production of shipping containers.

Recommendations on standardization of shipping packages were set forth in strict observance of the IAEA "Rulers for Safe Shipping of Radioactive Materials," and the "Rules for Shipping Radioactive Materials for COMECON Nations" elaborated on the basis of suggestions advanced by those countries.

The plan of recommendations was extended to packages for shipping all radioactive substances, with the exception of those requiring special packaging (e.g., high-level γ emission sources). Depending on mechanical strength and refractoriness, packages can be classified as either type A or type B. Packages are arbitrarily divided into three groups depending on the physical characteristics of the radiation emitted by the materials.

The proposed nomenclature for packages includes all packages, weighing anywhere from 6 kg to 2 tons, employed for shipping radioactive materials of any activity.

In addition to recommendations on standardization of shipping packages for radioactive materials, a plan of recommendations of standardized testing of shipping packages for radioactive materials is also being worked out at this time.

POLISH SUMMER SCHOOL ON IMPERFECTIONS IN CRYSTALS

AND CRYSTAL RESEARCH TECHNIQUES

A summer school devoted to "imperfections in crystals and methods for studying them" was held at Zakopane (Poland), in June 1966. A large group of lecturers from different countries was on hand to address over 60 students.

Review tutorial lectures on general aspects of the theory of imperfections in crystals, current topics in dislocation theory, the motion of point defects, the dynamic theory of electron scattering, and general problems in electron-microscopic study of crystal lattice defects were presented. Some of the lectures discussed the dynamical theory of x-ray scattering by perfect absorbing crystals, and the application of dynamic effects to the study of defects, as well as new techniques such as electron para-magnetic resonance and nuclear magnetic resonance, and advanced acoustical and optical techniques.

BOOK REVIEWS

Erich H. Schulz. VORKOMMNISSE UND STRAHLENUNFÄLLE IN KERNTECHNISCHEN ANLAGEN* (Cases and Radiation Accidents in Nuclear Facilities) [In German]

The book discusses and reviews over 1000 accidents involving exposures in nuclear facilities over more or less the past twenty years of development of nuclear science and industry in various countries throughout the world.

The book consists of four sections and several appendices.

The first two small sections present typical characteristics of major nuclear plants and facilities, such as reactors, accelerators, nuclear fuel production and processing facilities, and the like, and discuss national nuclear power development programs in ten of the world's most highly developed countries.

The third section offers a brief treatment of the basic recommendations of the international commission on radiation shielding, describes characteristic symptoms of overexposure in humans and some serious radiation injuries, and lists the most widespread formation reactions of radioactive isotopes and information on some reactors and radiochemical facilities in existence.

Here we find extensive tabular data on accidents and a detailed analysis of the most important cases. All the accidents are divided under the following ten headings:

1) uncontrolled runaways of critical assemblies, reactors, and nuclear chemical facilities; 2) power reactor accidents; 3) accidents at research reactors, experimental reactors, and material-testing reactors; 4) accidents at production reactors; 5) accidents involving maritime-propulsion reactors and space-propulsion reactors; 6) accidents at accelerator facilities; 7) accidents in radiochemical plants, and accidents occurring in the use of radioisotopes in industry and in scientific research and medical institutions; 8) accidents in shipping of radioactive and fissionable materials; 9) accidents in the Plowshare underground nuclear explosion testing program; and 10) accidents in testing and transportation of nuclear weapons. Accidents under the first three headings receive the most detailed analysis. A small concluding section presents some accident statistics concerning nuclear facilities and transportation of passengers in road and air carriers.

The appendices describe some accidents occurring at x-ray facilities in West Germany and in the use of radioactive preparations in medicine. The subject index is accompanied by a special index which facilitates locating specific accidents of interest to the reader.

This book will be useful to specialists in nuclear industry and nuclear science, and will be of great interest to readers concerned with nuclear safety in the design and use of nuclear facilities.

---

*K. Thiemig publ., Munich, 425 pages, 68 illustrations, 1966.

PUBLICATIONS OF GODDARD SPACE FLIGHT CENTER

VOL. I. SPACE SCIENCES*

This first volume of a collection of works of the Goddard Space Flight Center publishes 1963-1964 results. The extensive volume is divided into eight parts: astronomy and astrophysics (23 articles); 2) flight mechanics of artificial bodies and geodesy (27 articles); 3) solar physics (9 articles); 4) ionospheric physics (21 articles); 5) fields and particles (43 articles); 6) planetology (7 articles); 7) atmospheres of the planets (19 articles); 8) general topics (11 articles). Each article, as a rule, is accompanied by a detailed bibliography (mainly reports of NASA centers). The appendices offer a bibliographic list of articles related to the research published and an authors' index.

INTERNATIONALES LUMINESZENZ-SYMPOSIUM ÜBER DIE

PHYSIK UND CHEMIE DER SZINTILLATOREN† (International

Luminescence Symposium on Physics and Chemistry of Scintillators). [In German]

This is a collection of reports submitted at a symposium held in Munich, September 5-9, 1965, in seven sections. The first four sections deal with general topics. The first section takes up energy transport in a scintillator. This includes theoretical articles on various types of intermolecular bonds and the relative roles they play in energy transport, plus some experimental research.

The second section studies the time behavior of scintillators. Results of measurements of de-excitation time of some gaseous and liquid scintillators are cited, and a description is given of procedures for measuring short de-excitation times. An interesting article by J. B. Birks discusses the theory of the scintillation process in organic scintillators and possible improved methods for indentifying the mode of radiation recorded by a scintillation detector.

The third and fourth sections go into the physical and chemical properties of scintillators and changes they undergo in response to radiation. The last sections deal with the properties of specific scintillators and phosphors. A good deal of attention is given to compounds incorporating rare earths and halogens. Results of a study of different activators are cited. Some of the articles discuss inorganic phosphors such as CdF, $CuCl$, $LaMnO_4$, and others. Mention is made of the compound YVO_4 activated by europium, which is usable as a coating for kinescopes in color television. Many of the papers dealt with research on the electroluminescence of manganese-doped and copper-doped ZnS, Cds, and ZnO.

The book will be interesting to specialists on scintillators, but also to those physicists for whom scintillation detectors are a basic tool.

---

* U.S. Government Printing Office, Washington, 1666 pages, 1965.
† K. Thiemig publ., Munich, 471 pages, 1966.

NEUTRON DETECTORS*

This is a bibliography on neutron detectors, taking up such areas of application of these instruments as recording of neutron emission and neutron spectrometry and dosimetry. Most of the references, about 2000 in all, contain comments. The bibliography is compiled on the basis of material appearing from 1947 through 1965 in books, periodicals, reports of IAEA member nations, and the principal abstract journals.

PRACTICES IN THE TREATMENT OF LOW AND INTERMEDIATE-LEVEL RADIOACTIVE WASTES †

This book contains the proceedings of the international symposium on treatment of radioactive wastes of low and intermediate specific activity, held in Vienna in December 1965 [see Atomnaya Énergiya, 21, 72 (1966)]. 53 reports, and stenograms of the discussions, are published in their original languages (mostly in English, but seven in Russian, nine in French, and one in Spanish). The reports are grouped in four sections: 1) practises in the treatment of wastes in different countries (11 reports); 2) experience in the use of existing facilities (29 reports); 3) treatment of solid wastes (7 reports); and 4) special techniques (11 reports). The book ends with remarks by R. Berns on the occasion, a list of session chairmen and secretaries, a list of symposium participants, and an authors' index.

J. Selman. THE FUNDAMENTALS OF X-RAY AND RADIUM PHYSICS‡

This is a basic manual on the physics of x-radiation and γ-radiation, appearing in its fourth edition in the USA, and consisting of 23 sections: 1) simple mathematical relationships; 2) radiation measurement units; 3) physical meaning of energy; 4) the structure of matter; 5) static electricity; 6) electric current; 7) magnetism; 8) electromagnetism; 9) electric generators and motors; 10) generation and monitoring of high voltages; 11) generation of direct current; 12) x-radiation; 13) modern x-ray tubes; 14) electrical circuits for x-ray equipment; 15) x-ray screens and image intensifiers; 16) darkrooms in x-ray cabinets; 17) photographic processing of x-ray plates; 18) image quality of x-ray pictures;

---

*Bibliographic series, No. 18, IAEA, Vienna, 401 pages, 1966.
†IAEA, Vienna, 952 pages, 1966.
‡Charles C. Thomas publisher, Springfield, Illinois, USA, 4th edition, XXVI +468 pages, 1965.

19) methods for improving x-ray image quality; 20) special x-ray procedures; 21) radioactivity — radium; 22) radioactive isotopes and artificial radioactivity; 23) shielding and dosimetry in radiology.

All the chapters are written very simply and are within the reach of the average technical reader. The book ends in an appendix containing answers to questions posed in the body of the text, a small bibliography, and very detailed authors and subject indexes.

G. S. Vozzhenikov. AKTIVATSIONNYI ANALIZ V RUDNOI GEOFIZIKE * (Activation Analysis in Mining Geophysics)

This brochure describes activation methods for studying artificial radioactivity as used in ore-prospecting work. It also discusses activation assay of copper pyrite ores in boreholes, analyzes the prerequesites and explains the procedure of coreless determination of linear copper reserves in ore intervals of exploration boreholes, and cites examples from field practice.

The list of literature appended contains 55 references, 51 of them in Russian.

ADVANCES IN TRACER METHODOLOGY.†

This is the second volume appearing in a new periodical series, and contains the proceedings of the VI to the VIII American symposia on methods for utilizing labeled atoms, with symposium contributions grouped under several topic headings. After a tutorial review paper by M. Kamen, a well known specialist in radiometry, on the history of the discovery of isotope C^{14}, there follow six papers on various aspects of the production of tagged compounds (mainly C^{14} and H^3). Special analytical techniques are the subject matter of nine papers (chiefly dealing with H^3 and C^{14} liquid scintillation counters and methods for processing chromatograms). Five articles coming next deal with the use of labeled compounds in biochemistry. A section on clinical applications offers 13 reports (including papers on preparations using H^2, C^{14}, I^{131}, I^{125}, P^{32}, and other isotopes). A concluding article is devoted to the planning of radioisotope laboratories. There is a brief subject index.

81

APPLICATION OF FOOD IRRADIATION IN DEVELOPING COUNTRIES *

In August 1964, IAEA sponsored, jointly with FAO, a meeting of experts to discuss the potential use of ionizing radiation for lengthening the shelf and storage life of foodstuffs in developing countries. In 1966, IAEA published a symposium of articles, 16 in number, on the topic, with a report on the meeting.

A contribution by S. Goldblat (USA) presents the major problems involved in lengthening the storage time of foodstuffs. Fish constitutes one of the main sources of protein in the diet of peoples populating the African continent, and six papers deal with this food category: K. Shea (USA), D. Rhodes et al. (Britain), A. Kardashev (USSR), J. Daget (Chad), M. Boiset et al. (France), K. Abrahamsson et al. (Sweden) discuss various aspects of utilization of sources of ionizing radiation to lengthen storage time of fish products.

The remaining contributions deal with lengthening the storage life of vegetables, fruits, and fruit juices by irradiation treatment.

PROBLEME DES BAUTECHNISCHEN STRAHLENSCHUTZES. †

(Civil Engineering Problems in Radiation Shielding) [In German]

This is the sixth report of the West German society on the uses of atomic energy in shipbuilding and maritime practice, containing some of the reports delivered in late 1965 at a session of a special commission on radiation shielding, a combined organ of the above society and the Atomforum of West Germany.

The reports are devoted to experimental research on shielding compositions and structures, and certain theoretical aspects in biological shielding calculations.

Reports placed in the first group take up procedures for simplifying biological shielding calculations on the basis of pencil-beam experimental data; results of experiments designed to study the efficiency of shielding structures with holes or channels in the shields; and results of experimental and theoretical work on multilayer shielding compositions in recent research by a team of radiation shielding experts at a West German reactor. There is a treatment of procedures and experimental research findings pertaining to a model of power reactor shielding, with particular emphasis on the accuracy of computational methods, and a discussion of the characteristics of iron-water shields.

Several short papers in the second group are devoted to numerical methods for the solution of the Boltzmann transport equation, procedures for calculating transmission and reflection of radiation, and optimization of biological shielding in terms of weight and cost. Program and results of γ-ray buildup factor calculations in layered media are also given.

The book is written for specialists in the field.

---

* Technical Reports Series, No. 54, IAEA, Vienna, 180 pages, 1966.
† E. Bagye, Verlag K. Thiemig, Munich, 132 pages, 47 illustrations, 1966.

IAEA LABORATORY ACTIVITIES *; Third Report

This is the third report furnishing information on the principal results of IAEA laboratory research in 1965. Most of the brochure consists of notes and comments on work by the Vienna and Seibersdorf laboratories. These are grouped in seven sections: 1) physical research (standardization and dosimetry groups); 2) chemical research (analytical group and laboratory for measuring low-activity samples); 3) hydrological research; 4) medical physics; 5) agriculatural research; 6) electronics; 7) administrative problems. Most of the book is given over to a description of the activities of the International Laboratory for the Study of Marine Activity (Monaco), the International Center for Theoretical Physics (Trieste), and the Near East Regional Radioisotope Center for the Arab Countries (Cairo).

---

* Technical Reports Series, No. 55, IAEA, Vienna, 158 pages, 1966.

83

SIGNIFICANCE OF ABBREVIATIONS MOST FREQUENTLY ENCOUNTERED IN SOVIET PERIODICALS

FIAN	Physi. Inst. Acad. Sci. USSR
GDI	Water Power Inst.
GITI	State Sci.-Tech. Press
GITTL	State Tech. and Theor. Lit. Press
GONTI	State United Sci.-Tech. Press
Gosenergoizdat	State Power Press
Goskhimizdat	State Chem. Press
GOST	All-Union State Standard
GTTI	State Tech. and Theor. Lit. Press
IL	Foreign Lit. Press
ISN (Izd. Sov. Nauk)	Soviet Science Press
Izd. AN SSSR	Acad. Sci. USSR Press
Izd. MGU	Moscow State Univ. Press
LEIIZhT	Leningrad Power Inst. of Railroad Engineering
LET	Leningrad Elec. Engr. School
LETI	Leningrad Electrotechnical Inst.
LETIIZhT	Leningrad Electrical Engineering Research Inst. of Railroad Engr.
Mashgiz	State Sci.-Tech. Press for Machine Construction Lit.
MEP	Ministry of Electrical Industry
MES	Ministry of Electrical Power Plants
MESEP	Ministry of Electrical Power Plants and the Electrical Industry
MGU	Moscow State Univ.
MKhTI	Moscow Inst. Chem. Tech.
MOPI	Moscow Regional Pedagogical Inst.
MSP	Ministry of Industrial Construction
NI ZVUKSZAPIOI	Scientific Research Inst. of Sound Recording
NIKFI	Sci. Inst. of Modern Motion Picture Photography
ONTI	United Sci.-Tech. Press
OTI	Division of Technical Information
OTN	Div. Tech. Sci.
Stroiizdat	Construction Press
TOE	Association of Power Engineers
TsKTI	Central Research Inst. for Boilers and Turbines
TsNIEL	Central Scientific Research Elec. Engr. Lab.
TsNIEL-MES	Central Scientific Research Elec. Engr. Lab.-Ministry of Electric Power Plants
TsVTI	Central Office of Economic Information
UF	Ural Branch
VIESKh	All-Union Inst. of Rural Elec. Power Stations
VNIIM	All-Union Scientific Research Inst. of Metrology
VNIIZhDT	All-Union Scientific Research Inst. of Railroad Engineering
VTI	All-Union Thermotech. Inst.
VZEI	All-Union Power Correspondence Inst.

Note: Abbreviations not on this list and not explained in the translation have been transliterated, no further information about their significance being available to us. — Publisher.

SOVIET JOURNALS AVAILABLE IN COVER-TO-COVER TRANSLATION

This list includes all Russian journals which—to the publisher's knowledge—were available in cover-to-cover translation on June 30, 1965, or for which definite and immediate plans for cover-to-cover translation had been announced by that date. The list reflects only *current* publication arrangements, but the date and issue listed for first publication refer to translations available from any source. Thus, earlier volumes of a translation journal may have been published by an organization other than that listed as the current publisher, and possibly under a different title (and, for *Doklady Akademii Nauk SSSR*, in a different arrangement of sections).

Five bits of information are furnished, separated by bullets:

1. The abbreviation(s) by which the journals are most frequently referred to in Russian bibliographies (if the name of the journal is customarily spelled out, no abbreviation is given).
2. The transliterated full name of the journal.
3. The full name of the translation journal (in bold type).
4. The year, volume (in parentheses), and issue of first publication of the translation (parentheses are empty if the Russian journal does not use volume numbers).
5. The current publisher of the translation [AGI—American Geological Institute, AGU—American Geophysical Union, AIP—American Institute of Physics, CB—Consultants Bureau, CH—Clearing House for Federal Scientific and Technical Information, CS—The Chemical Society (London), FP—Faraday Press, IEEE— Institute of Electrical and Electronic Engineers, ISA—Instrument Society of America, PP—Pergamon Press].

For convenience in locating bibliographic references the journals are listed in alphabetical order of the *abbreviated* titles.

AÉ • Atomnaya énergiya • **Soviet Journal of Atomic Energy** • 1956(1)1 • CB

Akust. zh. • Akusticheskii zhurnal • **Soviet Physics—Acoustics** • 1955(1)1 • AIP

Astrofiz. • Astrofizika • **Astrophysics** • 1965(1)1 • FP

Astr(on). zh(urn). • Astronomicheskii zhurnal • **Soviet Astronomy—AJ** • 1957(34)1 • AIP

Avtomat. i telemekh. • Avtomatika i telemekhanika • **Automation and Remote Control** • 1956(27)1 • ISA

Avto(mat). svarka • Avtomaticheskaya svarka • **Automatic Welding** • 1959(12)1 • British Welding Research Association

Avtometriya • **Autometry** • 1965(1)1 • CB

Biokhim. • Biokhimiya • **Biochemistry** • 1956(21)1 • CB

Byul. éksp(erim). biol. (i med.) • Byulleten' éksperimental'noi biologii i meditsiny • **Bulletin of Experimental Biology and Medicine** • 1959(41)1 • CB

DAN (SSSR) • *see* Doklady AN SSSR

Defektoskopiya • **Soviet Defectoscopy** • 1965(1)1 • CB

Diff. urav. • Differentsial'nye uravneniya • **Differential Equations** • 1965(1)1 • FP

Dokl(ady) AN SSSR; DAN (SSSR) • Doklady Akademii Nauk SSSR • The translation of Doklady is published in various journals, according to subject matter. The sections of Doklady contained in each of the translation journals are listed in parentheses.

Doklady Biochemistry (biochemistry) • 1957(112)1 • CB

Doklady Biological Sciences Sections (anatomy, cytology, ecology, embryology, endocrinology, evolutionary morphology, parasitology, physiology, zoology) • 1957(112)1 • CB

Doklady Biophysics (biophysics) • 1957(112)1 • CB

Doklady Botany (botany, phytopathology, plant anatomy, plant ecology, plant embryology, plant physiology, plant morphology) • 1957(112)1 • CB

Doklady Chemical Technology (chemical technology) • 1956(106)1 • CB

Doklady Chemistry (chemistry) • 1956(106)1 • CB

Doklady Earth Sciences Sections (geochemistry, geology, geophysics, hydrogeology, lithology, mineralogy, paleontology, permafrost, petrography) • 1959(124)1 • AGI

Doklady Physical Chemistry (physical chemistry) • 1957(112)1 • CB

Doklady Soil Science (soil science) • 1964(154)1 • Soil Science Society of America

Soviet Mathematics—Doklady (mathematics) • 1960(130)1 • American Mathematical Society

Soviet Oceanography (oceanology) • 1959(124)1 • AGU

Soviet Physics—Doklady (aerodynamics, astronomy, crystallography, cybernetics and control theory, electrical engineering, energetics, fluid mechanics, heat engineering, hydraulics, mathematical physics, mechanics, physics, technical physics, theory of elasticity • 1956(106)1 • AIP

Élektrokhimiya • **Soviet Electrochemistry** • 1965(1)1 • CB

Élektrosvyaz' • combined with Radiotekhnika in **Telecommunications and Radio Engineering** • 1957(16)1 • IEEE

Élektrotekh. • Élektrotekhnika • **Soviet Electrical Engineering** • 1965(36)1 • FP

Éntom(ol). oboz(r). • Éntomologicheskoe obozrenie • **Entomological Review** • 1958(37)1 • Entomological Society of America

Fiz. goreniya i vzryva • Fizika goreniya i vzryva • **Combustion, Explosion, and Shock Waves** • 1965(1) • FP

Fiziol(ogiya) rast. • Fiziologiya rastenii • **Soviet Plant Physiology** • 1957(4)1 • CB

Fiz.-khim. mekh(anika) mater(ialov); FKhMM • Fizikokhimicheskaya mekhanika materialov • **Soviet Materials Science** • 1965(1)1 • FP

Fiz. met. i metallov.; FMM • Fizika metallov i metallovedenie • **Physics of Metals and Metallography** • 1957(5)1 • Acta Metallurgica

Fiz.-tekhn. probl. razr. polezn. iskopaem. • Fizikotekhnicheskie problemy razrabotki poleznykh iskopaemykh • **Soviet Mining Science** • 1965(1)1 • CB

Fiz. tv(erd). tela; FTT • Fizika tverdogo tela • **Soviet Physics—Solid State** • 1959(1)1 • AIP

FKhMM • *see* Fiz.-khim. mekhanika materialov

FMM • *see* Fiz. met. i metallov.

FTT • *see* Fiz. tverd. tela

Geliotekh. • Geliotekhnika • **Applied Solar Energy** • 1965(1)1 • FP

Geol. nefti i gaza • Geologiya nefti i gaza • **Petroleum Geology** • 1958(2)1 • Petroleum Geology, Box 171, McLean, Va.

Geomagnet. i aéronom. • Geomagnetizm i aéronomiya • **Geomagnetism and Aeronomy** • 1961(1)1 • AGU

Inzh.-fiz. zh. • Inzhenerno-fizicheskii zhurnal • **Journal of Engineering Physics** • 1965(8)1 • FP

Inzh. zh. • Inzhenernyi zhurnal • **Soviet Engineering Journal** • 1965(5)1 • FP

Iskusstv. sputniki Zemli • Iskusstvennye sputniki Zemli • **Artificial Earth Satellites** • 1958(1)1 • CB [superseded by Kosmich. issled.]

Izmerit. tekhn(ika) • Izmeritel'naya tekhnika • **Measurement Techniques** • 1958(7)1 • ISA

Izv. AN SSSR, o(td.) kh(im.) n(auk) (*or* ser. khim.) • Izvestiya Akademii Nauk SSSR: Otdelenie khimicheskikh nauk (*or* Seriya khimicheskaya) • **Bulletin of the Academy of Sciences of the USSR: Division of Chemical Science** • 1952(16)1 • CB

Izv. AN SSSR, ser. fiz(ich). • Izvestiya Akademii Nauk SSSR: Seriya fizicheskaya • **Bulletin of the Academy of Sciences of the USSR: Physical Series** • 1954(18)3 • Columbia Technical Translations

Izv. AN SSSR, ser. fiz. atm. i okeana • Izvestiya Akademii Nauk SSSR: Seriya fiziki atmosfery i okeana • **Izvestiya, Atmospheric and Oceanic Physics** • 1965( )1 • AGU

Izv. AN SSSR, ser. fiz. zemli • Izvestiya Akademii Nauk SSSR: Seriya fiziki zemli • **Izvestiya, Physics of the Solid Earth** • 1965( )1 • AGU

Izv. AN SSSR, ser. geofiz. • Izvestiya Akademii Nauk SSSR: Seriya geofizicheskaya • **Bulletin of the Academy of Sciences of the USSR: Geophysics Series** • 1957(7)1 • AGU [superseded by Izv. AN SSSR, ser. fiz. atm. i okeana and Izv. AN SSSR, ser. fiz. zemli]

Izv. AN SSSR, ser. geol. • Izvestiya Akademii Nauk SSSR: Seriya geologicheskaya • **Bulletin of the Academy of Sciences of the USSR: Geologic Series** • 1958(23)1 • AGI

Izv. AN SSSR, ser. neorgan. mat(er). • Izvestiya Akademii Nauk SSSR: Seriya neorganicheskie materialy • **Inorganic Materials** • 1965(1)1 • CB

Mass Spectrometry

Theory and Applications

By R. Jayaram

Geophysical Institute, University of Alaska

The first half of this unique book provides a lucid and thorough introduction to the principles of mass spectrometers. The second half features the applications of nonmagnetic mass spectrometers to upper atmospheric research, describing problems in the performance of satellite experiments and instruments for the direct study of the ion and neutral atom composition of the upper atmosphere. Other topics include composition studies using rocket- and satellite-borne mass spectrometers, the IGY rocket measurements of Arctic atmosphere composition above 100 km, an emission current regulator for rf mass spectrometers, a theory to determine ionic masses in rf spectrometers in flight, a two stage single frequency rf analyzer for exosphere research, the results of Soviet experiments with rf mass spectrometers, composition studies with quadrupole and time-of-flight mass spectrometers, a quadrupole mass spectrometer for D and lower E region composition measurements, a conventional magnetic mass spectrometer designed for an aeronomy satellite, and particular experimental and engineering problems.

CONTENTS: Introduction to mass spectrometers and spectrographs • Magnetic mass spectrometers • Time of flight mass spectrometers • Radio frequency mass spectrometers • Cyclotron resonance instruments • Massenfilter as a mass spectrometer • Applications of non-magnetic mass spectrometers to upper atmospheric research.

OF INTEREST TO: researchers and students in physics involved in mass spectrometry, atmospheric physics and space physics researchers, and instrumentation specialists working on analytical problems with special reference to mass spectrometry.

Approx. 220 pages   1966 $12.50

STUDIES OF

NUCLEAR REACTIONS

"Trudy" Volume 33 of the
Lebedev Physics Institute Series

Edited by Academician D. V. Skobel'tsyn

Director, Lebedev Physics Institute
Academy of Sciences of the USSR

Translated from Russian

Contains nine articles prepared by leading research workers at the Lebedev Physics Institute, one of the largest research centers of the Soviet Union, on such topics as the elastic scattering of charged particles on some light nuclei, interactions of protons and tritium, and inelastic scattering of neutrons on light and medium nuclei. Other articles deal with quantum mechanics and the theory of particle interactions, scattering, and nuclear reactions.

CONTENTS: Investigation of the interaction of protons with tritium at energies below the threshold of the (p,n)-reaction, A. B. Kurepin • Investigation of elastic scattering of charged particles on several light nuclei at low energies, Yu. G. Balashko • Analysis of the p—T interaction above the threshold of the T (p,n) He³ reaction, Yu. G. Balashko and I. Ya. Barit • Investigation of inelastic scattering of 14 Mev neutrons on light and medium nuclei, B. A. Benetskii • Theory of nuclear reactions and the many-body problems, G. M. Vagradov • Quantum-mechanical fundamentals of the theory of nuclear reactions, V. I. Serdobol'skii • On the phases of the elastic n—d-scattering process, V. N. Efimov and S. A. Myachkova • Method of time correlation functions in the description of the interaction of various particles with a complex system, and its applications, M. V. Kazarnovskii • Some possible ways of increasing the yield of nuclear reactions, L. N. Katsaurov.

222 pages   1966 $22.50
87 ill., 28 tables

Previously published in the Lebedev Physics Institute series:

OF INTEREST TO: nuclear physicists and theoretical and mathematical physicists investigating nuclear interactions.